NASA/TP—2006–214602

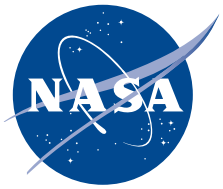

Shock Structure Analysis and Aerodynamics in a Weakly Ionized Gas Flow

R. Saeks
Accurate Automation Corporation, Chattanooga, Tennessee

S. Popovic
Old Dominion University, Norfolk, Virginia

A.S. Chow
Marshall Space Flight Center, Marshall Space Flight Center, Alabama

August 2006

The NASA STI Program Office…in Profile

Since its founding, NASA has been dedicated to the advancement of aeronautics and space science. The NASA Scientific and Technical Information (STI) Program Office plays a key part in helping NASA maintain this important role.

The NASA STI Program Office is operated by Langley Research Center, the lead center for NASA's scientific and technical information. The NASA STI Program Office provides access to the NASA STI Database, the largest collection of aeronautical and space science STI in the world. The Program Office is also NASA's institutional mechanism for disseminating the results of its research and development activities. These results are published by NASA in the NASA STI Report Series, which includes the following report types:

- TECHNICAL PUBLICATION. Reports of completed research or a major significant phase of research that present the results of NASA programs and include extensive data or theoretical analysis. Includes compilations of significant scientific and technical data and information deemed to be of continuing reference value. NASA's counterpart of peer-reviewed formal professional papers but has less stringent limitations on manuscript length and extent of graphic presentations.

- TECHNICAL MEMORANDUM. Scientific and technical findings that are preliminary or of specialized interest, e.g., quick release reports, working papers, and bibliographies that contain minimal annotation. Does not contain extensive analysis.

- CONTRACTOR REPORT. Scientific and technical findings by NASA-sponsored contractors and grantees.

- CONFERENCE PUBLICATION. Collected papers from scientific and technical conferences, symposia, seminars, or other meetings sponsored or cosponsored by NASA.

- SPECIAL PUBLICATION. Scientific, technical, or historical information from NASA programs, projects, and mission, often concerned with subjects having substantial public interest.

- TECHNICAL TRANSLATION. English-language translations of foreign scientific and technical material pertinent to NASA's mission.

Specialized services that complement the STI Program Office's diverse offerings include creating custom thesauri, building customized databases, organizing and publishing research results…even providing videos.

For more information about the NASA STI Program Office, see the following:

- Access the NASA STI Program Home Page at ***http://www.sti.nasa.gov***

- E-mail your question via the Internet to help@sti.nasa.gov

- Fax your question to the NASA Access Help Desk at 301–621–0134

- Telephone the NASA Access Help Desk at 301–621–0390

- Write to:
  NASA Access Help Desk
  NASA Center for AeroSpace Information
  7121 Standard Drive
  Hanover, MD 21076–1320
  301–621–0390

NASA/TP—2006–214602

Shock Structure Analysis and Aerodynamics in a Weakly Ionized Gas Flow

R. Saeks
Accurate Automation Corporation, Chattanooga, Tennessee

S. Popovic
Old Dominion University, Norfolk, Virginia

A.S. Chow
Marshall Space Flight Center, Marshall Space Flight Center, Alabama

National Aeronautics and
Space Administration

Marshall Space Flight Center • MSFC, Alabama 35812

August 2006

Acknowledgments

The authors wish to acknowledge the support provided by Robert M. Pap of the Accurate Automation Corp., NASA, and the U.S. Navy for the experimental and preliminary theoretical research programs on "Plasma Shock Wave Modification" under AAC corporate R&D, and SBIR contracts NAS8–00137 and N00178–01–C–1039, which paved the way for the theoretical research program on "Shock Structure Analysis and Aerodynamics" summarized herein.

Available from:

NASA Center for AeroSpace Information
7121 Standard Drive
Hanover, MD 21076–1320
301–621–0390

National Technical Information Service
5285 Port Royal Road
Springfield, VA 22161
703–487–4650

TABLE OF CONTENTS

TABLE OF CONTENTS (Continued)

LIST OF FIGURES

LIST OF FIGURES (Continued)

LIST OF TABLES

NOMENCLATURE

C	speed of sound
C_L	speed of light
C^s	speed of sound of specie s
D^s	diffusion parameter of specie s
E	electric field
e	electric charge
f	body force
f^s	body force on specie s
H	magnetic field
j^s	current density of specie s
k	Boltzmann's constant
l	mean free path
$\tilde{M}$	density effective of Mach number
$\hat{M}$	pressure effective of Mach number
$\bar{M}$	effective of Mach number
M^n	Mach number of flow normal to the shock
M^s	Mach number of specie s
m	mass of a neutral molecule
m^e	mass of an electron
m^s	mass of a particle of specie s

NOMENCLATURE (Continued)

n^s	number density (concentration) of specie s
$\overline{p}$	pressure with ionization
p^s	partial pressure of specie s
Q	heat addition
S^s	entropy of specie s
T^s	temperature of specie s
u	velocity
$\overline{u}$	velocity with ionization
u^{ed}	electron drift velocity
u^{er}	random electron velocity
u^s	velocity of specie s
ν^{en}	electron neutral collision frequency
ν^{in}	ion neutral collision frequency
β	shock angle
$\overline{\beta}$	shock angle with ionization
γ^s	specific heat ratio of specie s
Δ	shock width
ε_0	permittivity of free space
ε_I	ionization potential
ε^s	internal energy of specie s
ζ	second viscosity coefficient

NOMENCLATURE (Continued)

η	dynamic viscosity coefficient
ι_{shock}	shock intensity
$\bar{\rho}$	density with ionization
ρ^s	density of specie *s*
τ	shock standoff distance
$\bar{\tau}$	shock standoff distance with ionization
Φ	electric potential
Φ_I	ionization temperature
φ	mass flow
χ	turning angle
Ω^s	ohmic (joule) heating by specie *s*

Superscripts and Subscripts

0	initial value
bd	body
e	electron
ed	electron drift
dn	downstream flow
ds	downstream side of shock
i	ion
ie	applies to both ions and electrons, etc.
inv	inviscid

NOMENCLATURE (Continued)

m	mean flow condition in boundary layer
n	neutral molecule
s	generic species; i.e., *n*, *i*, or *e*
src	source
tp	flow variable along the upper surface of the lifting body
up	upstream flow
us	upstream side of shock
vis	viscous
w	flow condition at wall
∞	flow condition at top of boundary layer

TECHNICAL PUBLICATION

SHOCK STRUCTURE ANALYSIS AND AERODYNAMICS IN A WEAKLY IONIZED GAS FLOW

1. INTRODUCTION

Unlike the fully ionized case, the structure of a shock wave propagating through a weakly ionized gas is not well understood.[1] Interest in the weakly ionized case, however, has been rekindled by experimental research suggesting that the performance of a supersonic missile or aircraft can be significantly improved by weakly ionizing the air through which the associated shock wave propagates.[2–8]

Since the ion/neutral scattering cross section is large and the electron mass is negligible, one may assume that ions and neutral particles in the weakly ionized gas have the same temperature and velocity and that the electron momentum is negligible. Based on these assumptions together with a quasi-neutrality assumption, Appleton and Bray developed a "heavy particle/electron" model for a weakly ionized gas with both elastic and inelastic (ionizing) collisions,[9] while McIntyre, et al. used a derivative of this model to characterize the relaxation and recombination processes in a weakly ionized gas.[10]

Under the same assumptions, Magretova, et al. and Liu and Glass developed heavy particle/electron models for an ionizing shock wave propagating through a non-equilibrium weakly ionized gas.[11,12] Simulations using the Magretova, et al. model at high temperatures in the Mach 26–29 range, show a small electron temperature peak and a jump in both the charged and neutral particle densities at the shock, and simulations using the Liu and Glass model at room temperature and Mach 13 yield similar results.[11,12] (See ref. 1 for a review of the Magretova, et al. model and simulations.[1,11]) Popovic and Vuskovic and Saeks, et al. dropped the quasi-neutrality assumption in their heavy particle/electron models (though still requiring that the electron velocity equal the heavy particle velocity).[13,14] In addition to the effects indicated above, they saw a large electric field, on the order of 10^5–10^7 V m^{-1}, at the shock wave and a reduction in the shock intensity, which is consistent with the experimental observations.[2–8]

The object of this Technical Publication (TP) is to analyze the structure of a shock wave propagating through a weakly ionized gas and characterize its influence on the aerodynamics and performance of a missile or aircraft. For this purpose, an electrofluid dynamics model composed of six classical conservation laws and Gauss' Law was developed, while the remaining conservation laws are implied by the assumptions that $u^i = u^{n>0}$ and $T^i = T^n$ and that the electron momentum is negligible. Viscosity is included in the model to correctly define the shock thickness, but quasi-neutrality is not assumed since the spatial scale of the shock structure may be less than a Debye length. As such, both the electric field and the electron drift velocity are included in the model.

This model is divided into a fluid dynamics model and an electrodynamics model. The fluid dynamics model is derived in section 2.1 using the multispecies fluid flow model developed by Sutton and Sherman with the addition of the viscosity terms.[15] Since the electron velocity may be several orders of magnitude greater than the heavy particle velocity, an analysis of this model reveals that the electron body force term in the energy equation (equivalently the electron ohmic heating term) is the primary mechanism through which the electrodynamics interact with the fluid flow. As such, the role of the electrodynamics model is to provide sufficient electrodynamics equations to evaluate the body force/ohmic heating term in the energy equation. The resultant electrodynamics model, formulated in section 2.2, is made up of three individual species conservation laws plus Gauss' Law and the required auxiliary equations. The source and sink terms used in the electrodynamics model are summarized in section 2.3.

Although the electrofluid dynamics model is formulated in vector notation, the primary goal of this TP is to analyze the structure of a normal shock wave propagating through a weakly ionized gas and identify the underlying physical processes. As such, it suffices to solve a one-dimensional version of the electrofluid dynamics model, restricted to the region a few tens of micrometers upstream and downstream of the shock where the ionization interacts with the fluid flow. Indeed, in this region, the fluid dynamics model reduces to a pair of initial value problems upstream and downstream of the shock derived in section 3.1, which are connected by analytic intrashock and shock width models derived in section 3.2. The flow chart for a one-dimensional shock structure analysis algorithm based on the resultant model appears in section 3.3.

A detailed analysis of the structure of a Mach 4 shock wave at an altitude of 40,000 ft using a 1-eV source is presented in section 4.1 together with a discussion of the physics underlying the key features of the shock structure. Additional shock structure simulations appear in appendix A. The normally intuitive concepts of flow and shock intensity are formalized and used to summarize the properties of a series of shock structure simulations—as a function of Mach number, altitude, and the source temperature—in section 4.2. Furthermore, it is shown that the shock structure effectively bifurcates into two cases: (1) Where the ionization does not significantly effect the shock structure and (2) where the ionization reduces the shock to its minimum possible intensity, with a small transition region in between.

An analysis of the flow behind a shock wave propagating through a weakly ionized gas is developed in section 5. Given the bifurcation of the shock structure, the two cases are considered separately using a classical analysis for the case where the ionization does not significantly effect the shock structure, and a modified analysis for the case where the ionization reduces the shock to its minimum possible intensity. The required modified pressure and density ratio formulae are developed in section 5.1 and used to formulate a set of oblique shock curves for the case where the ionization reduces the shock to its minimum possible intensity in section 5.2. The modified oblique shock curves are used to determine if the shock is attached or detached and to compute the shock angle when it is attached, and an analysis of the flow behind the shock for the attached and detached cases is performed in section 5.3.

In section 6 the results of an aerodynamic analysis of a two-dimensional hypersonic lifting vehicle in which ionization is used to reduce the shock intensity to its minimum possible value, comparing its performance at various Mach numbers and angles of attack to an identical vehicle without ionization, are considered.

Finally, in section 7, the conclusion, the assumptions underlying the electrofluid dynamics model are reviewed, the shock structure analysis and simulations are compared with experiment, and the possible applications of the technology in aeronautics are commented upon.

2. ELECTROFLUID DYNAMICS MODEL

To formulate the electrofluid dynamics model, consider a fluid composed of neutral gas molecules, single positively charged ions, and electrons where each particle species is characterized by the variables summarized in table 1. Here the superscript, s, indicates the particular species ($s = n$, i, e for neutral molecules, ions, and electrons, respectively), whereas no superscript is used for the entire ionized gas treated as a single fluid. Furthermore, dual superscripts are used as required: $s = ed$ to denote the electron drift velocity, $s = ie$ to denote variables that apply to both the ions and electrons, etc. Clearly, $\rho^s = m^s n^s$ and $M^s = u^s / C^s$, while it follows from the ideal gas law that $p^s = n^s k T^s$, where k is Boltzmann's constant, and $\varepsilon^s = p^s / \left(\left(\gamma^s - 1\right)\rho^s\right)$ for a perfect gas where γ^s is the specific heat ratio for the given particle species.[15,16] In the following analysis a weakly ionized gas; i.e., $n^e, n^i \ll n^n$, is considered with no externally imposed electric or magnetic fields. An electric field due to charge separation may, however, be present over a distance of a few Debye lengths.[17] For nonrelativistic motion, however, the force due to a magnetic field, $\left(\pm u^s / C_L\right) eH$, is much less than that due to an electric field, eE, and as such, any magnetic fields due to charge transport may be ignored. Furthermore, $u^i = u^n$ and $T^i = T^n$ is assumed since the ions and neutrals have approximately the same mass and collision cross section and, therefore, flow together. See reference 17 for a detailed analysis of these effects, while a summary of all assumptions used in the derivation of the fluid dynamics model is provided in table 2.

Table 1. Variables and constants characterizing each particle species in a weakly ionized gas.

Variable	Symbol	Units	Variable	Symbol	Units
Velocity vector	u^s	m s^{-1}	Number density (concentration)	n^s	m^{-3}
Pressure	p^s	N m^{-2}	Internal energy per unit mass	ε^s	J kg^{-1}
Density	ρ^s	kg m^{-3}	Mass	m^s	kg
Temperature	T^s	K	Speed of sound	C^s	m s^{-1}
Mach number	M^s	1	Body force	f^s	N m^{-3}
Entropy	S^s	J kg^{-1} K^{-1}	Mass flow	φ	kg m^{-2} s^{-1}
Electric field	E	V m^{-1}	Current density	j^s	A m^{-2}
Electric potential	Φ	V	Ohmic (Joule) heating	Ω^s	J m^{-3} s^{-1}
Shock width	Δ	m	Mean free path	l	m
Dynamic viscosity	η	kg m^{-1} s^{-1}	Second viscosity	ξ	kg m^{-1} s^{-1}
Heat addition	Q	J m^{-3} s^{-1}	–	–	–
Constant	**Symbol**	**Units**	**Constant**	**Symbol**	**Units**
Electric charge	e	C	Boltzmann's Constant	k	J K^{-1}
Permittivity of free space	ε_0	C^2 N^{-1} m^{-2}	Speed of light	C_L	m s^{-1}
Mass of a neutral molecule	m^n	kg	Mass of an electron	m^e	kg
Ionization potential	ε_I	J	Ionization temperature	Φ_I	K
Specific heat ratio	γ^s	1	–	–	–

Table 2. Assumptions and bounds used in deriving the electrofluid dynamics model.

Physical Assumptions		
Approximation	**Implied Equality**	**Justification**
The neutrals and ions have the same velocity and temperature.	$u^n = u^i$ $T^n = T^i$	The neutrals and ions have (approximately) the same mass and collision cross section and therefore flow together. See ref. 17 for a detailed analysis of this effect.
There are no externally imposed electric or magnetic fields		The model is intended to analyze the effect of a weakly ionized gas on a shock wave in a free space environment without externally imposed fields.
Internally generated magnetic fields are ignored.	$H = 0$	For non-relativistic motion the magnetic force, $(\pm u^s/C_L)eH$, is much less than the electric force, eE, allowing H to be ignored.[17]
Steady state analysis	$\partial/\partial t = 0$	The model is intended for steady state applications.
Perfect gas	$p^s = n^s k T^s$ $\varepsilon^s = p^s \big/ \left(\gamma^s - 1\right)\rho^s$	The model is intended for aerodynamic applications in air (or other perfect gases).
Ions are singly ionized	$Z^i = 1$	Since the gas is weakly ionized, the probability of multiply ionizing a single molecule is small.
The are no radiative heat losses	$Q = 0$	Thermal radiation from the shock is negligible because of its small width.[18]
Parameter Bounds		
$n^e < 10^{-4} \times n^n$	$n^i < 10^{-3} \times n^n$	$T^e < 10^2 \times T^n$ $\quad u^e < 10^5 \times u^n$

Unlike the ions, the electrons will be accelerated by an electric field, where present, with their velocity limited by collisions with the heavy particles. Indeed, u^e may be expressed in the form $u^e = u^n + u^{ed} + u^{er}$ where u^{ed} is the electron drift velocity due to an electric field and u^{er} is the random electron velocity due to scattering. In general, the electron drift velocity, u^{ed}, can be modeled by a differential equation characterizing the acceleration of the electrons by the electric field less the momentum lost in electron neutral collisions.[17] In this application, however, the approximate expression, $u^{ed} = -eE \big/ m^e \nu^{en}$, suffices, where ν^{en} is the electron/neutral collision frequency. Typically, u^{ed} is two or more orders of magnitude greater than u^n, whereas the random electron velocity may be one to two orders of magnitude greater than u^{ed}.[17] Since the random electron velocity is due to the scattering of the electrons off of the neutrals, its direction is random, and as such, the mean random velocity of the electrons is zero, allowing the modeling of the mean electron velocity by

$$u^e = u^n - \frac{eE}{m^e \nu^{en}} \quad . \tag{1}$$

Note that in the presence of a positive flow, $u^n = u^i > 0$, u^e must also be positive. Indeed, if $u^e(x) < 0$, at some point, x, the electrons would flow upstream while the ions would flow downstream. The resultant increase in upstream electron density would, however, cause $E(x)$ to decrease via Gauss' Law; i.e., become more negative, which would increase u^e to a positive value. As such, a negative electron

velocity in the presence of a positive flow is unstable. Moreover, it follows from the above expression for u^e, that E is bounded above by $E < u^n m^e v^{en} / e$, which is approximated by $E<0$ since even a small positive E will produce a "weak electron trap".

The electrofluid dynamics model is divided into two components, (1) A fluid dynamics model developed in section 2.1, characterizing the fluid flow properties of the entire weakly ionized gas treated as a single fluid; and a electrodynamics model developed in section 2.2. The source and sink terms used in the electrodynamics model are summarized in section 2.3.

2.1 Fluid Dynamics Model

Following Sutton and Sherman,[15] define the fluid dynamics variables for the entire weakly ionized gas treated as a single fluid by letting

$$\rho \equiv \rho^n + \rho^i + \rho^e \tag{2}$$

and

$$p \equiv p^n + p^i + p^e \tag{3}$$

be the sum of the individual species densities and partial pressures, respectively, and

$$u \equiv \frac{\rho^n u^n + \rho^i u^i + \rho^e u^e}{\rho} \tag{4}$$

and

$$\varepsilon \equiv \frac{\rho^n \varepsilon^n + \rho^i \varepsilon^i + \rho^e \varepsilon^e}{\rho} \tag{5}$$

be the mass density weighted average of the individual species velocities and internal energies, respectively. Given the relatively small weight on the electrons in the fluid dynamics variables, they typically track the corresponding neutral particle variables within 1 percent, given the bounds for a weakly ionized gas indicated in table 2. This is not to imply that the ionization has no effect on the neutral particle flow (sec. 4), but rather that its effect on the neutral particle flow tracks its effect on the entire fluid. As such, one can use the fluid dynamics variables for the weakly ionized gas to approximate the neutral particle variables in the electrodynamics model developed in section 2.2.

Using the above defined fluid flow variables and following Sutton and Sherman with the addition of the viscous terms,[15] use the following set of fluid flow equations:

$$\nabla \bullet (\rho u) = 0 \tag{6}$$

$$\rho(u \bullet \nabla)u + \nabla\rho - \eta\nabla^2 u - (\zeta + \eta/3)\nabla(\nabla \bullet u) = f^n + f^i + f^e \tag{7}$$

and

$$\nabla \bullet \left(\rho \left(\frac{|u|^2}{2} + \varepsilon \right) u \right) + \nabla \bullet pu = f^n \bullet u^n + f^i \bullet u^i + f^e \bullet u^e + Q \tag{8}$$

to model the weakly ionized gas. Here, η and ζ are the dynamic and second viscosity coefficients, respectively; f^s, $s = n, i, e$ is the body force on the three particle species and Q is the heat added to the ionized gas. Note that, since the above equations define a fluid dynamics model for the entire weakly ionized gas treated as a single fluid, the interspecies collision processes are implicit in the equations, and do not require explicit models.

In the momentum and energy equations (7) and (8) we have expressed the body force, f^s, in terms of the individual particle species rather than the entire weakly ionized gas, since the electric field, which is the source of the body force in the present problem, effects each particle species differently. Letting f^s be the body force per unit volume due to the electric field on each of the three particle species in the energy equation (8), $f^n \bullet u^n = 0,$ while

$$f^e \bullet u^e = -en^e E \bullet u^e = -en^e u^e \bullet E = j^e \bullet E = \Omega^e \tag{9}$$

reduces to the ohmic (or Joule) heating of the ionized gas due to the body force on the electrons, where $j^e = -en^e u^e$ is the electron current density, and similarly, $f^i \bullet u^i = j^i \bullet E = \Omega^i$. Since the electron drift velocity is two or more orders of magnitude greater than the ion velocity, in the presence of an electric field, the ion ohmic heating can be neglected in comparison to the electron ohmic heating. As such, the body force terms in the energy equation reduce to $j^e \bullet E = \Omega^e$. Note that the ohmic heating term, Ω^e, only represents that part of the energy imparted to the electrons by the electric field, which is lost to the neutral particles via collisions, with the remainder going into the random electron velocity (see ref. 17 for a detailed analysis of the ohmic heating process).

Unlike the body force terms in the energy equation, the body force terms in the momentum equation are not multiplied by velocity, and as such, their effect on the fluid flow variables is normally negligible compared to Ω^e. Moreover, since the electric field only exists over a distance of a few Debye lengths on either side of the shock if one integrates in the direction normal to the shock over the interval $\left[x_{\text{up}}, x_{\text{dn}} \right]$ where E is non-zero:[17]

$$\int_{x_{up}}^{x_{dn}}\left[f^i(q)+f^e(q)\right]dq=\int_{x_{up}}^{x_{dn}}\left[n^i(q)-n^e(q)\right]eE(q)\,dq$$

$$=\int_{x_{up}}^{x_{dn}}\left[\varepsilon_0\frac{dE}{dx}(q)\right]E(q)\,dq=\frac{\varepsilon_0}{2}\int_{x_{up}}^{x_{dn}}\left[\frac{dE^2(q)}{dx}\right]dq$$

$$=\frac{\varepsilon_0}{2}E^2(q)\Big|_{x_{up}}^{x_{dn}}=\frac{\varepsilon_0}{2}\left[E(x_{dn})-E(x_{up})\right]$$

$$=\frac{\varepsilon_0}{2}[0-0]=0\ , \tag{10}$$

where the equality $\left(n^i-n^e\right)e=\varepsilon_0 dE/dx$ is the differential form of Gauss' Law in the direction normal to the shock. As such, the net first order effect of the ion and electron body force terms in the momentum equation is zero—sometimes called the washout effect—while $f^n=0$. Although higher order and/or local effects are not precluded, equation (10), together with the relatively small magnitude of the body forces compared to Ω^e, is sufficient justification to neglect the body force terms in the momentum equation.*

Finally, letting $\varepsilon=\left(\rho^n\varepsilon^n+\rho^i\varepsilon^i+\rho^e\varepsilon^u\right)\Big/\rho\approx p/(\gamma-1)\rho$ and substituting equations (9) and (10) into equations (6)–(8) yields the required fluid dynamics model for the ionized gas treated as a single fluid, as follows:

- Continuity equation:

$$\nabla\bullet(\rho u)=0\ . \tag{11}$$

- Navier Stokes equation:

$$\rho(u\bullet\nabla)u+\nabla\mathrm{p}-\eta\nabla^2u-(\zeta+\eta/3)\nabla(\nabla\bullet\mathrm{u})=0\ . \tag{12}$$

- Ionized gas energy equation:

$$\nabla\bullet\left(\rho\left(\frac{|u|^2}{2}+\frac{p}{(\gamma-1)p}\right)u\right)+\nabla\bullet pu=\Omega^{\mathrm{e}}\ . \tag{13}$$

* Since the electric field produced by charge separation across the shock only extends a few Debye lengths,[17] the number of electron/neutral collisions in the interval $\left[x_{up}, x_{dn}\right]$ may be insufficient to transfer the momentum imparted to the electrons by the electric field to the entire weakly ionized gas. In this case, the electron body force term drops out of the momentum equation (eq. (7)), negating the "washout effect." Since $E<0$, however, the remaining ion body force term in the momentum equation is additive to the ohmic heating term in the energy equation (eq. (8)), enhancing the interaction between the ionization and the fluid flow variables. As such, the "washout analysis" yields a conservative approximation in this case.

Although the heat addition term in the energy equation (eq. (8)) can be used to model the effects of an external heating source on the shock, our goal in the present paper is to characterize the effects of a weakly ionized gas on the shock, independently of thermal effects, while following Lowke and Murphy, thermal radiation from the shock is negligible.[18] As such, set $Q = 0$ in equation (13).

2.2 Electrodynamics Model

Given the fluid dynamics model of equations (11)–(13), it remains to add the appropriate electrodynamics equations required to evaluate Ω^e. To this end, define an electrodynamics model composed of the following equations.

- Electron velocity equation:

$$u^e = u - \frac{eE}{m^e \nu^{en}} \quad . \tag{14}$$

- Electron heating equation:

$$\frac{3}{2} n^e k \left(u^e \bullet \nabla \right) T^e + n^e k T^e \left(\nabla \bullet u^e \right) = \eta + \phi - \Omega^e + \sigma \quad . \tag{15}$$

- Ion continuity equation:

$$\nabla \bullet \left(n^i u - D^i \nabla \left(n^i \right) \right) = \dot{n}^{ie} \quad . \tag{16}$$

- Electron continuity equation:

$$\nabla \bullet \left(n^e u^e - D^e \nabla \left(n^e \right) \right) = \dot{n}^{ie} \quad . \tag{17}$$

- Poisson's equation:

$$\nabla^2 \Phi = -\frac{e}{\varepsilon_0} \left(n^i - n^e \right) \tag{18}$$

and

$$E = -\nabla \Phi \quad . \tag{19}$$

- Electron ohmic heating:

$$\Omega^e = -en^e E \bullet u^e \quad , \tag{20}$$

where the approximation $u^i \approx u^n \approx u$ is used to eliminate the species variables, u^n and u^i from the electrodynamics model.

The electron heating equation (eq. (15)) is the energy equation for the electrons without the kinetic energy term.[15] Here, Ω^e is the electron ohmic heating term defined in equation (9), η is the thermal energy lost in elastic collisions, using a standard "hard sphere" model, and ϕ is the thermal energy lost in inelastic; i.e., ionizing, collisions.[15] Finally, σ denotes the ionization source in the electron heating equation. For the present purposes, rather than attempting to model a realistic source, choose σ to maintain a prescribed minimum electron temperature in the region around the shock where the ionization interacts with the fluid flow, $T^e(x) \geq T^e_{src},\ x_{\text{up}} \leq x \leq x_{\text{dn}},$ where T^e_{src} is typically on the order of 1 eV. Detailed models for η and ϕ are developed by Sutton and Sherman, Hoffert and Lien, and summarized in section 2.3.[15,19]

In the charged particle continuity equations (eqs. (16) and (17)), $\dot{n}^{ie} = \dot{n}^{ie+} - \dot{n}^{ie-}$ characterizes the ionization/recombination rate. For the ionization rate, $\dot{n}^{ie+}$, a single step ionization model is used, where ionization is due to an electron colliding with a neutral and ionizing it from the ground state.[15,17] For the recombination rate, $\dot{n}^{ie-}$, a model developed by Stevefelt et al., which combines radiational and collisional recombination rate terms with an empirical correction term,is used.[20] Finally, D^i and D^e are the ion and electron diffusion parameters, respectively, though D^i may be replaced by the ambipolar ion diffusion parameter.[17] These models are developed by Sutton and Sherman and Raizer and summarized in section 2.3.[15,17]

The electric field, E, is expressed as the gradient of a scalar potential, Φ, which satisfies Poisson's equation, in equations (18) and (19), while the electron velocity, and electron ohmic heating equations (eqs. (14) and (20)) were derived in section 2.1.

Each of the terms used in the electrodynamics model, as well as the collision frequencies, ν^{en} and ν^{in}, and mean free path that appear throughout the model can be expressed in terms of the fluid dynamics variables, p, ρ, and u and/or the individual species parameters in the electrodynamics model. As such, the fluid dynamics and electrodynamics models of equations (11)–(20) constitute a self-consistent electrofluid dynamics model. Ignoring the explicit substitutions of equations (14) and (20), the resultant model is composed of one vector and six scalar equations in one vector and six scalar $(u, p, \rho, T^e, n^i, n^e,$ and $\Phi)$ unknowns.

2.3 Source and Sink Models

The ionization/recombination rate term, $\dot{n}^{ie} = \dot{n}^{ie+} - \dot{n}^{ie-}$, in the charged particle continuity equations (eqs. (16) and (17)) may expressed as the difference of the ionization rate, $\dot{n}^{ie+}$, and the recombination rate, $\dot{n}^{ie-}$. For the ionization rate, use the single step ionization model,

$$\dot{n}^{ie+} = \frac{2}{3} C_1 \left(\varepsilon_I e^{-\varepsilon_I / kT^e} \left(1 + \frac{\varepsilon_I}{kT^e} \right) \right) \left(\frac{8 \times 10^{-4} kT^e}{\pi m^e} \right)^{1/2} \left(\frac{\rho}{m^n} - n^i \right) n^e \quad , \tag{21}$$

where ionization is due to an electron colliding with a neutral and ionizing it from the ground state. This model is derived from the models in references 15 and 17, where ε_I is the ionization potential of a neutral molecule and C_I is an empirical constant,[14,17] while the n^i term in equation (21) is added to enforce the single ionization hypothesis. For the recombination rate model, use

$$\begin{aligned} \dot{n}^{ie-} = \Big[& 1.55 \times 10^{-16} \left(T^e \right)^{-0.63} + 3.61 \times 10^{-17} \left(T^e \right)^{-2.18} \left(n^e \right)^{0.37} \\ & + 3.8 \times 10^{-21} \left(T^e \right)^{-4.5} n^e \Big] n^e n^i \, , \end{aligned} \tag{22}$$

developed by Stevefelt, Boulmer, and Delpech, which combines radiational and collisional recombination rate terms with an empirical correction term.[20]

In the electron heating equation (eq. (15)), η is the thermal energy lost in elastic collisions, using a standard "billiard ball" model,[15]

$$\eta = \frac{3 m^e n^e}{m^n} \nu^{en} k \left(T - T^e \right) \, , \tag{23}$$

where ν^{en} is the electron/neutral collision frequency.[17] Similarly, $\phi = -\dot{n}^{ie+} \varepsilon_I$ is the thermal energy lost in inelastic; i.e., ionizing, collisions. For an electron to ionize a neutral molecule from the ground state, ε_I Joules are transferred from the electron to the molecule. Note that the ionizing energy is radiated by the molecule when it recombines and relaxes to the ground state and is normally not returned to the electrons.

Finally, D^i and D^e in the charged particle continuity equations are the ion and electron diffusion parameters

$$D^i = \frac{kT}{m^n \nu^{in}} \quad \text{and} \quad D^e = \frac{kT^e}{m^e \nu^{en}} \, , \tag{24}$$

where ν^{in} is the ion/neutral collision frequency, though D^i may be replaced by the ambipolar ion diffusion constant $D^a = kT^e / m^n \nu^{in}$.[17]

3. SOLUTION OF THE FLUID DYNAMICS EQUATIONS ACROSS A SHOCK WAVE

The purpose of this section is to develop a procedure for analyzing the structure of a shock wave propagating through a weakly ionized gas using the electrofluid dynamics model developed in section 2. Of course, one could simply solve equations (11)–(20) in one dimension, but this would require a priori knowledge of the downstream boundary conditions and a full downstream solution of the fluid dynamics equations to capture the shock. Alternatively, one can analyze the shock structure without explicit knowledge of the downstream boundary conditions by assuming that the shock wave exists and (without loss of generality) that it is located at $x_{us} = 0$ while ignoring the effect, if any, of the downstream boundary conditions on the intrashock flow. Indeed, this approach is implicit in the classical case where one uses the Rankine-Hugoniot equations to compute the pressure and density ratios across the shock, combined with analytic shock width and intrashock flow models, if required, to analyze the shock structure without explicit reference to the downstream boundary conditions.[16]

Over the past few years, several authors have modified the Rankine-Hugoniot equations to include the effect of ionization on the pressure and density ratios across the shock wave.[21,22] In practice, however, the effect of the ionization on the shock structure is spread out over a region a few tens of microns upstream and downstream of the shock as indicated in figure 1. As such, Murray and Saeks proposed to replace the single control volume used to define the modified Rankine-Hugoniot equations with a sequence of control volumes upstream and downstream of the shock, starting with the given upstream flow and chaining the pressure and density ratios across each control volume to compute the pressure and density ratios across the entire region where the ionization interacts with the flow.[21]

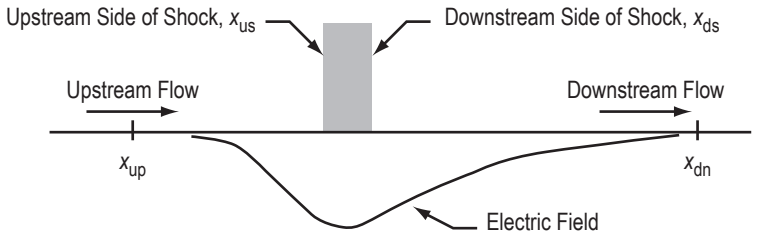

Figure 1. One dimensional geometry for shock structure analysis.

In the present analysis, this process is taken to the limit, letting the thickness of the control volumes go to zero with the chain of pressure and density ratios converging to initial value problems in the regions upstream and downstream of the shock connected by an analytic intrashock model. The initial value problems in the regions upstream and downstream of the shock, connected by an inviscid (zero thickness) shock are formulated in section 3.1, while the inviscid shock is replaced by a viscous intra shock model and an associated shock width model in section 3.2. Finally, a computational algorithm for analyzing the structure of a shock wave propagating through a weakly ionized gas, without reference to

the downstream boundary conditions, is obtained by combining these techniques with a one-dimensional version of the electrodynamics model in section 3.3.

Although the electrofluid dynamics model using vector notation is defined in section 2, for the actual shock structure analysis the one-dimensional geometry used for this TP is illustrated in figure 1. The flow is moving forward along the x-axis, which is translated so that the upstream side of the shock is located at x_{us}. The subscript "us" is also used to denote the fluid flow and electrodynamic variables at the upstream side of the shock; $p_{us} = p(x_{us})$, E_{us}, etc. Similarly, the downstream side of the shock is located at x_{ds}, with the subscript "ds" used to denote the variables at the downstream side of the shock. Unlike a classical shock, the ionization can affect the flow upstream of the shock via electron and ion diffusion across the shock. As such, let x_{up} be a point upstream of the region where the ionization begins to interact with the flow, and use the subscript "up" to denote x and the variables at x_{up}, and similarly for a point x_{dn} and the variables at x_{dn}, downstream of the region where the ionization ceases to interact with the flow. As such, the structure of a shock wave propagating through a weakly ionized gas may be fully characterized by the fluid flow and electrodynamic variables in the interval $\left[x_{up}, x_{dn}\right]$.

3.1 Modified Rankine-Hugoniot Analysis

To formulate the initial value problems that subsume the Modified Rankine-Hugoniot equations in the regions upstream and downstream of the shock where the ionization interacts with the fluid flow, start with a one-dimensional version of the fluid dynamics equations (eqs. (11)–(13)):

$$\frac{d}{dx}(\rho u) = 0 \quad , \tag{25}$$

$$\rho u \frac{du}{dx} + \frac{dp}{dx} - \eta' \frac{d^2 u}{dx^2} = 0 \quad , \tag{26}$$

and

$$\frac{d}{dx}\left(\rho\left(\frac{u^2}{2} + \frac{p}{(\gamma-1)\rho}\right)u\right) + \frac{d}{dx}(pu) = \Omega^e \quad . \tag{27}$$

where $\eta' = (\zeta + 4\eta/3)$. To simplify the analysis, treat the viscosity term in equation (26) as an external force rather than an intrinsic part of the momentum equation by computing the second derivative using data from a previous iteration of the shock structure analysis algorithm or smoothing and extrapolating previously computed data points on the present iteration (sec. 3.3). In either case, this process decouples the second derivative from the unknown velocity, allowing us to treat it as an independent variable, which

is denoted by $\widehat{d^2u}/dx^2$. Although this process will smooth out some higher order effects, it is sufficient for the present purpose.

From equation (25), it follows that the mass flow, $\varphi \equiv \rho u$ is a constant, and $\frac{d\rho}{dx} = -\frac{\rho}{u}\frac{d}{dx}u$. Using the equality $\varphi = \rho u$ to eliminate ρ as a variable in equations (26) and (27), yields

$$\frac{dp}{dx} = -\varphi\frac{du}{dx} + \eta'\widehat{\frac{d^2u}{dx^2}} \tag{28}$$

and

$$\varphi\frac{d}{dx}\left(\frac{u^2}{2} + \frac{pu}{(\gamma-1)\varphi}\right) + \frac{d}{dx}(pu) = \Omega^e \quad , \tag{29}$$

while expanding equation (29) yields

$$\varphi u\frac{du}{dx} + \frac{p}{(\gamma-1)}\frac{du}{dx} + \frac{u}{(\gamma-1)}\frac{dp}{dx} + p\frac{du}{dx} + u\frac{dp}{dx} = \Omega^e \quad , \tag{30}$$

and

$$\varphi u\frac{du}{dx} + \frac{\gamma p}{(\gamma-1)}\frac{du}{dx} + \frac{\gamma u}{(\gamma-1)}\frac{dp}{dx} = \Omega^e \quad . \tag{31}$$

Substituting equation (28) into equation (31) yields the series of equalities

$$\varphi u\frac{du}{dx} + \frac{\gamma p}{(\gamma-1)}\frac{du}{dx} + \frac{\gamma u}{(\gamma-1)}\left(-\varphi\frac{du}{dx} + \eta'\widehat{\frac{d^2u}{dx^2}}\right) = \Omega^e \quad , \tag{32}$$

$$-\frac{\varphi}{(\gamma-1)}u\frac{du}{dx} + \frac{\gamma p}{(\gamma-1)}\frac{du}{dx} + \frac{\gamma u}{(\gamma-1)}\eta'\widehat{\frac{d^2u}{dx^2}} = \Omega^e \quad , \tag{33}$$

$$\frac{1}{(\gamma-1)}(\gamma p - \varphi u)\frac{du}{dx} = \Omega^e - \frac{\gamma u}{(\gamma-1)}\eta'\widehat{\frac{d^2u}{dx^2}} \quad , \tag{34}$$

and the desired expression for

$$\frac{du}{dx} = \frac{(\gamma-1)}{(\gamma p - \varphi u)}\Omega^e - \frac{\gamma u}{(\gamma p - \varphi u)}\eta' \widehat{\frac{d^2u}{dx^2}} \ , \tag{35}$$

while substituting equation (35) into equation (28) yields

$$\begin{aligned}\frac{dp}{dx} &= -\varphi\left(\frac{(\gamma-1)}{(\gamma p - \varphi u)}\Omega^e - \frac{\gamma u}{(\gamma p - \varphi u)}\eta' \widehat{\frac{d^2u}{dx^2}}\right) + \eta' \widehat{\frac{d^2u}{dx^2}} \\ &= -\frac{(\gamma-1)\varphi}{(\gamma p - \varphi u)}\Omega^e + \left(\frac{\gamma\varphi u}{(\gamma p - \varphi u)} + 1\right)\eta' \widehat{\frac{d^2u}{dx^2}} = -\frac{(\gamma-1)\varphi}{(\gamma p - \varphi u)}\Omega^e \\ &\quad + \left(\frac{(\gamma p + (\gamma-1)\varphi u)}{(\gamma p - \varphi u)}\right)\eta' \widehat{\frac{d^2u}{dx^2}} \ .\end{aligned} \tag{36}$$

Equations (35) and (36) define a set of "fluid state" equations that can be used to compute $p(x)$ and $u(x)$, given Ω^e, $\widehat{d^2u/dx^2}$, and initial values for p and u, and one can express the remaining fluid flow variables in terms of p and u. In practice, however, the "fluid state" variables M and C are prefered; i.e., the Mach number and speed of sound of the flow. Indeed, with the aid of the equalities $u = CM$ and $p = \varphi C / \gamma M$, one can transform equations (25) and (26) into an equivalent set of "fluid state" equations,

$$\frac{dC}{dx} = \frac{(\gamma-1)}{2\varphi}\frac{\left(1-\gamma M^2\right)}{\left(1-M^2\right)}\frac{\Omega^e}{C} + \frac{\gamma(\gamma-1)}{2\varphi}\frac{M^3}{\left(1-M^2\right)}\eta' \widehat{\frac{d^2u}{dx^2}} \tag{37}$$

and

$$\frac{dM}{dx} = \frac{(\gamma-1)}{2\varphi}\frac{\left(1+\gamma M^2\right)M}{\left(1-M^2\right)}\frac{\Omega^e}{C^2} + \frac{\gamma}{2\varphi}\frac{\left(2+(\gamma-1)M^2\right)M^2}{\left(1-M^2\right)}\frac{\eta'}{C}\widehat{\frac{d^2u}{dx^2}} \ , \tag{38}$$

in M and C. Finally, use Sutherland's equation to compute η.[23] Indeed, in this application temperatures less than 200 K are rarely encountered, and as such, Sutherland's formula may be approximated by

$$\eta = \frac{1.458\times10^{-6}\times T^{3/2}}{(110.4+T)} \approx 1.458\times10^{-6}\times\sqrt{T} = 1.458\times10^{-6}\times\sqrt{\frac{m^n}{\gamma k}}\times C \ . \tag{39}$$

Furthermore, in this application, the "fluid state" equations are used in the regions upstream and downstream of the shock but not in the shock. As such, it is not expected to encounter extreme compression or expansion waves, allowing the approximation of the second viscosity by the dynamic viscosity.[16] Setting $\eta' = \zeta + \eta/3 \approx 7\eta/3$, yields

$$\eta' \approx \frac{7}{3} \times 1.458 \times 10^{-6} \times \sqrt{\frac{m^n}{\gamma k}} \times C = \alpha C \quad , \tag{40}$$

where $\alpha = 1.69 \times 10^{-7}$. Substituting equation (40) into equations (37) and (38) and setting $u = CM$ now yields the desired form for the "fluid state" equations,

$$\frac{dC}{dx} = \frac{(\gamma-1)}{2\varphi} \frac{\left(1-\gamma M^2\right)}{1-M^2} \frac{\Omega^e}{C} + \frac{\alpha\gamma(\gamma-1)}{2\varphi} \frac{M^3 C}{\left(1-M^2\right)} \frac{\widehat{d^2 CM}}{dx^2} \tag{41}$$

and

$$\frac{dM}{dx} = \frac{(\gamma-1)}{2\varphi} \frac{\left(1+\gamma M^2\right) M}{1-M^2} \frac{\Omega^e}{C^2} - \frac{\alpha\gamma}{2\varphi} \frac{\left(2+(\gamma-1)M^2\right) M^2}{\left(1-M^2\right)} \frac{\widehat{d^2 CM}}{dx^2} \quad , \tag{42}$$

which can be solved for C and M given Ω^e, $\widehat{d^2 u}/dx^2$ and initial values for C and M. Moreover, given the "fluid state" variables, $C(x)$ and $M(x)$, one may compute the remaining fluid flow variables via

$$u = CM; \ \rho = \varphi / CM; \ \text{and} \ \ p = \varphi C / \gamma M \quad . \tag{43}$$

The most significant feature of equations (41) and (42) is the singularity at $M = 1$, which is a manifestation of the physical fact that the flow cannot pass through Mach 1 continuously.

Indeed, since $\Omega^e \geq 0$, the Mach number of the upstream supersonic flow is reduced by the ohmic heating process, eventually producing a shock wave where it jumps across the singularity at Mach 1 to a subsonic value. Since the sign of $(1 - M^2)$ changes at Mach 1, the Mach number of the resultant subsonic flow then begins to increase under the influence of the ohmic heating process. Unlike the supersonic flow, however, the subsonic flow cannot jump across the singularity, and is accelerated toward Mach 1 by the singularity in equation (42), with the rate of acceleration damped by the viscosity term.[16] Moreover, if the flow reaches Mach 1, the sign of $(1 - M^2)$ changes, trapping it at Mach 1. This results in a Mach number curve typical of that shown in figure 2 (a), while the pressure curve follows an inverse trajectory illustrated in figure 2 (b). In general, whenever the flow is supersonic, M and u decrease in the ionization, while p and ρ increase, and vice-versa when the flow is subsonic. See section 4.1 for a detailed analysis of a Mach 4 flow in 40,000-ft air that has been weakly ionized by a 1-eV generator.

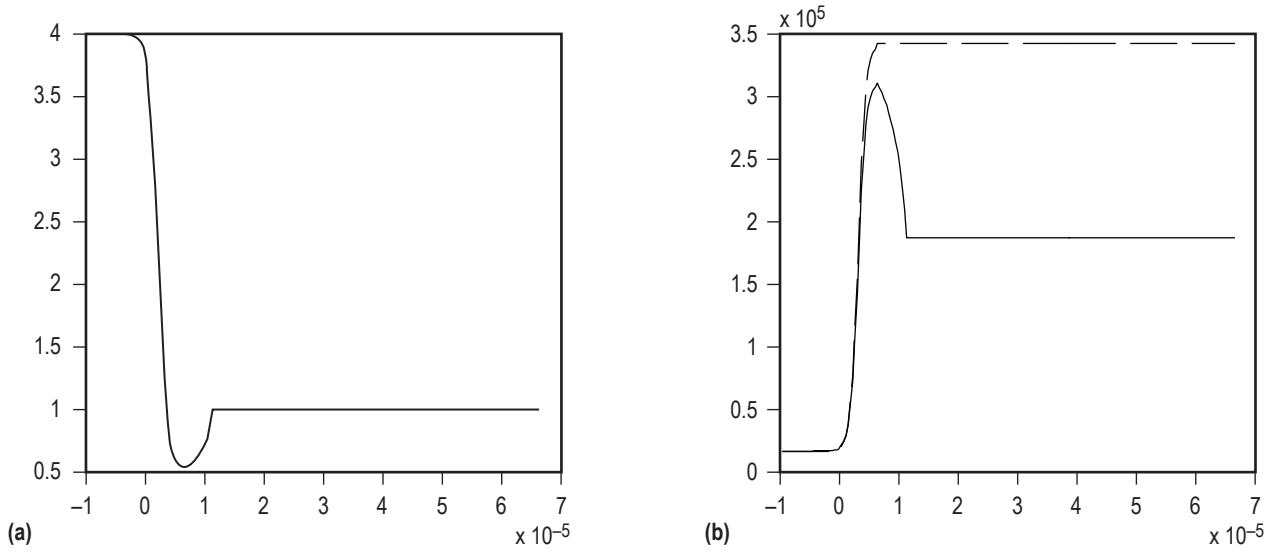

Figure 2. (a) Mach number and (b) pressure across a Mach 4 shock at 40,000 ft with a 1-eV source.

3.1.1 Solution of the Fluid Dynamics Equations Across a Shock Wave

The solution of the fluid dynamics equations across a shock wave is as follows:

(1) Given Ω^e and $\widehat{d^2u/dx^2}$, initialize equations (41) and (42) at x_{up} with the upstream flow variables, M_{up}, C_{up}, and solve (41) and (42) for $M(x)$ and $C(x)$ in the interval $[x_{\text{up}},\ x_{\text{us}}]$, where x_{up} is a point upstream of the region where the ionization interacts with the flow, and x_{us} is the point at the upstream side of the shock.

(2) Use the (classical) Rankine-Hugoniot equations to compute the flow variables at a point, $x_{\text{ds}} = x_{\text{us}} + \delta$, at the downstream side of an inviscid shock, given the fluid flow variables at x_{us}, where δ is a single step in the numerical process used to compute the flow variables.[16]

(3) Initialize equations (41) and (42) with M_{ds} and C_{ds} at x_{ds}, and solve (41) and (42) for $M(x)$ and $C(x)$ in the interval $[x_{\text{ds}},\ x_{\text{dn}}]$, where x_{dn} is a point downstream of the region where the ionization interacts with the fluid flow.

This process yields a complete solution of the fluid dynamics equations in the region around the shock where the ionization interacts with the flow, excepting the inviscid shock, which will be replaced by a viscous intrashock model in section 3.2.

3.2 Intrashock Model

Although an inviscid fluid dynamics model producing an ideal (zero-thickness) shock is used in classical shock structure analysis,[16,24] in this application a viscous intrashock model is required to properly model the electron energy losses in the shock. To this end, the inviscid shock used in section 3.1 is replaced with an analytic intrashock model derived from the Navier-Stokes equation.[16]

Following Landau and Lifshitz, in the one-dimensional case,[16] if the inviscid fluid dynamics model indicates the presence of a shock in the interval between x_{us} and x_{ds}, with pressure p_{us} at the upstream side of the shock and p_{ds} at the downstream side of the shock, one approximates the viscous effects in the shock by interpolating p^{inv} in the interval $[x_{us},\ x_{ds}]$ with a hyperbolic tangent,

$$p^{vis}(x) = \frac{1}{2}\left[(p_{ds} - p_{us})\tanh\left(\frac{2x - x_{us} - x_{ds}}{2\Delta}\right) + (p_{ds} + p_{us})\right] \ ;\ x_{us} < x < x_{ds}$$

$$p^{vis}(x) = p^{inv}(x) \ ;\ x < x_{us},\ x_{ds} < x \ , \tag{44}$$

and similarly for $\rho^{vis}(x)$ and $u^{vis}(x)$. Here, the shock width, Δ, is typically a few mean free paths for the upstream neutral gas.[16,24] Note, in the following, the superscripts "*inv*" and "*vis*" have normally been dropped, distinguishing between the inviscid and viscous models by context.

Even though Δ is termed the "shock width" in the literature,[16,24] it is, in actuality, the slope of the hyperbolic tangent at the center of the shock. Indeed, less than half (46 percent) of the pressure (density, velocity, etc.) jump across the shock takes place over a distance of Δ, as illustrated in figure 3, while a distance of 5Δ is required for 99 percent of the jump. As such, 5Δ is used when it is desired to model the distance required for "most" of the jump across the shock.

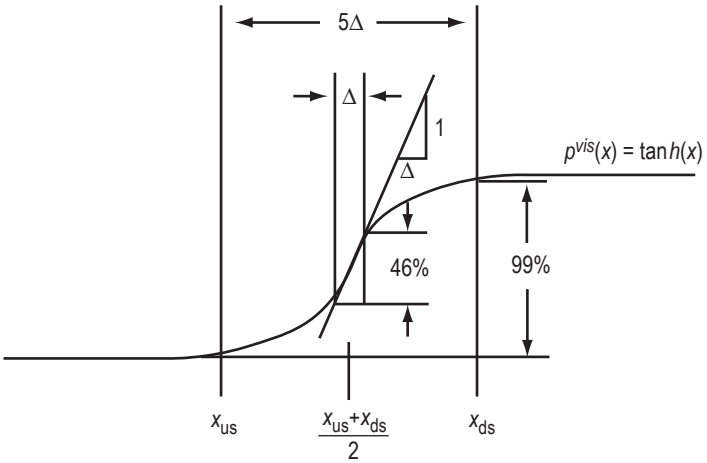

Figure 3. Effective shock width required to model 99 percent of the jump across the shock.

Although Shapiro provides an analytic formula for the shock width, Δ, it is quite complex.[24] Alternatively, Landau and Lifshitz provide an estimate of Δ, in the form (ref. 16)

$$\Delta \sim \frac{8a}{\rho^2 \left(p_{\mathrm{ds}} - p_{\mathrm{us}}\right)\left(\partial^2 \left(1/\rho\right)/\partial p^2\right)_s} \ , \tag{45}$$

together with estimates for $a \sim \lambda / C^2$ and $\left(\partial^2 \left(1/\rho\right)/\partial \mathrm{p}^2\right)_s \sim 1/\rho p$, where λ is the upstream mean free path for the neutral gas. Substituting these expressions into equation (23) and evaluating *p* at the center of the shock, $p = \left(p_{\mathrm{ds}} + p_{\mathrm{us}}\right)/2,$ yields

$$\frac{\Delta}{\lambda} \sim \frac{4}{\gamma} \frac{\left(p_{\mathrm{ds}} + p_{\mathrm{us}}\right)}{\left(p_{\mathrm{ds}} - p_{\mathrm{us}}\right)} \ , \tag{46}$$

which may be used to compute the shock width. Indeed, if one divides equation (46) by p_{us}, and substitutes the classical Rankine-Hugoniot pressure jump formula into the resultant expression,[16] equation (46) reduces to

$$\frac{\Delta}{\lambda} \sim \frac{4}{\gamma} \frac{\left(p_{\mathrm{ds}} + p_{\mathrm{us}}\right)}{\left(p_{\mathrm{ds}} - p_{\mathrm{us}}\right)} = \frac{4}{\gamma} \frac{\frac{p_{\mathrm{ds}}}{p_{\mathrm{us}}} + 1}{\frac{p_{\mathrm{ds}}}{p_{\mathrm{us}}} - 1} = \frac{4}{\gamma} \frac{\frac{2\gamma M_{\mathrm{us}}^2 - (\gamma - 1)}{(\gamma + 1)} + 1}{\frac{2\gamma M_{\mathrm{us}}^2 - (\gamma - 1)}{(\gamma + 1)} - 1} = \frac{4}{\gamma^2} \frac{\gamma M_{\mathrm{us}}^2 + 1}{M_{\mathrm{us}}^2 - 1} \ , \tag{47}$$

yielding an alternative expression for the shock width in terms of the Mach number of the flow at the upstream side of the shock.

The shock widths predicted by equation (47) range between 2 and 3 mean free paths for Mach numbers greater than 2 in a monotonic gas, increasing to infinity below Mach 2, and the shock width for a diatomic gas is ≈20 percent greater than the shock width for a diatomic gas. As such, the shock widths predicted by equation (47) are consistent with those predicted by Shapiro and Shapiro and Kline up to Mach 10,[24,25] while properly accounting for the difference between monotonic and diatomic gases.[24] Above Mach 10, however, equation (47) converges to $4/\gamma,$ while Shapiro's model diverges.

Unfortunately, equation (47) is not applicable in the presence of ionization, since M_{us} does not account for the effect of the ionization on the shock width. As such, in the presence of ionization, revert to equation (46) to compute the shock width directly from the pressure distribution, *p*. Indeed, with the upstream side of the shock at x_{us} and the downstream side of the shock at $x_{\mathrm{ds}} = x_{\mathrm{us}} + 5\Delta$ (using the "99 percent" approximation of fig. 3), $p_{\mathrm{us}} = p\left(x_{\mathrm{us}}\right)$ and $p_{\mathrm{ds}} = p\left(x_{\mathrm{us}} + 5\Delta\right),$ while equation (46) reduces to

$$\frac{\Delta}{\lambda} = \frac{4}{\gamma} \frac{\left(p\left(x_{\mathrm{us}} + 5\Delta\right) + p\left(x_{\mathrm{us}}\right)\right)}{\left(p\left(x_{\mathrm{us}} + 5\Delta\right) - p\left(x_{\mathrm{us}}\right)\right)} \ , \tag{46}$$

which can be solved for Δ, given $p(x)$. Indeed, since $p_{ds} > p_{us}$, the expression on the right-hand side of equation (48) is a bounded positive continuous function of Δ, and the expression on the left-hand side of equation (48) goes from 0 to ∞ as Δ goes from 0 to ∞. As such, the two expressions must cross for some $\Delta > 0$, guaranteeing that equation (48) has a positive real solution. Moreover, since the viscous and inviscid variables coincide at the upstream and downstream sides of the shock, one can use either p^{vis} or p^{inv} in equation (48). As such, to incorporate the viscous intrashock model into the solution of equations (41) and (42) add the following steps to the solution described in section 3.1.1:

(4) Solve equation (48) for Δ using p^{inv}.

(5) Interpolate the fluid flow variables between x_{us} and $x_{ds} = x_{us} + 5\Delta$ with hyperbolic tangents.

3.3 Computational Process

Although the electrofluid dynamics model of equations (11)–(20) is potentially applicable to a wide variety of electrofluid dynamics problems, the development of a complete computational electrofluid dynamics code to implement the model is well beyond the scope of the present investigation, where it suffices to solve the electrofluid dynamics equations for a one-dimensional flow a few tens of microns on either side of the shock. A flow chart for the shock structure analysis algorithm developed for this purpose appears in figure 4. In the flow chart, the subscripts "k" and "j" denote the inner and outer loop iteration indices, respectively. The fluid flow variables, p_j, ρ_j, and u_j and the electric field, E_j from the jth outer loop iteration are fed back to initialize the (j+1)th outer loop iteration while the electron density from the (j, k)th inner loop iteration is fed back to initialize the (j, k+1)th inner loop iteration. Finally, the computational process is initialized with the upstream fluid dynamics variables; p_{up}, ρ_{up}, and u_{up}; and "initial values" for the fluid dynamics variables, p_0, ρ_0, and u_0, and the electric field, E_0. Also note that the ohmic heating term is the only interface from the electrodynamics model to the fluid dynamics model, and the fluid flow variables connect the fluid dynamics model to the electrodynamics model.

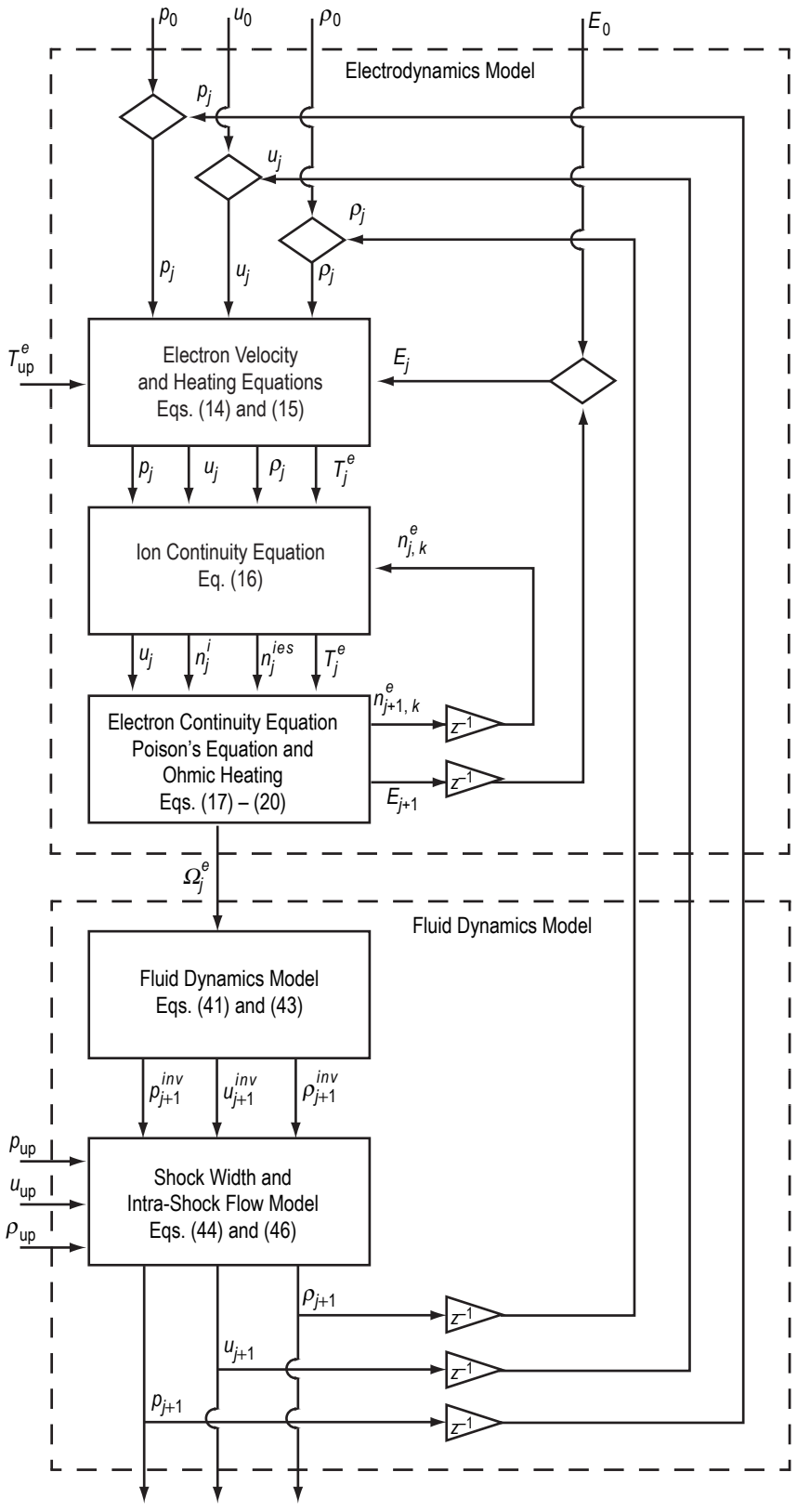

Figure 4. Shock structure analysis algorithm flow chart.

The shock structure analysis algorithm illustrated in figure 4 is composed of the following five processes:

(1) Electron velocity and heating equations.

(2) Ion continuity equation.

(3) Electron continuity equation and Poisson's equation.

(4) One-dimensional fluid dynamics problem with ohmic heating over an interval a few tens to hundreds of microns on either side of the shock wave.

(5) Analytic intrashock model into the solution of the one-dimensional fluid dynamics problem.

4. SHOCK STRUCTURE IN A WEAKLY IONIZED GAS

The purpose of this section is to summarize the results of a series of shock structure simulations using the electrofluid dynamics model developed in sections 2 and 3 together with the iterative algorithm summarized in section 3. Section 4.1 provides a detailed analysis of the structure of a Mach 4 flow through a normal shock wave in 40,000-ft air that has been weakly ionized with a 1-eV source—additional analyses appear in appendix A. In section 4.2, the concept of "shock intensity" as the geometric mean of the pressure and density jumps across the shock is formalized, allowing the summarization of the results of a shock structure simulation in a single plot, and comparison of the results of a large number of simulations parameterized by Mach number, altitude, and source temperature.

4.1 Shock Structure Analysis

The purpose of this section is to summarize the results of a shock structure analysis for a Mach 4 flow at an altitude of 40,000 ft with a 1-eV source, while providing some insight into the underlying physical phenomena. In the electrofluid dynamics model developed in section 2, the source maintains a minimum electron temperature (typically between 0.5 and 1.5 eV) across the region where the ionization interacts with the flow (between x_{up} and x_{dn} in the geometry defined in figure 1). Such a source will produce electron and ion fractions on the order of 10^{-7}–10^{-5}. Since the ions and electrons are created and annihilated simultaneously, however, the generator by itself will not produce an electric field and the associated ohmic heating required for the electrodynamics model to interact with the fluid dynamics model. Rather, the electric field is due to a jump in the ionization rate at the shock wave, with the additional electrons diffusing farther upstream than the ions, thereby producing a negative electric field across the shock wave and the associated ohmic heating.

In previous analyses the jump in ionization rate across the shock has been attributed to:

- A jump in the electron temperature across the shock driven by the differential term in the electron heating equation (eq. (15)):[13,14,26–28] In the inviscid case, where the loss terms in the electron heating equation are negligible in the shock, one can show that the electron temperature ratio across the shock is equal to the pressure ratio raised to the $2/3$ power, producing an orders-of-magnitude increase in the ionization rate at the shock. When one incorporates the true shock thickness into the model, however, the loss terms in the electron heating equation (primarily the transfer of electron energy to the neutrals via ohmic heating) damp out much of the electron temperature jump.

- The jump in ionization across the shock:[11,12] Since the ionization in this model is due to electron neutral collisions, the ionization rate is proportional to the product of the gas density and the electron density.[15,17] As such, when the gas density jumps across the shock the ionization rate increases, producing additional electrons that further increase the ionization rate (in a positive feedback mode damped by the loss of electrons due to transport and recombination), resulting in a jump in the ionization rate across the shock that exceeds the jump in neutral density across the shock.

Indeed, in our 40,000 ft Mach 4 example with a 1-eV source, the electron temperature jump across the shock is completely damped out by the ohmic heating losses as illustrated in figure 5 (a), while the ionization rate illustrated in figure 5 (b) tracks $n \times n^e$ (figs. 6 (a) and 8 (a)), indicating that it is due to the jump in gas density across the shock. In particular, the ionization rate continues to increase, tracking the increase in electron density, downstream of the point where the gas density saturates.

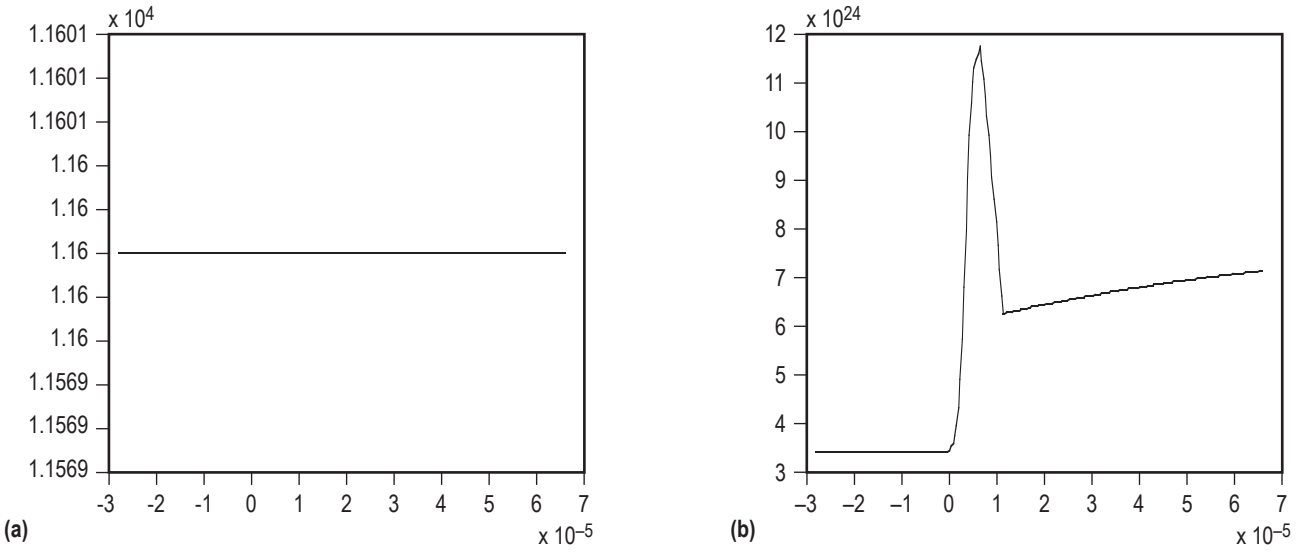

Figure 5. (a) Electron temperature and (b) ionization rate across a Mach 4 shock at 40,000 ft with a 1-eV source

Although the electron diffusion constant is typically several orders of magnitude greater than the ion diffusion constant,[17] when one incorporates the effect of the electric field, with the attractive forces between the ions and electrons increasing the ion diffusion length; i.e., ambipolar diffusion,[17] and the electron drift velocity decreasing the electron diffusion length, the electron diffusion length is typically only a few tens of microns greater than the ion diffusion length, yielding an electron density which is only slightly more diffuse than the ion density as indicated in figure 6 (a). This is, however, sufficient to generate a negative electric field on the order of 10^5–10^7 V/m at the shock, as indicated in figure 6 (b). Finally, given the electron density and the electric field one can evaluate the electron velocity and the ohmic heating term which serves as the interface between the electrodynamics model and the fluid dynamics model, as indicated in figures 7 (a) and 7 (b). Here, the sharp drop in electron velocity across the shock is due to the increase in the electron/neutral collision frequency, which roughly tracks the increase in pressure,[17] across the shock.

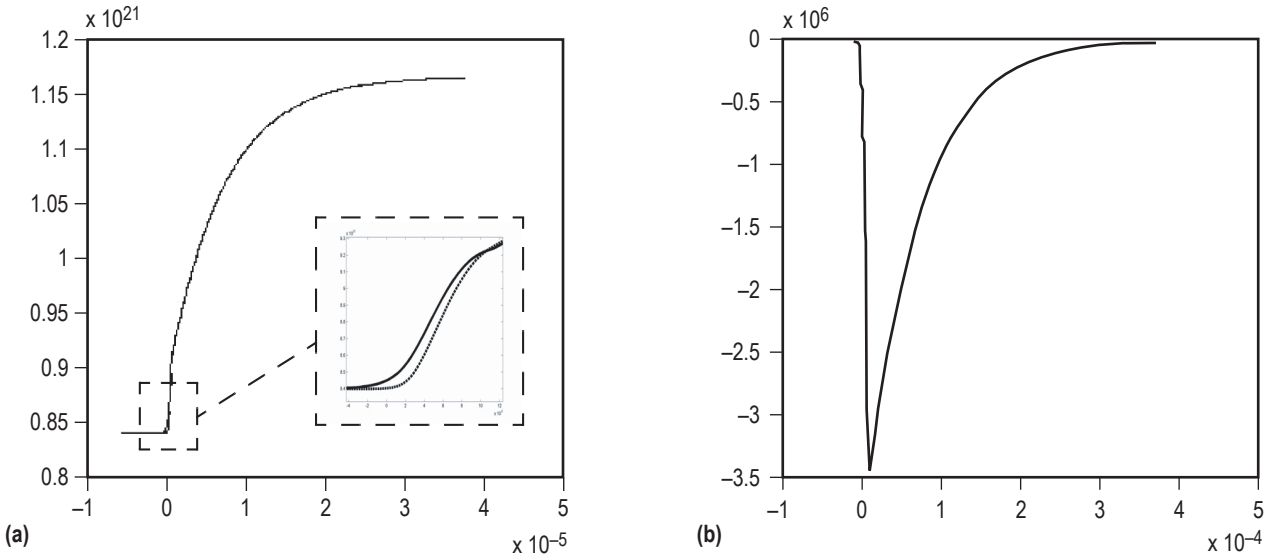

Figure 6. (a) Electron and ion densities and (b) electric field across a Mach 4 shock at 40,000 ft with a 1-eV source.

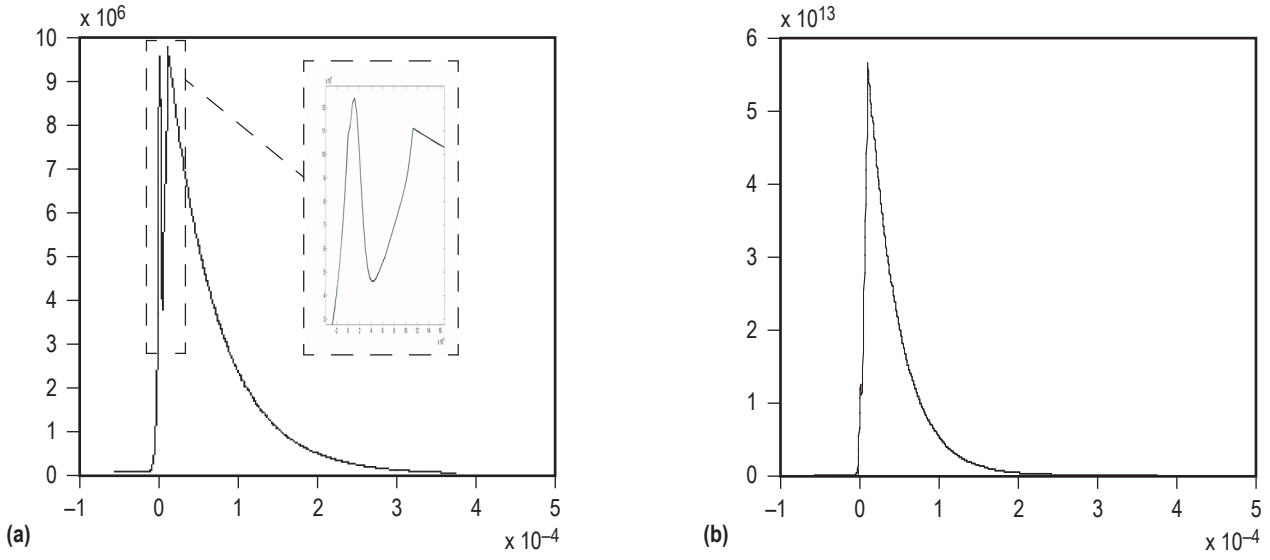

Figure 7. (a) Electron velocity and (b) ohmic heating across a Mach 4 shock at 40,000 ft with a 1-eV source.

The primary fluid dynamics variables for our Mach 4, 40,000 ft flow with a 1-eV source are illustrated in figures 2 and 8.

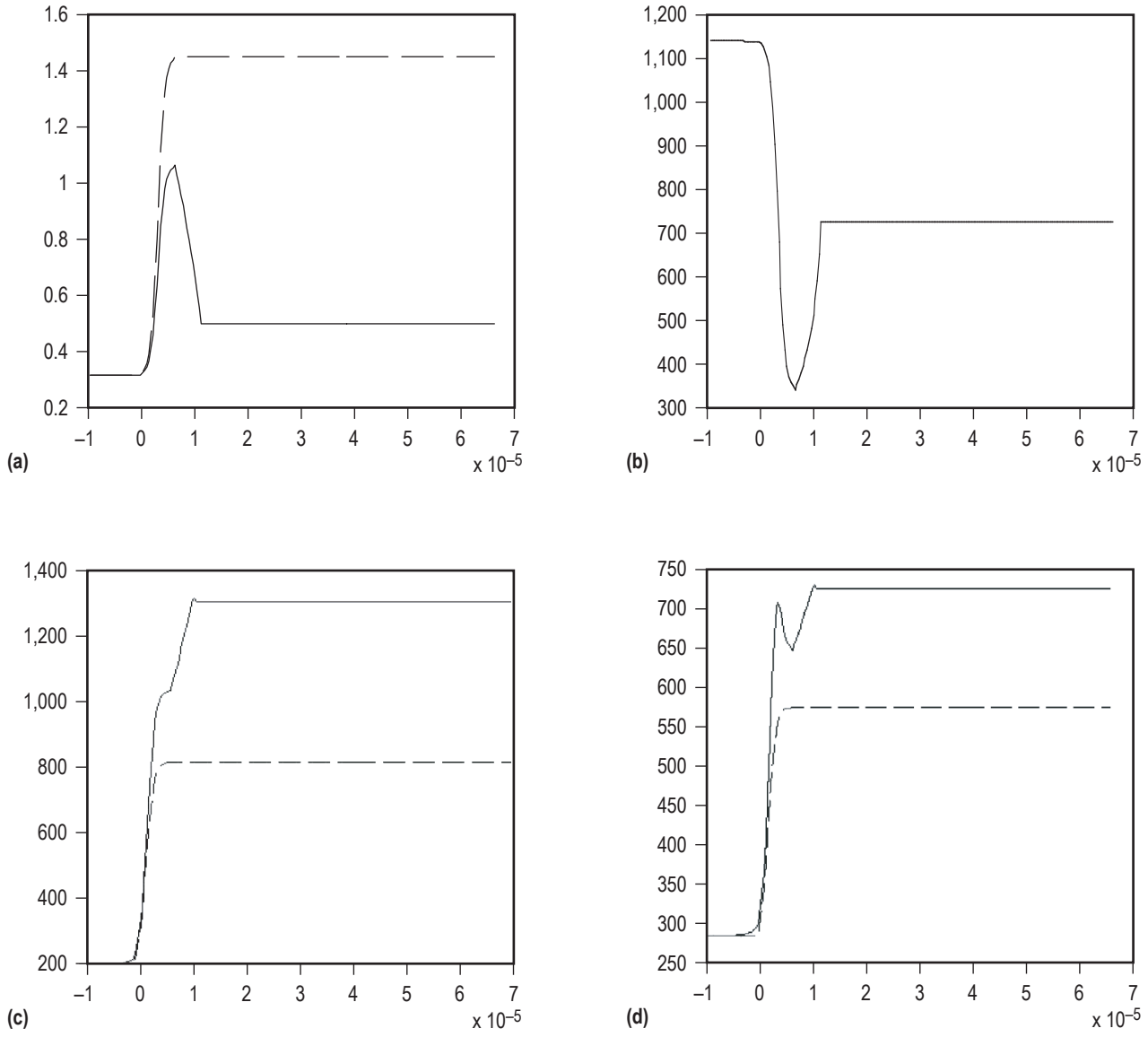

Figure 8. (a) Density, (b) velocity, (c) temperature, and (d) speed of sound across a Mach 4 shock at 40,000 ft with a 1-eV source.

Unlike the classical case where the upstream flow is constant, the diffusion of electrons (and ions) across the shock (fig. 6 (a)) extends the ohmic heating term upstream of the shock (fig. 7 (b)), where it effects the upstream flow. In particular, the pressure and density increase while the Mach number and flow velocity decrease upstream of the shock. Fortunately, the decrease in pressure ratio across the shock, due to the decreased upstream Mach number, more than compensates for the pressure increase at the upstream side of the shock and yields a net decrease in the pressure at the downstream side of the shock. A similar analysis is applicable to the density at low Mach numbers. At high Mach numbers, however, where the density ratio approaches its limiting value, the drop in density ratio may be insufficient to compensate for the increase in density at the upstream side of the shock, yielding a net increase density at the downstream side of the shock.

In the shock, the ionization further reduces the pressure and density, while increasing the Mach number and velocity. This effect was analyzed in detail using the modified Rankine-Hugoniot equations.[14,21,22] Moreover, the ionization in the shock increases the shock width (eq. (46)).

The ionization continues to decrease the pressure and density, and increase the Mach number and velocity downstream of the shock. This effect may dissipate at some subsonic Mach number (fig. 10 (c)), or as in the present example, may drive the Mach number back to 1, where it is "trapped" by the singularity in the "fluid state" equations (eqs. (41) and (42)) since a subsonic flow cannot jump across Mach 1. Indeed, given the nature of this singularity, as the Mach number approaches 1, the flow is accelerated at an increasing rate towards Mach 1. As such, the downstream Mach number is driven back to Mach 1 in many of our simulations, while the pressure and density are driven to corresponding minimum values (sec. 5). This results in the "overshoot" effect observed in figures 2 and 8, where the fluid flow variables jump across the shock to an intermediate value (between their "no ionization" value and their final value), and then drop to their final value downstream of the shock.

The temperature and speed of sound across the shock are plotted in figures 8 (c) and 8 (d), respectively. Although the ionization reduces both the downstream pressure and density, it reduces the downstream density more than the downstream pressure, thereby causing the downstream temperature to increase with ionization and similarly for the downstream speed of sound. Finally, the "kink" in the speed of sound curve can be explained by examining the $\left(1-\gamma M^2\right)/\left(1-M^2\right)$ term in equation (41), which changes sign at both $M=1$ and $M=1/\sqrt{\gamma}$. As such, if the Mach number drops below $1/\sqrt{\gamma}$ downstream of the shock before returning to Mach 1 (as in this example—see figure 2 (a)), dC/dx changes sign four times. Specifically, C increases upstream of the shock where $M>1$, decreases immediately downstream of the shock where $1/\sqrt{\gamma}<M<1$, increases while $M<1/\sqrt{\gamma}$, and decreases again as M approaches Mach 1 downstream—$1/\sqrt{\gamma}<M<1$.

For a point of comparison, selected plots from two additional shock structure analyses are presented in figures 9 and 10. The first example in figure 9 is the same as above with the source increased from 1 to 1.4 eV, chosen to illustrate the sensitivity of the shock structure to the source temperature. As above, the electron temperature spike is completely damped, but the ionization rate increases rapidly with the increase in gas density across the shock as illustrated in figure 9 (a). This, in turn, causes the electron density, the electric field, and the electron velocity to increase, combining to increase the ohmic heating, shown in figure 9 (b), by almost two orders of magnitude. As such, the ionization upstream of the shock is sufficient to reduce the Mach number of the flow at the upstream side of the shock to Mach 2, while increasing the pressure at the upstream side of the shock to 6×10^4 Pa, illustrated in figures 9 (c) and 9 (d), respectively. This, in turn, increases the Mach number and decreases the pressure in the shock. Finally, the ionization in the shock is sufficient to drive the downstream Mach number back to 1 and the downstream pressure to its maximum value of 1.8×10^5 Pa within the shock, thereby eliminating the overshoot observed in the previous example.

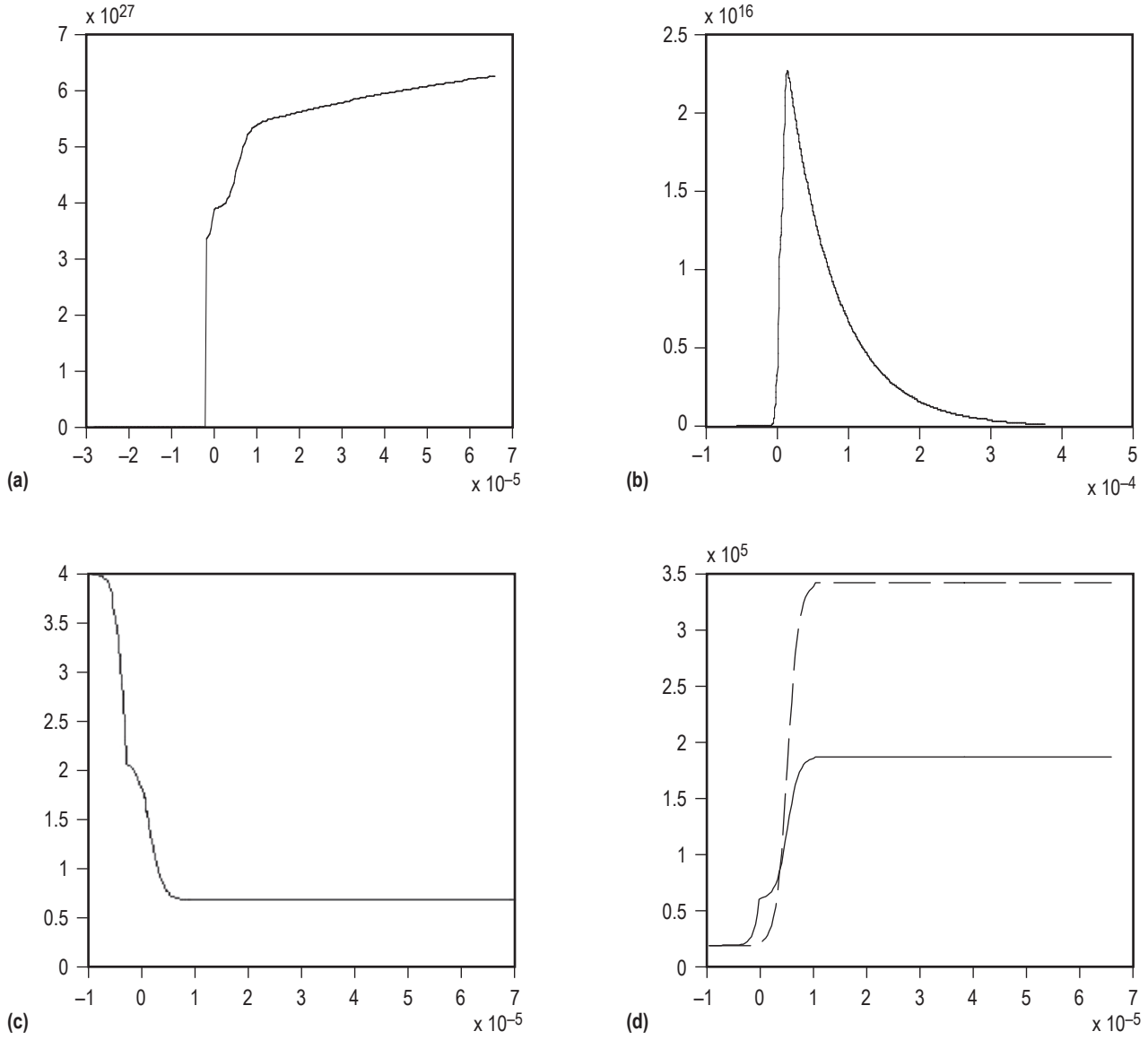

Figure 9. Shock structure analysis for a Mach 4 shock at 40,000 ft with a 1.4-eV source: (a) Ionization rate, (b) ohmic heating, (c) Mach number, and (d) pressure.

The second example shown in figure 10 is a Mach 12 flow at an altitude of 10,000 ft with a 1-eV source, chosen to illustrate some of the effects which occur at high Mach numbers. In this example, the downstream pressure jump due to the high Mach number and the associated increase in the electron/neutral collision frequency,[17] reduces the downstream electron velocity by an order of magnitude, as illustrated in figure 10 (a). This, in turn, reduces the downstream ohmic heating, shown in figure 10 (b), to a point where it is insufficient to drive the pressure to its minimum value, as indicated in figure 10 (c), and similarly for the density (not shown). Moreover, in this case, the electron temperature losses due to ohmic heating are insufficient to fully damp out the jump in electron temperature at the shock, as indicated in figure 10 (d).

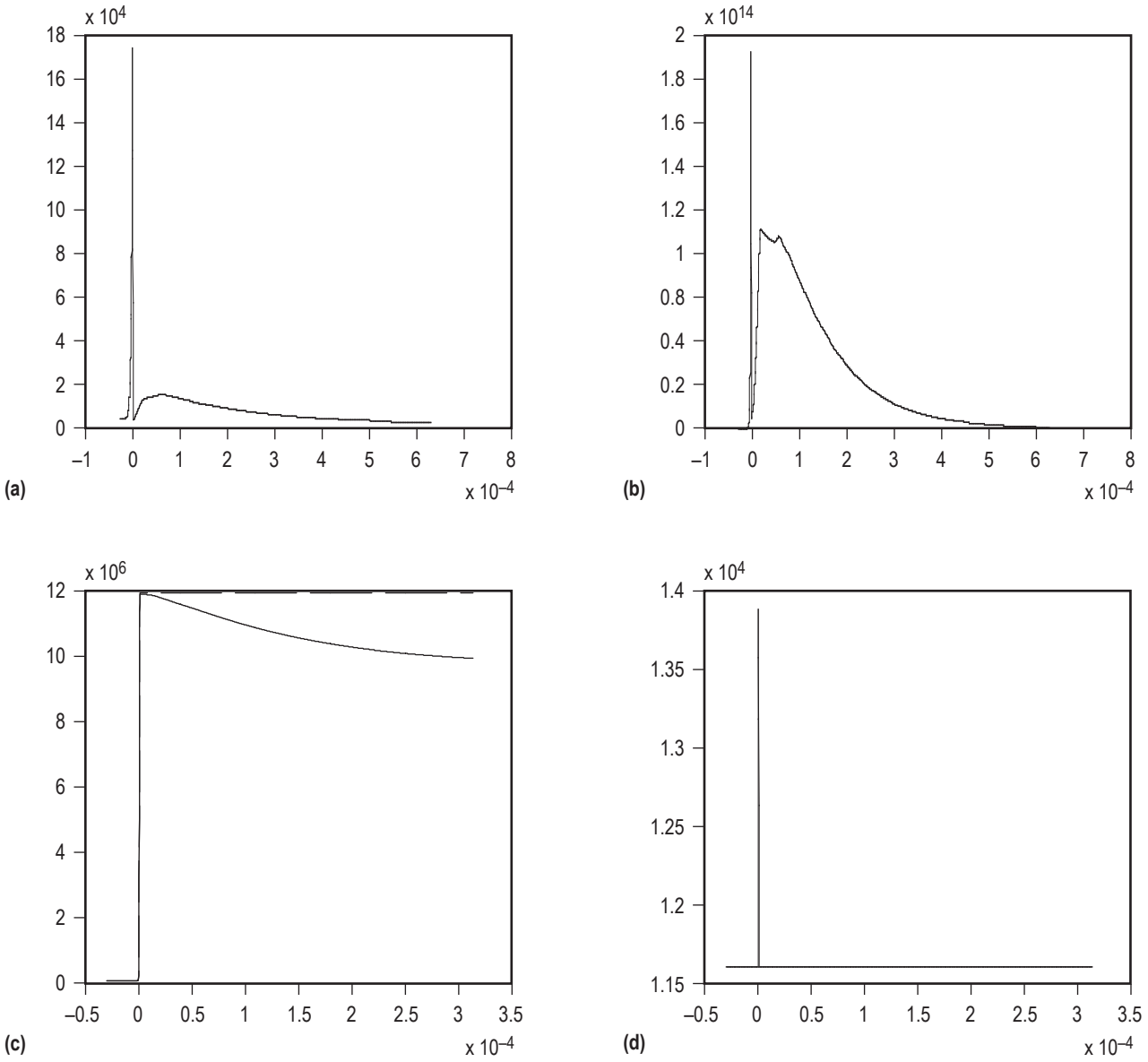

Figure 10. Shock structure analysis for a Mach 12 shock at 10,000 ft with a 1-eV Source: (a) Electron velocity, (b) ohmic heating, (c) pressure, and (d) electron temperature.

4.2 Shock Intensity

The term "shock intensity" is commonly used as a qualitative measure of the pressure and/or density jump across a shock wave. The goal of this section is to formalize this concept, with the goal of using it to quantify the effect of ionization on the shock structure without resorting to the full set of plots used in section 4.1. To this end, the intensity of a flow at x is defined as the geometric mean of the pressure and density at $x, \iota(x) = \sqrt{p(x)\rho(x)}$. Since p and ρ increase and decrease together, while $u = \varphi/\rho, \iota(x)$

simultaneously characterizes the combined effect of the shock on p, ρ, and u. Moreover, with the aid of some algebra, it follows that

$$\iota(x) = \sqrt{p(x)\rho(x)} = \left(\frac{\varphi}{\sqrt{\gamma}}\right)\frac{1}{M(x)} \quad . \tag{49}$$

As such, $\iota(x)$ defines a single parameter that simultaneously characterizes the effect of both the ionization and the shock on the primary flow variables.

Finally, define the intensity of a shock wave as the ratio of the downstream flow intensity to the upstream flow intensity:

$$\iota_{\text{shock}} = \frac{\sqrt{p_{dn}\rho_{dn}}}{\sqrt{p_{up}\rho_{up}}} = \frac{\left(\frac{\varphi}{\sqrt{\gamma}}\right)\frac{1}{M_{dn}}}{\left(\frac{\varphi}{\sqrt{\gamma}}\right)\frac{1}{M_{up}}} = \frac{M_{up}}{M_{dn}} \quad . \tag{50}$$

Since the downstream flow is subsonic, the inequality, $M_{\text{dn}} \le 1$, lower bounds ι_{shock} downstream by

$$M_{\text{up}} \le \iota_{\text{shock}} \quad , \tag{51}$$

implying that there is a limit to the extent to which ionization can reduce the intensity of a shock wave (by 62 percent at high Mach numbers in air); i.e., if the upstream Mach number of the flow is 3, then the "intensity ratio" across the shock cannot be reduced below 3 by ionization. Although this appears to contradict several experiments where ionization appeared to fully disperse a shock wave,[7,14,29,30] this is believed to be an artifact of the Schlieren and shadowgraph diagnostics used in these experiments (sec. 7).

The normalized flow intensity, $\iota(x)/\sqrt{p_{\text{up}}\rho_{\text{up}}}$ $\left(\text{which equals the shock intensity at } x = x_{\text{dn}}\right)$, for the 40,000-ft, Mach 4, 1-eV example of section 4.1 is plotted in figure 11, together with the downstream lower bound implied by equation (51) and the normalized flow intensity without ionization.

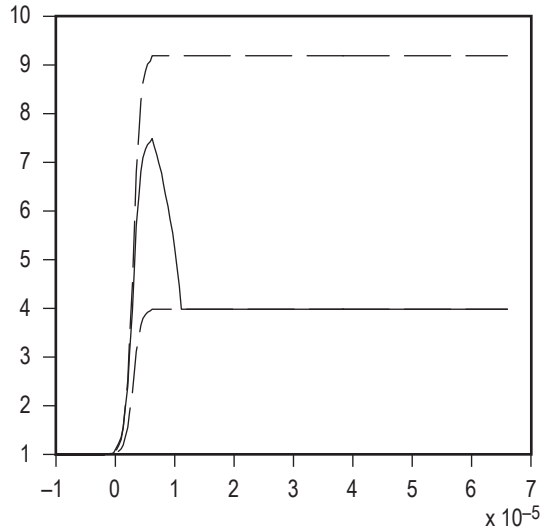

Figure 11. Normalized flow intensity for a Mach 4 flow at 40,000 ft with its downstream lower bound (lower dashed line) and the "no ionization" case (upper dashed line).

The normalized flow intensity for a series of simulations at a fixed altitude (40,000 ft), parameterized by the Mach number and the source temperature appear in figure 12, while the normalized flow intensity for a series of simulations at a fixed source temperature (1 eV), parameterized by the Mach number and the altitude appear in figure 13. Although the downstream flow intensity is M_{up}; i.e., the minimum possible value, in most of the simulations in figures 12 and 13, one can quantify the effect of ionization in these simulations by the distance downstream of the shock required for the flow intensity to reach M_{up}. The trends observed in these plots and the underlying physical processes are summarized below.

4.2.1 Source Temperature

Since the ionization rate can be expressed in the form $r\left(T^e\right)n^e n$, where $r\left(T^e\right)$ is an increasing function of electron temperature,[15,17] the ionization rate increases when T^e is increased at constant Mach number and altitude. This, causes n^e to increase, further increasing the ionization rate and the electron density in a positive feedback mode damped by the loss of electrons due to transport and recombination. The resultant increase in electron density causes an increase in the electric field, which in turn, increases the electron drift velocity. As such, all three variables that define the ohmic heating process increase, which causes Ω^e to increase cubically and the shock intensity to decrease via the "fluid state" equations (41) and (42). As such, the shock intensity decreases with increasing electron temperature. This is consistent with the simulations presented in figure 12, while the cubic increase in Ω^e accounts for the high sensitivity of the shock intensity to small increases in electron temperature.

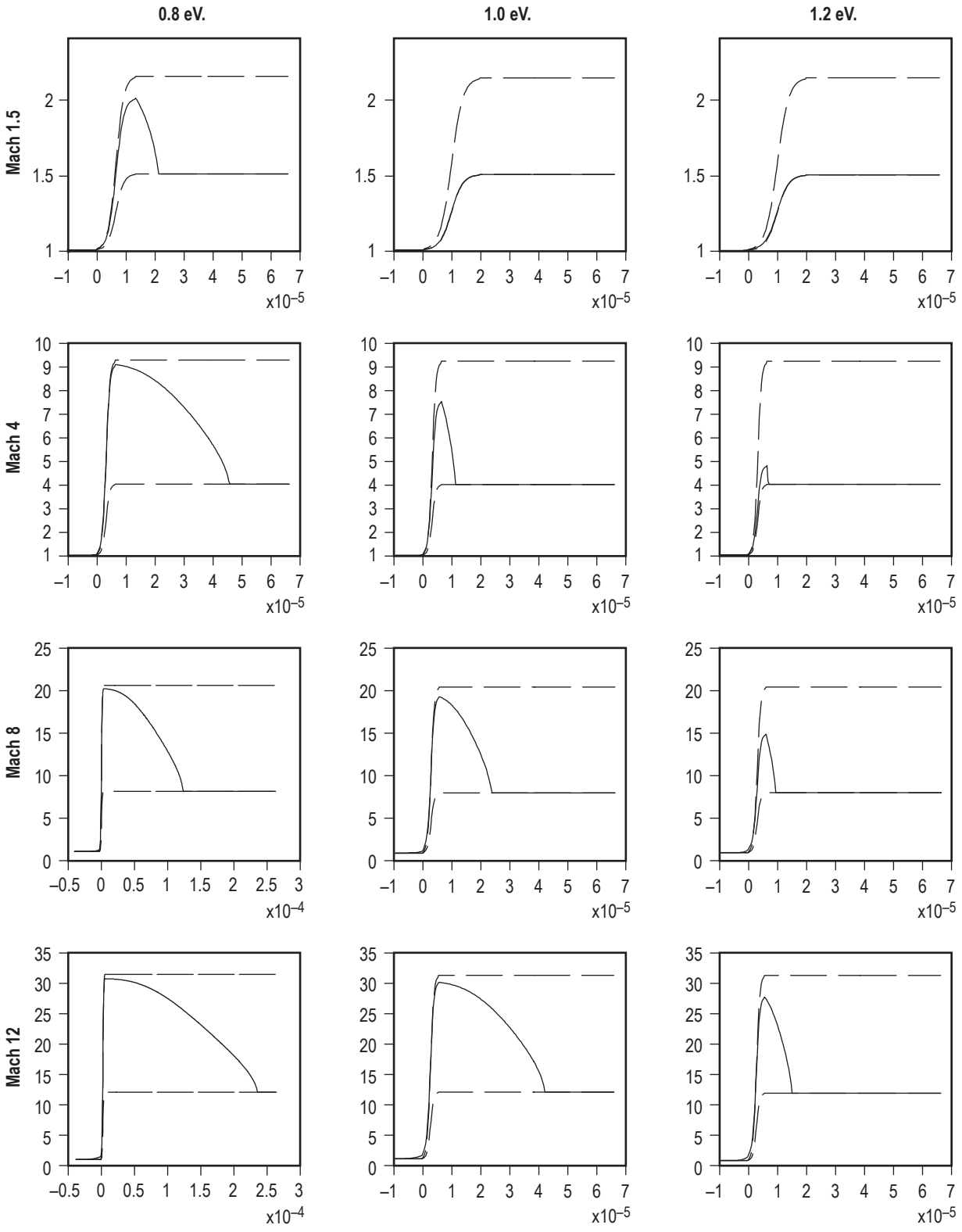

Figure 12. Normalized flow intensity versus Mach number and source temperature at 40,000 ft. (Note the change in scale on the Mach 8 and 12, 0.8-eV plots.)

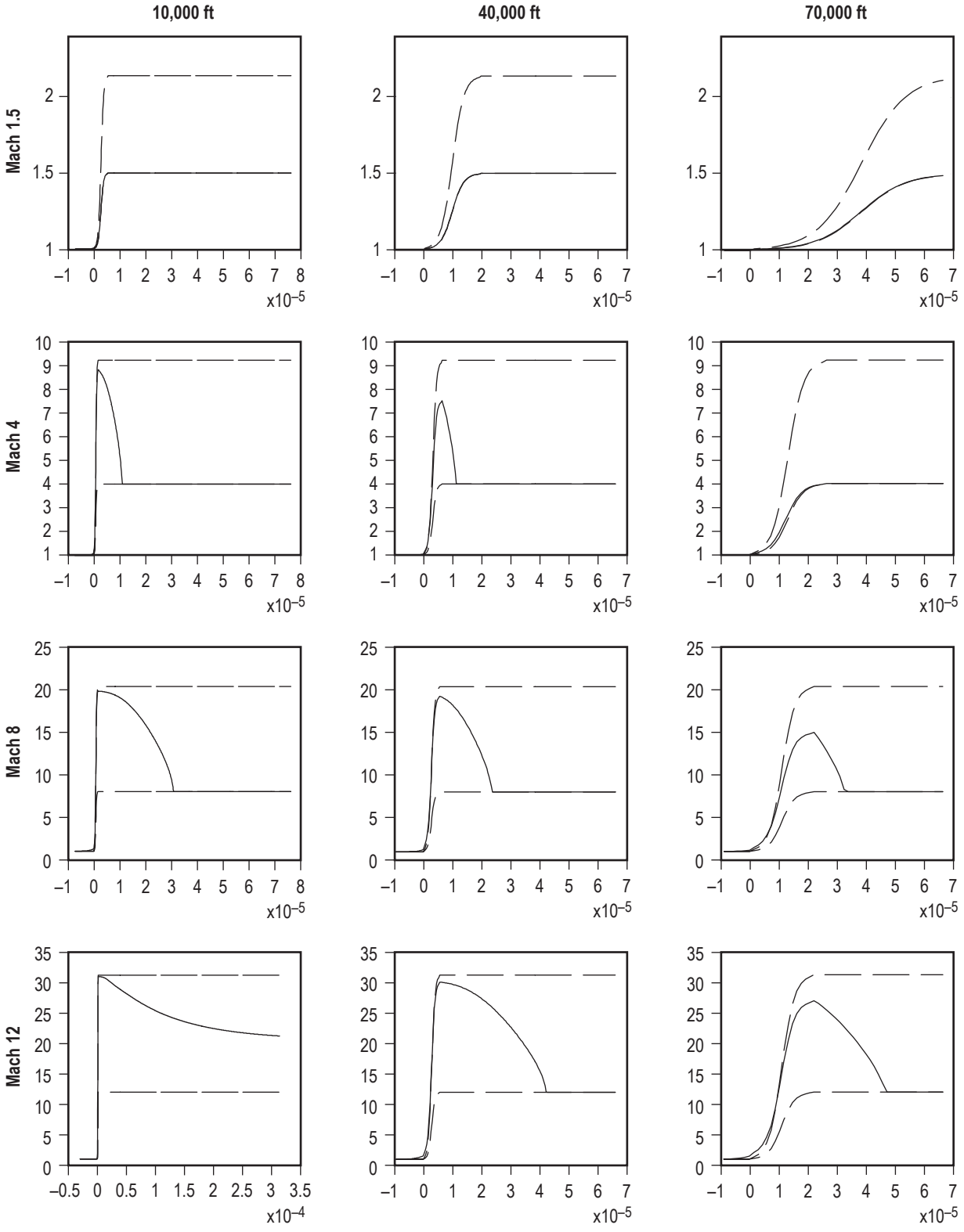

Figure 13. Normalized flow intensity versus Mach number and altitude with a 1-eV source. (Note the change in scale on the Mach 12, 10,000-ft plot.)

4.2.2 Mach Number

When one increases the Mach number at constant electron temperature and altitude, the downstream pressure and density increase. The increase in downstream density causes the ionization rate, $r(T^e)n^e n$, to increase, producing additional electrons that further increase the ionization rate and electron density as indicated above. On the other hand, the increase in downstream pressure increases the electron/neutral collision frequency, which reduces the electron drift velocity and the ohmic heating term. Finally, the increase in upstream velocity required to increase the Mach number at constant altitude, increases the mass flow, φ, which scales down the ohmic heating term, Ω^e, in the "fluid state" equations (eqs. (41) and (42)), reducing the effect of the ionization on the shock wave.

Although the downstream density can theoretically increase by a factor of 6 (in air), the ionization reduces the increase in downstream density Indeed for the 40,000-ft 1-eV simulations of figure 12, the density ratio across the shock only increases from 1.28 at Mach 1.5 to 1.81 at Mach 12. As such, the effect of the increased downstream density can be neglected compared to the effect of the increased downstream pressure and mass flow, which increase from 1.76 to 85 and 136 to 1,085, respectively. As such, the increased downstream pressure and mass flow dominate the increase in downstream density, causing the shock intensity to decrease with increasing Mach number, which is consistent with the simulations presented in figures 12 and 13.

4.2.3 Altitude

When one increases the altitude at constant electron temperature and Mach number, the gas density and pressure decrease, while the mass flow decreases with the decreasing density. Replicating the above analyses, the decreased density decreases Ω^e, while the decreased pressure decreases the electron/neutral collision frequency, increasing the electron drift velocity and Ω^e. and the decreased mass flow scales up the ohmic heating term, Ω^e, in the "fluid state" equations (eqs. (41) and (42)). Given these contradictory effects, one cannot predict the effect of an altitude change on the shock intensity, as indicated by the simulations in figure 13.

4.2.4 Summary Conclusion

Finally, note that the decreased effect of ionization at high Mach numbers (and possibly altitudes) does not preclude its application since one can readily compensate for these effects with a small increase in the electron temperature given the high sensitivity of ohmic heating process to changes in T^e.

Although the continuity of the electrofluid dynamics model with respect to the underlying parameters is manifested by the distance downstream of the shock required for the flow intensity to reach its minimum value in the simulations of figures 12 and 13, the effect of the ionization on the downstream flow $\left(x \geq x_{\text{dn}}\right)$ is "almost" binary.

Indeed, the effect of ionization is either negligible with the downstream intensity roughly equal to the "no ionization" case, or the ionization level is sufficient to drive the downstream flow intensity to M_{up} with a small transition region between the two extremes (indicated by the 10,000 ft, Mach 12, 1-eV

simulation in fig. 13). This is due to the singularity in equations (41) and (42), which literally draws the flow intensity to M_{up}, if the Mach number begins to approach to 1. Indeed, our simulations indicate that a change in electron temperature of 0.01 eV is usually sufficient to cause the downstream flow intensity to jump from one extreme to the other, allowing us to treat the downstream flow as "effectively binary." In the following we refer to the two extreme cases as "with ionization" and "without ionization," respectively, ignoring the transitory case.

Indeed, this effect suggests the possibility of analyzing the impact of ionization on the underlying missile or aircraft, without recourse to a full shock structure analysis, by reducing the analysis to the two cases, "with ionization" and "without ionization" (sec. 5). Also note that if ionization is used to reduce the flow intensity for a normal or detached shock wave, the underlying missile or aircraft must be designed to operate in the transonic flow behind the shock wave.

5. TWO-DIMENSIONAL AERODYNAMICS

The purpose of this section is to analyze the air flow through and behind a shock wave propagating through a weakly ionized gas. Given the bifurcation of the shock structure indicated in section 4, the two cases are analyzed separately, using a classical analysis "without ionization," and a modified analysis "with ionization" developed in this section. Modified pressure and density ratio formulae with ionization are developed in section 5.1 and used to formulate modified oblique shock curves in section 5.2. The modified oblique shock curves are used to determine if the shock is attached or detached and to compute the shock angle when it is attached, "with ionization." Analysis of the flow behind the shock for both the attached and detached cases is performed in section 5.3.

5.1 Modified Pressure and Density Ratios

The purpose of this section is to develop an analytical model for the pressure and density ratios across the shock with ionization. Begin by defining "pressure and density effective Mach numbers" to quantify the effect of ionization by matching the pressure and density ratios with ionization to the pressure and density ratios without ionization at a lower Mach number. Recall that the pressure and density ratios without ionization are given by the normal shock relations:[16,31]

$$\frac{p_{\mathrm{dn}}}{p_{\mathrm{up}}} = \frac{2\gamma M_{\mathrm{up}}^2 - (\gamma - 1)}{(\gamma + 1)} \quad \text{and} \quad \frac{\rho_{\mathrm{dn}}}{\rho_{\mathrm{up}}} = \frac{(\gamma + 1) M_{\mathrm{up}}^2}{(\gamma + 1) M_{\mathrm{up}}^2 + 2} \ . \tag{52}$$

As such, one may define "pressure and density effective Mach numbers" by replacing the downstream pressure and density, p_{dn} and ρ_{dn}, in equation (52) with the downstream pressure and density, $\overline{p}_{\mathrm{dn}}$ and $\overline{\rho}_{\mathrm{dn}}$, with ionization, and the actual upstream Mach number, M_{up}, with pressure and density effective Mach numbers, $\hat{M}_{\mathrm{up}}$ and $\tilde{M}_{\mathrm{up}}$, satisfying

$$\frac{\overline{p}_{\mathrm{dn}}}{\mathrm{p}_{\mathrm{up}}} = \frac{2\gamma \hat{M}_{\mathrm{up}}^2 - (\gamma - 1)}{(\gamma + 1)} \quad \text{and} \quad \frac{\overline{\rho}_{\mathrm{dn}}}{\rho_{\mathrm{up}}} = \frac{(\gamma + 1) \tilde{M}_{\mathrm{up}}^2}{(\gamma - 1) \tilde{M}_{\mathrm{up}}^2 + 2} \ , \tag{53}$$

Here an "upper bar" is used to distinguish the parameters with and without ionization. Since $\overline{p}_{\mathrm{dn}} < p_{\mathrm{dn}}$ and $\overline{\rho}_{\mathrm{dn}} < \rho_{\mathrm{dn}}$, while the expressions in equation (53) are monotonically increasing, $1 \le \hat{M}_{\mathrm{up}} \le M_{\mathrm{up}}$ and $1 \le \tilde{M}_{\mathrm{up}} \le M_{\mathrm{up}}$. Unfortunately, $\hat{M}_{\mathrm{up}}$ and $\tilde{M}_{\mathrm{up}}$ do not, in general, coincide (except when there is no ionization or $M_{\mathrm{up}} = 1$). As such, following the model used to define shock intensity, define the effective Mach number of a flow with ionization to be the geometric mean of $\hat{M}_{\mathrm{up}}$ and $\tilde{M}_{\mathrm{up}}$:

$$\overline{M}_{\mathrm{up}} \equiv \sqrt{\hat{M}_{\mathrm{up}} \tilde{M}_{\mathrm{up}}} \ . \tag{54}$$

Clearly, when there is no ionization, $\bar{M}_{\text{up}} = \sqrt{M_{\text{up}} M_{\text{up}}} = M_{\text{up}}$, while based on simulations using the structure analysis algorithm with ionization,

$$\bar{M}_{\text{up}} = \sqrt{\hat{M}_{\text{up}} \tilde{M}_{\text{up}}} = \sqrt{M_{\text{up}}} \quad . \tag{55}$$

Although we are not aware of any physical justification for equation (55), numerous simulations were performed that ranged from Mach 1.5 to Mach 12, with electron temperatures between 0.6 and 1.4 eV, at altitudes between 10,000 and 70,000 ft in which equation (55) is satisfied with an average of 4 percent error and a standard deviation of 0.5 percent. As such, equation (55) is used as an empirical model in the remainder of the analysis. See appendix B for an approximate but fully analytic derivation of the same result.

Given the bifurcation of the downstream flow indicated in section 4.2, the above equations completely define the effective Mach number (except for the transitory case). In particular, $\bar{M}_{\text{up}} = \sqrt{M_{\text{up}}}$ with ionization and $\bar{M}_{\text{up}} = M_{\text{up}}$ without ionization.

By combining equation (55) with equations (50) and (53), one may solve for $\hat{M}_{\text{up}}$ and $\tilde{M}_{\text{up}}$ in terms of M_{up}, with ionization. Indeed, in this case,

$$\begin{aligned} M_{\text{up}}^2 = \iota_{\text{shock}}^2 &= \frac{\bar{p}_{\text{dn}} \bar{\rho}_{\text{dn}}}{p_{\text{up}} \rho_{\text{up}}} \\ &= \left[\frac{2\gamma \hat{M}_{\text{up}}^2 - (\gamma - 1)}{(\gamma + 1)} \right] \left[\frac{(\gamma + 1) \tilde{M}_{\text{up}}^2}{(\gamma - 1) \tilde{M}_{\text{up}}^2 + 2} \right] = \frac{\tilde{M}_{\text{up}}^2 \left[2\gamma \hat{M}_{\text{up}}^2 - (\gamma - 1) \right]}{(\gamma - 1) \tilde{M}_{\text{up}}^2 + 2} \quad . \end{aligned} \tag{56}$$

Now, upon substituting equation (55) (in the equivalent form $\hat{M}_{\text{up}}^2 = M_{\text{up}}^2 \big/ \tilde{M}_{\text{up}}^2$) into equation (56), it reduces to

$$M_{\text{up}}^2 = \frac{\tilde{M}_{\text{up}}^2 \left[2\gamma \left(M_{\text{up}}^2 \big/ \tilde{M}_{\text{up}}^2 \right) - (\gamma - 1) \right]}{(\gamma - 1) \tilde{M}_{\text{up}}^2 + 2} = \frac{\left[2\gamma \tilde{M}_{\text{up}}^2 - (\gamma - 1) \tilde{M}_{\text{up}}^2 \right]}{(\gamma - 1) \tilde{M}_{\text{up}}^2 + 2} \quad , \tag{57}$$

which can be solved for $\tilde{M}_{\text{up}}^2$ and $\hat{M}_{\text{up}}^2$, in terms of M_{up}^2, yielding the expressions

$$\tilde{M}_{\text{up}}^2 = \frac{2 M_{\text{up}}^2}{1 + M_{\text{up}}^2} \quad , \tag{58}$$

and

$$\hat{M}_{up}^2 = \frac{M_{up}^2}{\tilde{M}_{up}^2} = \frac{M_{up}^2}{\left[\frac{2M_{up}^2}{1+M_{up}^2}\right]} = \frac{1+M_{up}^2}{2} \quad . \tag{59}$$

In combination with the equality $\tilde{M}_{up}^2 = \hat{M}_{up}^2 = M_{up}^2$ without ionization, equations (58) and (59) fully characterize the effective Mach numbers (except for the transitory case).

Finally, upon substituting equations (58) and (59) into equation (53), one may express the pressure and density ratios across the shock with ionization directly in terms of the actual upstream Mach number via

$$\frac{\bar{p}_{dn}}{p_{up}} = \frac{\gamma M_{up}^2 + 1}{(\gamma+1)} \quad \text{and} \quad \frac{\bar{\rho}_{dn}}{\rho_{up}} = \frac{(\gamma+1)M_{up}^2}{\gamma M_{up}^2 + 1} \quad . \tag{60}$$

By comparing these expressions with the classical normal shock relations of equation (52), one may verify that the pressure and density ratios across a normal shock wave are always reduced with ionization. Comparing the corresponding temperature ratio

$$\frac{\bar{T}_{dn}}{T_{up}} = \frac{\frac{\bar{p}_{dn}}{p_{up}}}{\frac{\bar{\rho}_{dn}}{\rho_{up}}} = \frac{\frac{\gamma M_{up}^2 + 1}{(\gamma+1)}}{\frac{(\gamma+1)M_{up}^2}{\gamma M_{up}^2 + 1}} = \left(\frac{\gamma M_{up}^2 + 1}{(\gamma+1)M}\right)^2 \tag{61}$$

with the classical temperature ratio;[16] however, one concludes that the downstream temperature ratio across a normal shock wave is increased with ionization, which is consistent with the simulations.

Finally, one can compare the pressure and density ratios with ionization computed numerically using the above described shock structure analysis simulations with the pressure and density ratios predicted by equation (60). Indeed, in a total of 43 simulations ranging from Mach 1.5 to Mach 12, with electron temperatures between 0.6 and 1.4 eV, at altitudes between 10,000 and 70,000 ft, the normal shock relations of equation (60) match the simulated data with an accuracy of 5 percent and 3 percent for the pressure and density ratios with ionization, respectively, and standard deviations of 0.7 percent and 0.3 percent, respectively.

Although the analytical model of equation (60) was "calibrated" using a single data point from the numerical data (eq. (55)), which is indirectly an average of the product of the computed pressure and density ratios over the entire array of simulations), its ability to predict the individual pressure and density ratios with the indicated accuracy supports the voracity of both models.

Finally, note that the possibility of deriving the expression $\bar{M}_{up} = \sqrt{M_{up}}$ for the effective Mach number from first principles has not been totally exhausted and remains an open question. (Also see app. B for an approximate but fully analytic derivation of this expression.)

5.2 Oblique Shock Curves With Ionization

Given the bifurcation of the shock structure identified in section 4.2, one can use the classical oblique shock curves to determine if a shock wave is attached or detached and to compute the shock angle without ionization.[31] The purpose of this section is to develop a set of modified oblique shock curves with ionization. To derive the oblique shock curves with ionization, analyze the geometry shown in figure 14, where χ is the turning (or nose cone) angle of the flow and $\bar{\beta}$ is the shock angle with ionization. Invoking the standard trigonometric analysis used to express the density ratio across the shock in terms of χ and $\bar{\beta}$,[31] yields

$$\frac{\rho_{up}}{\bar{\rho}_{dn}} = \cot\left(\bar{\beta}\right)\tan\left(\bar{\beta} - \chi\right) \ . \tag{62}$$

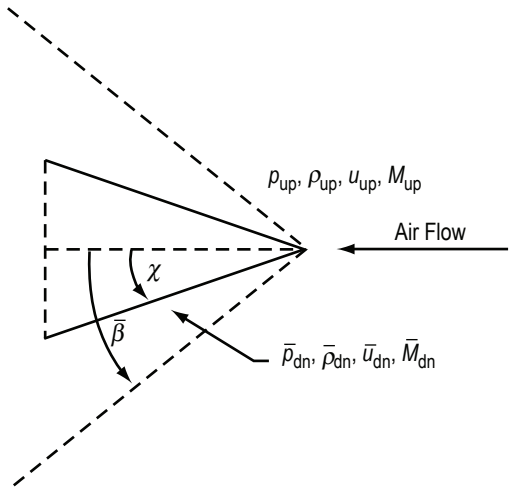

Figure 14. Geometry for the oblique shock curves.

Then equation (58) is used to express the Mach number of the normal air flow through the shock wave as a function of the density ratio across the shock with ionization:

$$\bar{M}_{\text{up}}^{n} = \sqrt{\frac{1}{(\gamma+1)\dfrac{\rho_{\text{up}}}{\bar{\rho}_{\text{dn}}} - \gamma}} = \sqrt{\frac{1}{(\gamma+1)\cot\left(\bar{\beta}\right)\tan\left(\bar{\beta}-\chi\right)-\gamma}} \quad . \tag{63}$$

Finally, express the normal upstream Mach number in terms of the actual upstream Mach number, $M_{\text{up}} = M_{\text{up}}^{n} \Big/ \left(\sin\left(\bar{\beta}\right)\right)$, obtaining the desired relationship,

$$M_{\text{up}} = \frac{1}{\sin\left(\bar{\beta}\right)}\sqrt{\frac{1}{(\gamma+1)\cot\left(\bar{\beta}\right)\tan\left(\bar{\beta}-x\right)-\gamma}} \quad , \tag{64}$$

between the upstream Mach number, the shock angle with ionization, and the turning angle. The resultant oblique shock curves with ionization are plotted in figure 15 along with the classical obliques shock curves "without ionization." Note that for any given Mach number the shock curve "with ionization" is always to the right of the corresponding shock curves without ionization, demonstrating the broadening of the shock wave with ionization, which has been widely observed experimentally.[3,6,29,30,32] Carried to the limit, this implies that in many cases of interest where the shock would normally be attached, the shock with ionization is detached; i.e., the horizontal line for the specified turning angle in figure 15 is above the specified Mach number curve.

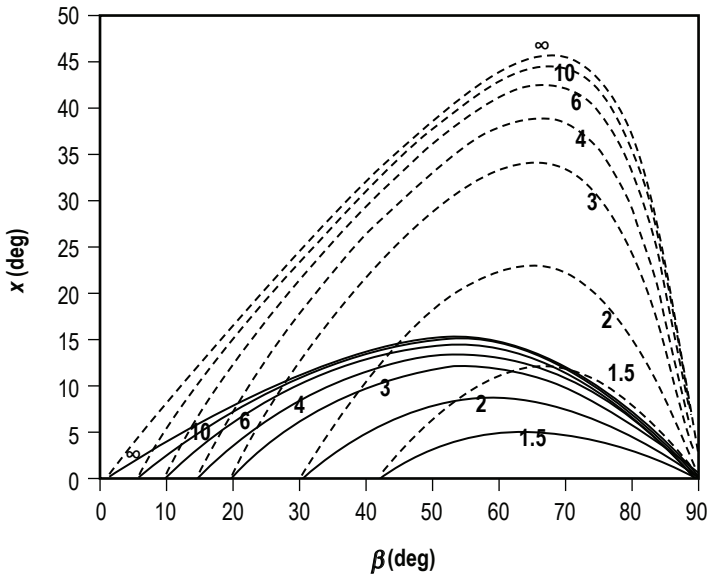

Figure 15. Oblique shock curves with ionization (solid) and without ionization (dashed).

5.3 Downstream Flow

This purpose of the section is to analyze the flow downstream of a shock wave with ionization. To this end, the modified oblique shock curves developed in section 5.2 are used to determine if the shock is attached or detached and to compute the shock angle when it is attached. The flow through an attached shock and around a two-dimensional wedge is analyzed in sections 5.3.1 and 5.3.2. Unlike the classical case without ionization, where the shock is attached for most realistic turning angles and Mach numbers, with ionization the shock is often detached for medium and large turning angles and/or low Mach numbers. As such, the flow through a detached shock and around a two-dimensional wedge is analyzed in section 5.3.3.

5.3.1 Attached Shocks With Ionization

The analysis of the flow through an attached shock and around a two-dimensional wedge with ionization is similar to the classical analysis of the flow through an attached shock and around a two-dimensional wedge with the exception of the pressure and density ratios across the shock,[31] and the fact that the Mach number of the downstream flow normal to the shock is always 1 (eq. (51)). The resultant flow pattern is illustrated in figure 16, where an "upper bar" is used to denote variables that change with ionization. As in the classical case the attached shock is also wedge shaped with a shock angle $\bar{\beta}$ determined from the oblique shock curves with ionization (fig. 15), or by solving equation (54) for $\bar{\beta}$, given the wedge angle χ and the upstream Mach number M_{up}. Moreover, it follows from equation (64) that a streamline crossing the shock at a point x, will turn by an angle of $\bar{\beta} - \chi$ as it passes through the shock, and then flow parallel to the wedge.[31]

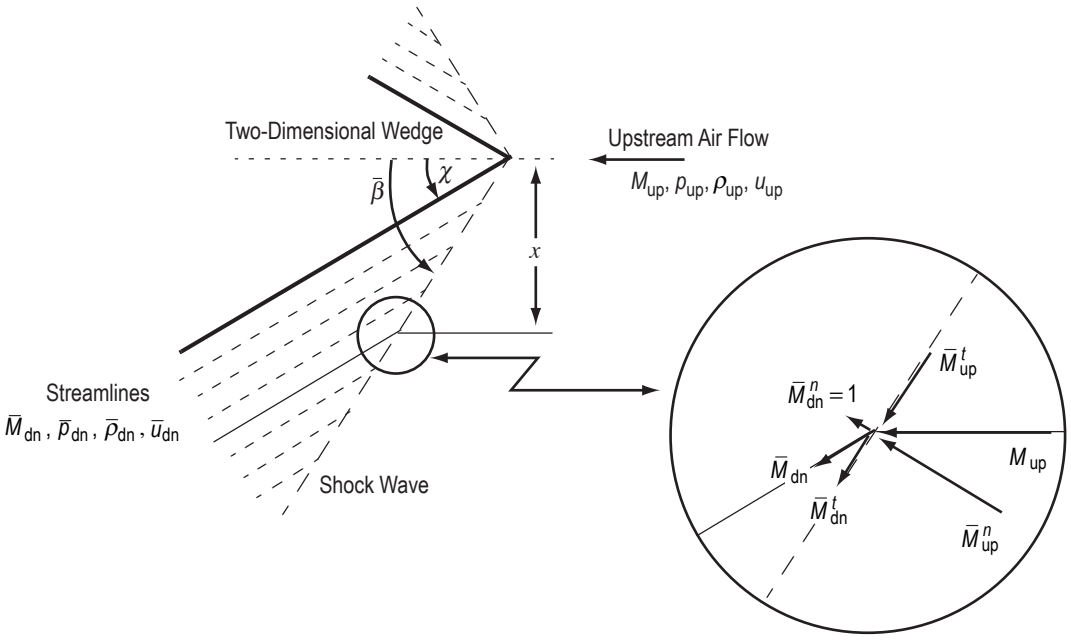

Figure 16. Flow through an attached shock and around a two-dimensional wedge with ionization.

To compute the pressure and density, $\bar{p}_{\text{dn}}$ and $\bar{\rho}_{\text{dn}}$, in the streamline at the downstream side of the shock, one invokes the modified pressure and density ratios with ionization of equation (60), using the Mach number of the upstream flow normal to the shock, $\bar{M}_{\text{up}}^{n} = M_{\text{up}} \sin\left(\bar{\beta}\right)$, in lieu of the actual upstream Mach number, obtaining

$$\frac{\bar{p}_{\text{dn}}}{p_{\text{up}}} = \frac{\gamma\left(M_{\text{up}} \sin\left(\bar{\beta}\right)\right)^2 + 1}{\left(\gamma + 1\right)} \quad \text{and} \quad \frac{\bar{\rho}_{\text{dn}}}{\rho_{\text{up}}} = \frac{\left(\gamma + 1\right)\left(M_{\text{up}} \sin\left(\bar{\beta}\right)\right)^2}{\gamma\left(M_{\text{up}} \sin\left(\bar{\beta}\right)\right)^2 + 1} \quad . \tag{65}$$

Furthermore, since the angle between the shock and the streamline downstream of the shock is $\bar{\beta} - \chi$, while the Mach number of the downstream flow normal to the shock with ionization is 1, $\bar{M}_{\text{dn}} = 1 \Big/ \sin\left(\bar{\beta} - \chi\right)$.

Finally, since the flow in the streamlines downstream of the shock and parallel to the wedge is neither compressive or expansive, it follows from Bernoulli's equation that the above flow parameters, evaluated immediately behind the shock, are constant over the entire downstream portion of the streamline.[16] Moreover, since the shock angle is independent of the point where the streamline crosses the shock, the downstream flow parameters are same for all streamlines. As such, the downstream flow is uniform over the entire downstream region between the two-dimensional wedge and the shock, and it is supersonic since $\sin\left(\bar{\beta} - \chi\right) < 1$, as in the classical case. The flow through an attached shock and around a two-dimensional wedge with ionization, is summarized as follows:

(1) The shock is a two-dimensional wedge with a shock angle, $\bar{\beta}$, given by the oblique shock curves with ionization for the specified wedge angle, χ, and upstream Mach number.

(2) The streamlines turn by an angle of $\bar{\beta} - \chi$ when they cross the shock, and they flow downstream in parallel with the surface of the wedge.

(3) The flow variables are supersonic and constant throughout the region between the two-dimensional wedge and the shock and along the surface of the wedge. $\bar{p}_{\text{dn}}$ and $\bar{\rho}_{\text{dn}}$ are given by equation (63), while $\bar{M}_{\text{dn}} = 1 \Big/ \sin\left(\bar{\beta} - \chi\right)$.

As such, the attached shock and the flow through the shock and along the surface of the two-dimensional wedge with ionization are the same as for an attached shock and the flow around a two-dimensional wedge without ionization, except for the shock angle and the numerical values of the flow variables.

5.3.2 Attached Shocks With Ionization Near the Vertex

Rather than ionizing the entire volume of a shock, one would like to restrict the ionization to a volume near the vertex of the two-dimensional wedge to reduce the energy required for ionization. This is illustrated in figure 17 where it has been assumed that the ionization level in the volume covering the part of the shock near the vertex of the two-dimensional wedge is sufficient to drive the shock intensity to its minimum and that there is no ionization around the outer part of the wedge.

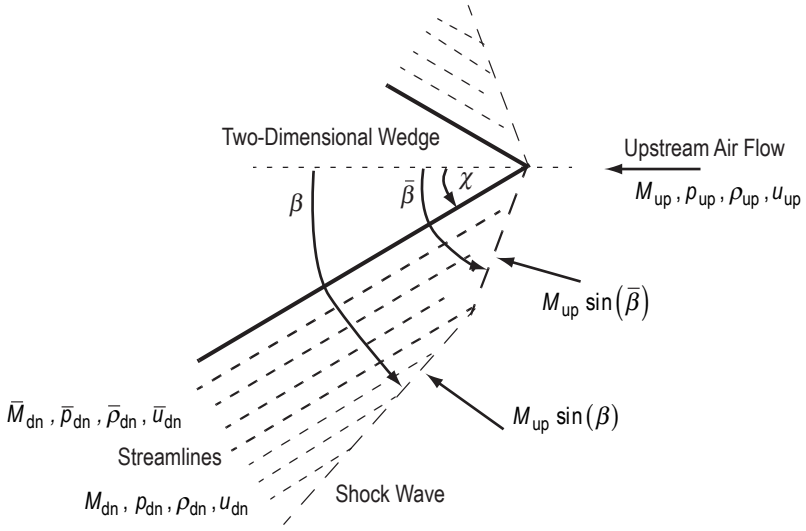

Figure 17. Flow through an attached shock and around a two-dimensional wedge with ionization near the vertex.

The streamlines through both parts of the shock flow in parallel with the surface of the wedge without expanding or contracting. Near the surface of the wedge the shock angle, $\bar{\beta}$, the angle between shock and the streamlines downstream of the shock, $\bar{\beta} - \chi$, and the downstream flow variables— $\bar{M}_{dn}$, $\bar{p}_{dn}$, $\bar{\rho}_{dn}$, and $\bar{u}_{dn}$ —are the same as in section 5.3.1, where the ionization covers the entire shock. Away from the surface of the wedge the shock angle, β, the angle between shock and the streamline downstream of the shock, $\beta - \chi$, and the downstream flow variables— M_{dn}, p_{dn}, ρ_{dn}, and u_{dn} —are the same as without ionization. To verify this, recall that the criteria, for the streamlines between the shock and the two-dimensional wedge to be compatible with the fluid flow equations, are as follows:

(1) They must fill the region between the shock and the two-dimensional wedge.

(2) They must vary continuously downstream of the shock satisfying Bernoullis equation.

(3) The angle between the shock and the streamline downstream of the shock must be consistent with the upstream Mach number and properties of the shock at the point where the streamline crosses the shock.

The first two items are clearly satisfied by the flow illustrated in figure 17 where the flow variables are constant in each streamline since the flow in the streamlines is neither compressive or expansive. Furthermore, as indicated in the derivation of section 5.3.1, the angle between the shock and the a streamline downstream of the shock is only dependent on the upstream Mach number and the properties of the shock at the point where the streamline crosses the shock.

Finally, since the flow variables along the surface of the two-dimensional wedge are the limiting values of the flow variables in the streamlines approaching the surface of the wedge, the performance of a two-dimensional missile or aircraft modeled by the wedge with ionization near the vertex of the wedge will be indistinguishable from the case where the "entire" volume around the shock is ionized. As a matter of practice, however, the ionized volume near the vertex should be wide enough to guarantee that the entire boundary layer is contained in the region where the ionization effects the flow variables (sec. 6.2).

5.3.3 Detached Shocks With Ionization

The flow pattern for the detached case with ionization is shown in figure 18, where an "upper bar" is used to denote the variables that change with ionization. Although the shock wave is detached and normal to the flow at the vertex of the two-dimensional wedge, it does not stand off from the vertex. Indeed, the stand-off distance, τ, for a detached shock is

$$\bar{\tau} = \frac{2r}{3\left[\bar{\rho}_{\mathrm{dn}}/\rho_{\mathrm{up}} - 1\right]} \ , \tag{66}$$

where r is the radius of curvature of the vertex.[32] As such, $\tau = 0$ for an ideal wedge. Moreover, the local shock angle, $\bar{\beta}(x)$, of the detached shock decreases with increasing x, starting at 90° for $x = 0$ (at the vertex). As such, the flow along each streamline is different, while the limiting values of the flow variables as the streamlines approach the surface of the wedge are required for aerodynamic analysis.

To analyze the flow immediately behind the shock, in a streamline that crosses the shock at x, compute the pressure and density via the modified pressure and density ratios with ionization of equation (58), using the Mach number of the upstream flow normal to the shock at x, $\bar{M}^{n}_{\mathrm{up}}(x) = M_{\mathrm{up}} \sin\left(\bar{\beta}(x)\right)$. This yields

$$\frac{\bar{p}_{\mathrm{dn}}(x)}{p_{\mathrm{up}}} = \frac{\gamma\left(M_{\mathrm{up}} \sin\left(\bar{\beta}(x)\right)\right)^2 + 1}{(\gamma+1)} \ \text{ and } \ \frac{\bar{\rho}_{\mathrm{dn}}(x)}{\rho_{\mathrm{up}}} = \frac{(\gamma+1)\left(M_{\mathrm{up}} \sin\left(\bar{\beta}(x)\right)\right)^2}{\gamma\left(M_{\mathrm{up}} \sin\left(\bar{\beta}(x)\right)\right)^2 + 1} \ . \tag{67}$$

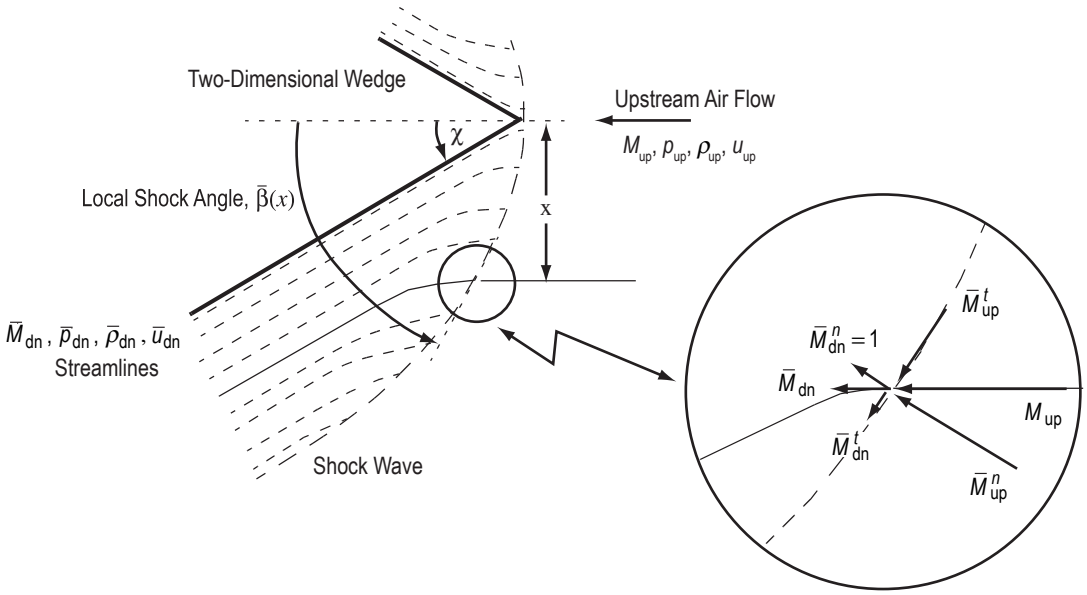

Figure 18. Flow through a detached shock and around a two-dimensional wedge with ionization.

As in the attached case, $\bar{M}^n_{\mathrm{dn}} = 1$ with ionization. Unlike the attached case, however, the angle between the shock and the streamline immediately behind the shock is unknown. As such, use the fact that the shock does not effect tangential velocity; i.e., $\bar{u}^t_{\mathrm{dn}}(x) = \bar{u}^t_{\mathrm{up}}(x)$, allowing computation of the tangential Mach number immediately behind the shock via

$$\begin{aligned}\bar{M}^t_{\mathrm{dn}}(x) &= \frac{\bar{u}^t_{\mathrm{dn}}(x)}{\bar{C}_{\mathrm{dn}}(x)} = \frac{\bar{u}^t_{\mathrm{dn}}(x)}{C_{\mathrm{up}}}\frac{C_{\mathrm{up}}}{\bar{C}_{\mathrm{dn}}(x)} = \frac{\bar{u}^t_{\mathrm{up}}(x)}{C_{\mathrm{up}}}\frac{C_{\mathrm{up}}}{\bar{C}_{\mathrm{dn}}(x)} \\ &= \bar{M}^t_{\mathrm{up}}(x)\frac{C_{\mathrm{up}}}{\bar{C}_{\mathrm{dn}}(x)} = M_{\mathrm{up}}\cos\left(\bar{\beta}(x)\right)\frac{C_{\mathrm{up}}}{\bar{C}_{\mathrm{dn}}(x)}\ ,\end{aligned} \tag{68}$$

where $\bar{C}_{\mathrm{dn}}(x) = \sqrt{\gamma \bar{p}_{\mathrm{dn}}(x)/\bar{\rho}_{\mathrm{dn}}(x)}$. Given $\bar{M}^t_{\mathrm{dn}}(x)$, one may now compute the angle, $\bar{\theta}$, between the shock and the streamline crossing the shock at *x* immediately behind the shock, in terms of the local shock angle via

$$\bar{\theta}(x) = \operatorname{atan}\left(\frac{1}{\bar{M}^t_{\mathrm{dn}}(x)}\right) = \operatorname{atan}\left(\frac{C_{\mathrm{dn}}(x)}{C_{\mathrm{up}}M_{\mathrm{up}}\cos\left(\bar{\beta}(x)\right)}\right), \tag{69}$$

while

$$\bar{M}_{\mathrm{dn}}(x) = \sqrt{\left(\bar{M}^n_{\mathrm{dn}}(x)\right)^2 + \left(\bar{M}^t_{\mathrm{dn}}(x)\right)^2} = \sqrt{1 + \left(\bar{M}^t_{\mathrm{dn}}(x)\right)^2} > 1\ . \tag{70}$$

As such, unlike a classical detached shock, the flow immediately behind the shock in a streamline is supersonic. Furthermore, since the flow in a streamline is compressive downstream of the shock, Bernoulli's equation implies that the Mach number of the flow decreases along the streamline.[16] Since the streamline is already downstream of the shock, however, the Mach number of the flow cannot drop below 1 (without a second shock). As such, the flow is supersonic over the entire length of the streamline. Moreover, this analysis is independent of x, and as such, the flow is supersonic over the entire region between the two-dimensional wedge and the detached shock.

Finally, to estimate the flow variables along the surface of the wedge, observe that

$$\lim_{x\to 0} \bar{M}_{\mathrm{dn}}(x) = \lim_{x\to 0} \sqrt{1+\left(\bar{M}^{t}_{\mathrm{dn}}(x)\right)^{2}} = \lim_{x\to 0} \sqrt{1+\left(\bar{M}_{\mathrm{up}} \cos\left(\bar{\beta}(x)\right) \frac{C_{\mathrm{up}}}{\bar{C}_{\mathrm{dn}}(x)}\right)^{2}} = 1 \tag{71}$$

immediately behind the shock since $\beta(x) = 90°$ at the $x = 0$ where the shock wave is locally normal. Since the flow cannot drop below Mach 1 anywhere in the streamline, this implies that $\lim_{x\to 0} \bar{M}_{\mathrm{dn}}(x) = 1$ over the entire downstream part of the streamline, while Bernoulli's equation implies that in the limit as $x \to 0$, all of the flow variables are constant over the entire downstream part of the streamline.

Since the shock is locally normal at $x = 0$, one can compute the flow variables in the limiting streamlines as $x \to 0$, via the modified pressure and density ratios with ionization of equation (60) using the actual upstream Mach number:

$$\lim_{x\to 0} \frac{\bar{p}_{\mathrm{dn}}(x)}{p_{\mathrm{up}}} = \frac{\gamma M^{2}_{\mathrm{up}} + 1}{(\gamma + 1)} \quad \text{and} \quad \lim_{x\to 0} \frac{\bar{\rho}_{\mathrm{dn}}(x)}{\rho_{\mathrm{up}}} = \frac{(\gamma + 1) M^{2}_{\mathrm{up}}}{\gamma M^{2}_{\mathrm{up}} + 1} \ , \tag{72}$$

while

$$\lim_{x\to 0} \bar{M}_{\mathrm{dn}}(x) = 1 \ . \tag{73}$$

Finally, since the flow along the surface of the two-dimensional wedge is determined by the limiting value of the flow in the streamlines as $x \to 0$, the flow variables along the surface of the two-dimensional wedge with ionization are also given by equations (72) and (73).

The above flow through a detached shock and around a two-dimensional wedge with ionization may be summarized as follows:

(1) The shock is normal at the vertex of the two-dimensional wedge with a stand off distance $\bar{\tau} = 0$.

(2) The local shock angle, $\bar{\beta}(x)$, is 90° at $x = 0$; i.e., at the vertex of the two-dimensional wedge), decreasing with increasing x.

(3) The streamlines cross the shock and turn by an angle, $\bar{\theta}(x)$, immediately behind the shock, continuing to turn downstream until they reach a steady state value.

(4) The pressure, density and Mach number of the flow in a streamline immediately behind the shock are given by equations (57) and (60).

(5) The Mach number in a streamline decreases downstream of the shock but remains supersonic while the pressure and density increase downstream. As such, the flow variables are supersonic throughout the region between the two-dimensional wedge and the shock.

(6) The pressure and density along the surface of the two-dimensional wedge are given by equation (72) while the Mach number along the surface of the two-dimensional wedge is 1.

Note, the above analysis implies that the flow variables along the surface of the two-dimensional wedge are the same as those that would result from a two-dimensional analysis with a normal shock wave.

6. AERODYNAMICS AND PERFORMANCE OF A HYPERSONIC LIFTING BODY

Over the past decade, the driving force behind much of the research in shock structure analysis has been its potential application to aeronautics.[2,5,6,32,34,35] Indeed, the reduction in pressure and density behind a shock wave propagating through a weakly ionized gas suggest the possibility of reducing both wave (pressure) drag and friction drag on the underlying missile or aircraft. Unfortunately, these effects may be compromised by the broadening of the shock wave, which increases the Mach number of the normal airflow through the shock and the pressure and density behind the shock.

Indeed, our simulations indicate that ionization may increase drag on a cylindrical missile at zero angle of attack. For a lifting body (or a missile/aircraft at a high angle of attack), however, the broadening of the shock wave can be beneficial, increasing the lift on the lower surface of the lifting body, without requiring an increased angle of attack which would also increase drag.

The purpose of this section is to use the aerodynamic tools developed in section 5 to analyze the aerodynamics and performance of a hypersonic lifting body with ionization at various Mach numbers and angles of attack, comparing its performance to a lifting body of the same design without ionization. For this purpose a two-dimensional hypersonic lifting body whose geometry is indicated in figure 19 will be used. The analysis of the flow along the lower forward surface of the lifting body with ionization is performed via the techniques developed in section 5. Since the ionization does not extend behind the shock, however, one can use classical techniques to analyze the flow along the lower rear and upper surfaces of the lifting body.[24,31]

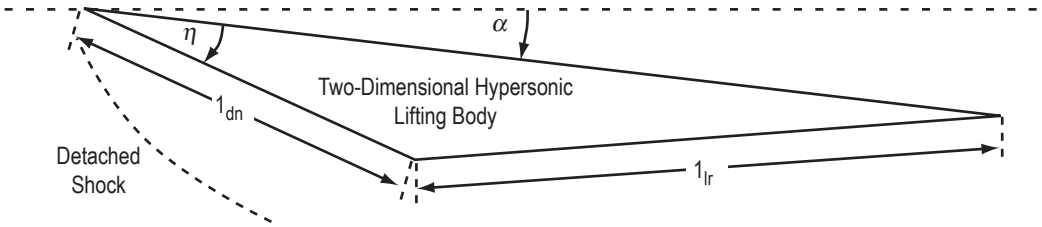

Figure 19. Geometry of two-dimensional hypersonic lifting body.

A summary of an aerodynamic performance analysis of the two-dimensional hypersonic lifting body with and without ionization, parameterized by altitude, Mach number, and angle-of-attack appears in section 6.1, while the energy required by the ionization system is evaluated, and the trade-offs between ionization energy and the aerodynamic performance of the lifting body are reviewed in section 6.2. Finally, a summary of the classical two-dimensional aerodynamic analysis techniques employed in the analysis appears in appendix C.

6.1 Aerodynamic Analysis

In the following, a Mach 4 lifting body operating at 70,000 ft with the operational and geometric parameters indicated in table 3 is considered. The lift over drag (L/D) curves for the lifting body with and without ionization at various angles of attack appear in figure 20 (a). Indeed, the L/D curves with ionization are consistently higher than without ionization, peaking at 8.27 at an angle of attack of 2.41° with ionization, whereas the peak L/D without ionization is 4.21 at $\alpha = 5.04°$. Note, the "kink" in the L/D curve with ionization is at the point where the shock detaches. Since L/D is maximized with an attached shock in this example, the "with ionization" curves in figures 20 and 21 are truncated at $\alpha = 3.38°$, where the shock detaches (except for the L/D curve). There are, however, some combinations of Mach number and nose cone angle where one may want to consider the possibility of flying with a detached shock, such as the Mach 2, 70,000-ft case summarized in table 4.

Table 3. Parameters of lifting body.

M_{up}	Altitude	η	l_{dn}	l_{lr}	Width
4	70,000	10°	5 m	10 m	1 m

From the lift and drag curves of figures 20 (b) and (c), it is apparent that the L/D increase with ionization is due to increased lift with drag only minimally decreased (table 4). Also note that even though the air temperature along the lower forward surface of the lifting body with ionization is twice that without ionization (fig. 21), the temperature increase in the boundary layer is smaller with ionization since the Mach number of the air flow along the boundary layer is smaller, resulting in similar skin temperatures with and without ionization as shown in figure 20 (d). Finally, the air flow variables along the lower forward, lower rear, and upper surfaces of the lifting body are plotted against angle of attack with and without ionization in figure 21.

From the point of view of the aircraft designer, one would prefer to compare the two vehicles trimmed to provide the same lift, and hence carry the same payload and fuel fraction, rather than trimmed at the point of maximum L/D. As such, assume that the lifting body without ionization is trimmed to maximize L/D, as above, while the lifting body with ionization is trimmed to provide the same lift as without ionization. To this end, one would trim the lifting body with ionization in the above Mach 4 example, to fly at an angle of attack of 0.58°, generating the same 88,300 N of lift as the optimally trimmed vehicle without ionization, but with reduced drag and skin temperature (table 4). Although the L/D in this case is less than in the optimally trimmed case (7.55 versus 8.27), it allows one to compare the performance of alternative aircraft designed to carry the same payload and fuel fraction, with and without ionization.

Finally to characterize the effect of Mach number and altitude on the performance of the lifting body, the key performance parameters for the two-dimensional lifting body of figure 19 with and without ionization, are tabulated for Mach numbers ranging 2 to 12 and altitudes ranging from 40,000 ft to 100,000 ft in tables 4 and 5.

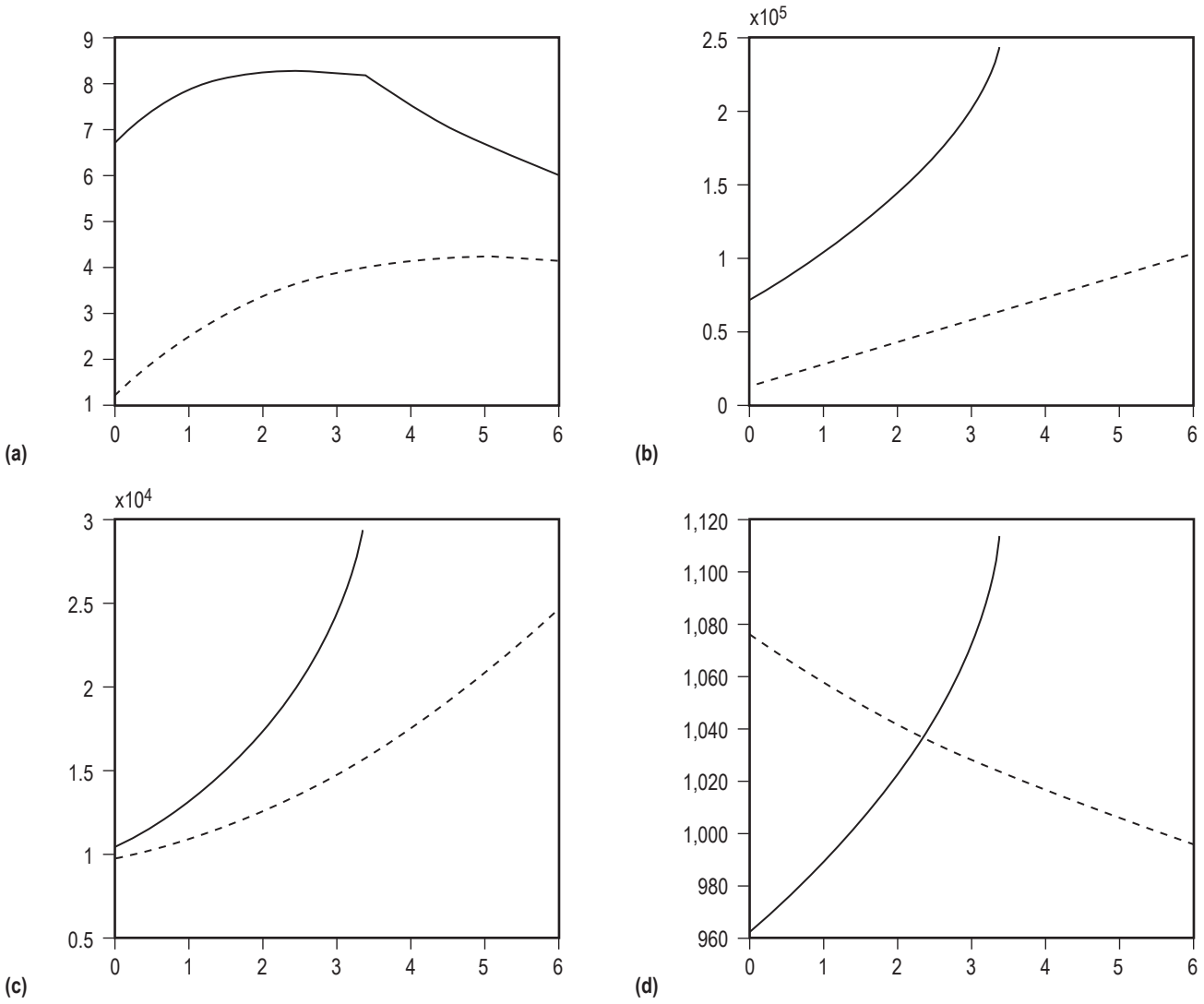

Figure 20. Performance of a Mach 4 two-dimensional lifting body at 70,000 ft versus angle of attack with (solid) and without (dashed) ionization: (a) L/D, (b) lift, (c) drag, and (d) skin temperature.

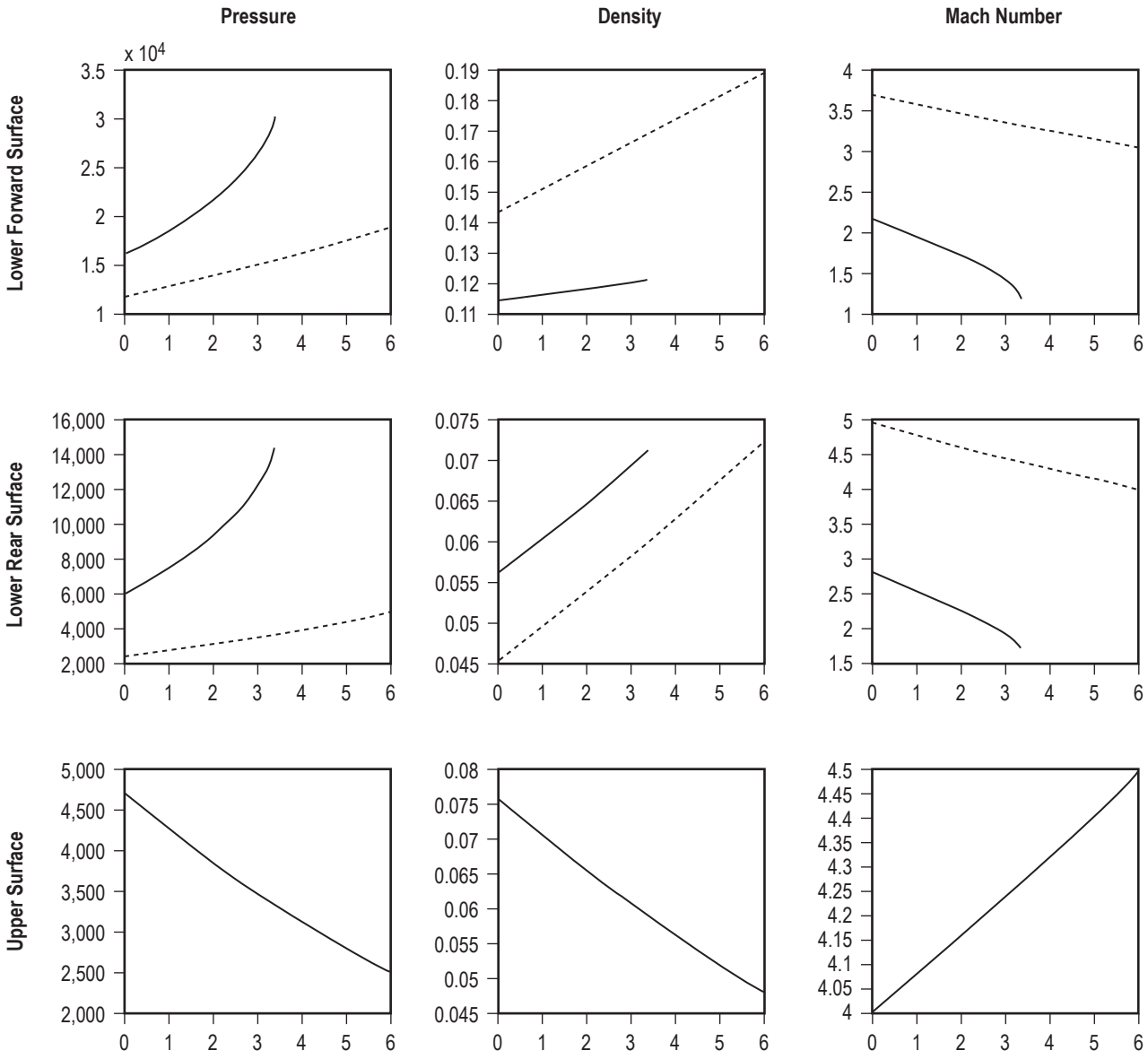

Figure 21. Air flow variables for Mach 4 two-dimensional lifting body at 70,000 ft versus angle of attack with (solid) and without (dashed) ionization.

Table 4. Performance of a two-dimensional lifting body at 70,000 ft versus Mach number with and without ionization.

Mach	Parameter	With Ionization Max L/D	With Ionization =Lift	Without Ionization Max L/D	Parameter	With Ionization Max L/D	With Ionization =Lift	Without Ionization Max L/D
2	Angle of attack L/D Drag	0° 7.41 6,876 N	** ** **	5.41° 4.61 10,297 N	Shock angle Lift Skin temperature*	Detached 50,100 N 491 K	** ** **	46° 47,500 N 417 K
3	Angle of attack L/D Drag	2.03° 8.5 13,900 N	0.83° 7.93 8,610 N	5.54° 4.31 15,900 N	Shock angle Lift Skin temperature*	55.3° 117,900 N 686 K	44.3° 68,300 N 637 K	32.9° 68,300 N 670 K
4	Angle of attack L/D Drag	2.41° 8.27 19,700 N	0.58° 7.55 11,700 N	5.04° 4.21 21,000 N	Shock angle Lift Skin temperature*	44.2° 163,000 N 1,039 K	36.6° 88,300 N 976 K	27.2° 88,300 N 1,004 K
6	Angle of attack*** L/D Drag	1.64° 8.2° 29,500 N	0° 7.34 19,200 N	4.14° 4.19 32,300 N	Shock angle Lift*** Skin temperature*	35.3° 241,900 N 2,030 K	30° 141,000 N 1,941 K	21.9° 134,000 N 1,925 K
8	Angle of attack L/D Drag	1.06° 8.31 41,100 N	** ** **	3.4° 4.16 44,000 N	Shock angle Lift Skin Temperature*	31.5° 341,800 N 3,404 K	** ** **	19.2° 182,700 N 3,192 K
10	Angle of attack L/D Drag	1.02° 8.44 60,800 N	** ** **	2.75° 4.2 56,100 N	Shock angle Lift Skin temperature*	30.5° 513,500 N 5,210 K	** ** **	17.5° 235,600 N 4,812 K
12	Angle of attack L/D Drag	0.6° 8.56 75,400 N	** ** **	2.11° 4.26 67,400 N	Shock angle Lift Skin temperature*	28.7° 645,000 N 7,334 K	** ** **	16.2° 287,300 N 6,788 K

* Measured at the lower forward surface of the lifting body.
** Requires a negative angle of attack, which is not supported by our code.
*** Approximation for the equal lift case.

Table 5. Performance of a Mach 4 two-dimensional lifting body versus altitude with and without ionization.

Alt (ft)	Parameter	With Ionization Max L/D	With Ionization =Lift	Without Ionization Max L/D	Parameter	With Ionization Max L/D	With Ionization =Lift	Without Ionization Max L/D
40,000	Angle of attack* L/D Drag	2.22° 8.44 71,200 N	0.26° 7.41 41,000 N	4.94° 4.30 79,000 N	Shock angle Lift Skin temperature*	43.2° 600,800 N 963 K	35.5° 304,100 N 905 K	27.1° 304,100 N 939 K
70,000	Angle of attack* L/D Drag	2.41° 8.27 19,700 N	0.58° 7.55 11,700 N	5.04° 4.21 21,000 N	Shock angle Lift Skin temperature*	44.2° 163,000 N 1,039 K	36.6° 88,300 N 976 K	27.2° 88,300 N 1,004 K
100,000	Angle of attack* L/D Drag	2.65° 8.06 5,530 N	0.72° 7.3 3,220 N	5.33° 4.1 5,720 N	Shock angle Lift Skin temperature*	45.6° 44,700 N 1,094 K	36.9° 23,500 N 1,021 K	27.5° 23,500 N 1,043 K

* Measured at the lower forward surface of the lifting body.

Note that a negative angle of attack would be required to match the lift with ionization to the optimal lift without ionization in the Mach 2, 8, 10, and 12 cases at 70,000 ft. Since this would not take advantage of the available lift with ionization and is not supported by our code, an "equal lift" analysis was not performed in these cases, indicated by "**" in table 4. Also note that some type of active cooling system would be required to deal with the skin temperatures for the Mach 8–12 cases.

6.2 Energy Requirements

Since the energy used by the ionization system could (theoretically) have been used to increase the engine thrust, it should be incorporated into the L/D analysis to properly evaluate the performance of the ionization system on the lifting body of section 6.1. To this end, the "effective" drag of the energy used by the ionization system has been included in the L/D and drag of a lifting body with ionization (trimmed to provide the same lift as an optimally trimmed lifting body without ionization), and it has been compared to the L/D and drag without ionization.

To estimate the energy requirements for an ionization system, assume that ionization is only used near the vertex of the two-dimensional nose cone of the lifting body (fig. 22). As indicated in section 5.3.2, the shock in the ionized region takes the angle determined by the oblique shock curves with ionization of section 5.2, and the flow variables in the streamlines through the ionized part of the shock take on the values determined by the modified pressure and density ratios with ionization of section 5.2. Similarly, the shock angle in the region without ionization and the flow variables in the streamlines passing through that part of the shock are characterized by the classical oblique shock curves and pressure and density ratios. Furthermore, both sets of streamlines flow in parallel with the surface of the lifting body, while the flow along the surface of the lifting body is determined by the streamlines that "pass through" the boundary layer. As such, it would be theoretically possible to limit the ionized region to the thickness of the boundary layer, 1 mm or less at the far end of the lower rear surface of the lifting body. In practice, however, it is unlikely that one could focus an ionization source that precisely. As such, for the purpose of the present analysis, assume that the ionized part of the shock is 1.5 cm across (a half wavelength for an X-Band microwave source). Since the lifting body is 1-m wide, this implies that the source is required to ionize an area of 1.5×10^{-2} m^2.

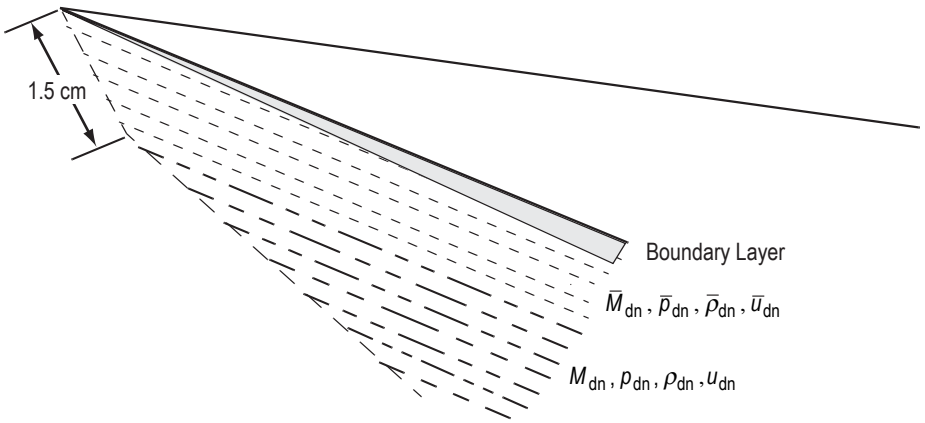

Figure 22. Shock, flow, and boundary layer with ionization near the nose of the lifting body.

The minimum power required to drive the shock intensity to its minimum value for the five flight regimes with equal lift with and without ionization (tables 4 and 5), was evaluated using the shock structure analysis algorithm of section 4, and is summarized in table 6 together with the equivalent drag force (power/upstream velocity). The effective drag with ionization is then taken to be the sum of the actual drag with ionization plus the equivalent drag of the power required by the ionization source. The effective L/D and drag reduction are then computed, both of which are reduced by the equivalent drag of the power required by the ionization source. Finally, following Beaulieu et al., define the energy effectiveness of the ionization system as the ratio of the effective drag reduction divided by the equivalent drag of the power required by the ionization source.[34] These data are summarized in table 6 for the five flight regimes with equal lift with and without ionization.

Table 6. Power required for ionization and effective drag with ionization for the lifting body at 70,000 ft.

Flight Regime	Mach 3 (70,000 ft)	Mach 4 (70,000 ft)	Mach 6 (70,000 ft)	Mach 4 (40,000 ft)	Mach 4 (100,000 ft)
Power to ionize 1.5×10^{-2} m^2 of the shock	2.42×10^3 W	5.22×10^3 W	1.08×10^4 W	1.94×10^4 W	2.45×10^5 W
Equivalent drag force (Power / upstream velocity)	2.72 N	4.4 N	6.208 N	16.9 N	202 N
Drag with ionization (table 4)	8,610 N	11,700 N	19,200 N	41,000 N	3,220 N
Effective drag with ionization (drag with ionization + equivalent drag)	8,612 N	11,704 N	19,206 N	41,017 N	3,422 N
Effective L/D	7.931	7.544	7.341	7.414	6.86
Effective drag reduction (drag without ionization – effective drag with ionization)	7,288 N	9,296 N	13,094 N	37,983 N	9,142 N
Energy effectiveness (effective drag reduction / equivalent drag of ionization power)	2.68×10^3	2.11×10^3	2.11×10^3	2.25×10^3	4.53×10^1

With the exception of the Mach 4, 100,000-ft case, the energy effectiveness of the ionization system exceeds 2,000, indicating that an ionization system would significantly increase the performance of the lifting body, even if one were to increase the power required by the ionization system by an order of magnitude (or two) to incorporate thermal and volumetric inefficiencies in the analysis. Indeed, such a system would achieve a net performance gain even in the 100,000-ft case, though with reduced energy effectiveness. Finally, note the nonmonotonicity of the data with altitude, which is consistent with the observations based on the simulations of section 4.

7. CONCLUSIONS

In this section the assumptions underlying the electrofluid dynamics model are reviewed, a qualitative comparison of the above analysis and simulations with the available experimental data is provided, and the potential applications of the shock structure modification technology in aeronautics are commented upon.

7.1 Electrofluid Dynamics Model

The driver for the shock structure analysis is the electrofluid dynamics model of equations (11)–(20). Indeed, this model is composed of 6 classical conservation laws (for either the entire weakly ionized gas or the individual species), plus Gauss' Law, and the required auxiliary equations. The remaining conservation laws are implied by the assumptions that $u^i = u^n$, $T^i = T^n$, and that the electron momentum is negligible. As such, the efficacy of the resultant analysis is dependent on these assumptions and the remaining assumptions summarized in table 2.

Of equal significance are the assumptions that are not made, as follows:

- Not assuming quasi-neutrality and including the resultant electric field and electrostatic body forces/ohmic heating in the model.
- Treating the electron velocity as an independent variable.
- Including viscosity in the model.

Although, to our knowledge, all previous shock structure analysis models have assumed that $u^e = u^n = u^i$, the electron velocity may increase by several orders of magnitude in the electric field across the shock, significantly impacting the shock structure.[1,9,12,13] In particular, the increased electron velocity decreases the electron drift length while increasing the electron body force/ohmic heating term in the energy equation, making it the primary coupling mechanism between the ionization and the fluid flow.

Similarly, the viscosity in the fluid dynamics model significantly influences the shock structure. In particular, the jump in electron temperature across the shock is driven by the pressure jump, which is independent of shock width, but the loss mechanisms, which reduce the electron temperature jump in the shock, are dependent on the shock thickness. Furthermore, the viscosity of the flow dampens the rapid decrease of the flow intensity as it converges to its minimum value downstream of the shock and enhances the decrease of the Mach number upstream of the shock.

Finally, note that the thermal radiation term, Q, can be used to add a thermodynamic model to the electrofluid flow model. Such a model might include thermal radiation, if significant, an external heat

source, or a feedback system in which Q is dependent on the fluid flow variables. Since Q is additive to Ω^e, it will either add or subtract from the ohmic heating produced by the electrodynamics model, but should not fundamentally modify the shock structure.

7.2 Comparison With Experiment

The experimental literature on ionized gas/shock wave interaction can be divided into the following:

- Macroscopic effects—where one observes the effect of the ionization indirectly, via its effect on the shock wave.

- Microscopic effects—where one observes the effect of the ionization directly via its effect on the fluid flow and electrodynamic variables across the shock

Unfortunately, the available electron temperature and density measurements, are not sufficiently precise to permit a quantitative comparison with the simulations of section 4, where a 0.01-eV change in electron temperature can fundamentally effect the shock structure. As such, this review is restricted to a qualitative comparison.

The most common macroscopic effects include the following:[3–8,32,36]

- Reduction in shock intensity.

- Broadening of the shock wave.

- Increased standoff distance for a detached shock wave.

- An enhancement of the observed effect when an external electric field is applied in the direction opposite to the flow, and a degradation of the observed effect when an external electric field is applied in the direction of the flow.[5,37]

- The apparent complete dispersion of the shock wave with sufficiently high ionization levels.[5,7,14]

- Asymetric time constants associated with the change in shock structure (changing in microseconds when the ionization is turned on, but requiring milliseconds to revert back to the original shock structure when the ionization is turned off).[38]

The first three items are due to the reduced density ratio across the shock in the presence of ionization. Indeed, these observations are all made with either Schlieren or shadowgraph images, which are proportional to either the derivative of the second derivative of the density,[39] and as such, the intensity of these images is reduced when the density ratio across the shock decreases in the presence of ionization.

The observed broadening of the shock wave is also attributable to the reduced density ratio across the shock in the presence of ionization via the equality

$$\frac{\rho_{dn}}{\rho_{up}} = \frac{1}{\cot(\beta)\tan(\beta - x)} \quad , \tag{74}$$

which is used in the derivation of the oblique shock curves,[31] where β is the shock angle and χ is the nose cone angle. Similarly, the shock standoff distance increases with decreasing density ratio (eq. (66)).

Since the electric field that drives the changes in shock structure in the above analysis (via the ohmic heating term) is always negative; i.e., in the direction opposite to the flow, an externally imposed electric field in the direction opposite the flow will enhance its effect, whereas an externally imposed electric field in the direction of the flow will detract from the effect of the ionization.

Although the apparent complete dispersion of the shock wave in the presence of ionization would appear to contradict the fact that the shock intensity cannot be driven below a minimum value;[5,7,14] the Schlieren and shadowgraph diagnostics used in these experiments image the derivative and second derivative of the gas density, respectively.[39] As such, they are dependent on the distance upstream and downstream of the shock over which the ionization interacts with the fluid flow as well as the density ratio. Indeed, as the ionization level increases in these simulations, the distance upstream and downstream of the shock over which the ionization interacts with the fluid flow continues to increase after the shock intensity and flow density have reached minimum values. As such, the (average) amplitude of the Schlieren and shadowgraph images will continue to decrease with increasing ionization levels. This is illustrated in figure 23 for a Mach 2 shock at 70,000 ft, which roughly approximates the environment where the experimental observations were made. Although the downstream density increases slightly for the 1.4-eV case (probably numerical error for this example, which is on the fringes of instability), the distance over which the density jumps across the shock is about 40 μm for the 1-eV case and about 150 μm for the 1.4-eV case. As such, depending on the spacial resolution of the diagnostic systems employed the (average) amplitude of the Schlieren and shadowgraph images for the 1.4-eV case will be about a third of that for the 1-eV case.

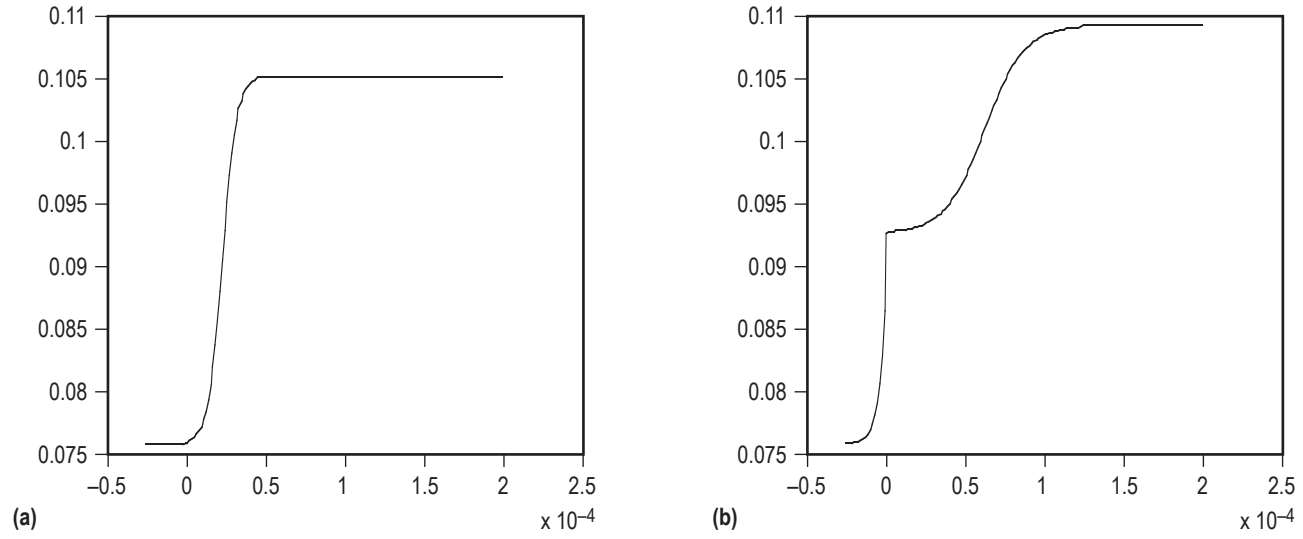

Figure 23. Density for a Mach 2 shock at 70,000 ft with (a) 1-eV and (b) 1.4-eV sources.

Finally, note that the asymmetric time constants observed experimentally,[38] cannot be modeled by our steady state electrofluid dynamics model. Given the complex feedback loops coupling the fluid flow and electrodynamic variables in the model of figure 4, however, such an effect would not be unreasonable.

Unlike the macroscopic effects, high (spatial) resolution instrumentation is required to directly observe the microscopic effects of ionization on the shock structure. To increase the spatial scale of the region around the shock wave, most researchers work at low pressures (typically 3–5 Torr), thereby facilitating the direct observation of the fluid flow and electrodynamic variables within the shock wave. Liu, Whitten, and Glass; and Liu and Glass use a Mach-Zehnder interferometer to observe the structure of Mach 13–16 shock waves in 5 Torr argon, in a 10-cm by 18-cm. hypervelocity shock tube.[12,40] In these experiments they observe a "small" electron temperature peak at the shock and a factor of 2 jump in electron density behind the shock wave. In a similar series of experiments in Mach 17–21 neon, McIntyre et al., saw an order-of-magnitude or more jump in electron density at the shock and observed the increased ionization rate at the shock indirectly via measurements of the excited state populations.[10] Moreover, they saw an overshoot in the heavy particle concentration behind the shock, which is consistent with the overshoot in our simulations. Finally, Chan and Hershkowitz saw an electron temperature peak at the shock and the associated electronic double layer.[41]

In a recent paper, Bletzinger, Ganguly, and Garscadden reported on an experimental program in 3–5 Torr nitrogen, performed in a 3-cm-diameter shock tube with an electric shock driven Mach 1.76 shock wave propagating through a 20 ma weakly ionized gas.[35] They summarized the results of these experiments as follows:

> [*W*]*e have provided direct evidence for the large jump in ionization potential, the fast increase of electron excitation temperature as indicated by the sudden increase in emission rate, and the increase in the emission rate and the increase in* n^e *caused by the formation of strong double layers, at the shock front, in non-equilibrium ionizations. One of the important implications of the strong- double-layer-induced local electron heating is that a very localized energy dispersion and gas heating at the shock front is possible so that shock wave dispersions and modifications of the shock jump conditions cannot always be determined from the steady state or spatially averaged gas properties.*[35]

In particular, Bletzinger et al., observed the following:[35]

- A negative electric field across the shock.
- An increased ionization rate at the shock.
- The formation of a double layer at the shock.
- A drop in the density ratio across the shock.

Based on these observations, Bletzinger et al., concluded that the electron temperature peaks at the shock and that the observed shock wave dispersion is due to local ohmic heating at the shock, induced by the double layer. As such, the microscopic shock structure model resulting from the Bletzinger et al. experiments is qualitatively identical to the model predicted by the above described shock structure analysis and

simulations.[35] The experimental and theoretical models differ quantitatively in certain respects—a 10-eV electron temperature jump in the experimental model versus <1 eV in the analytical model and a 150 percent electron density ratio in the experimental model versus more than an order of magnitude in the analytical model.

7.3 Application in Aeronautics

The potential applications of the shock structure modification in a weakly ionized gas are dependent on the trade-offs between its various effects, as follows:

- Reducing the pressure and density jump across the shock.
- Broadening of the shock wave.
- Increasing the temperature jump across the shock.

For the lifting body of section 6, the broadening of the shock wave is the primary source of the increased L/D with ionization—increasing the Mach number of the normal air flow through the shock and hence the pressure below the lifting body at a lower angle of attack than without ionization, thereby increasing lift without a commensurate increase in drag. Moreover, in this application, the skin temperature of the lifting body is essentially unchanged, since the decreased downstream Mach number with ionization compensates for the increased downstream air flow temperature (eq. (97)).

The above analysis would also apply to a missile or aircraft flying at a high angle of attack, or the flow in a duct or inlet, where a broad shock angle is also beneficial. Moreover, for a "blunt" nosed missile or aircraft, where the shock angle is already "broad," the additional broadening of the shock wave with ionization will only minimally increase the Mach number of the normal air flow while decreasing the pressure and density behind the shock with a commensurate decrease in wave and friction drag. For a "fine" nosed missile or aircraft, however, the broadening of the shock wave with ionization will counteract the reduction of the pressure and density jumps across the shock, possibly increasing drag.

APPENDIX A — ADDITIONAL SHOCK STRUCTURE ANALYSIS DATA

The purpose of this appendix is to expand on section 4.1 by providing detailed shock structure analysis plots for some additional cases (figs. 24–26).

A.1 Shock Structure of a Mach 4 Flow at 40,000 ft With a 1.4-eV Source

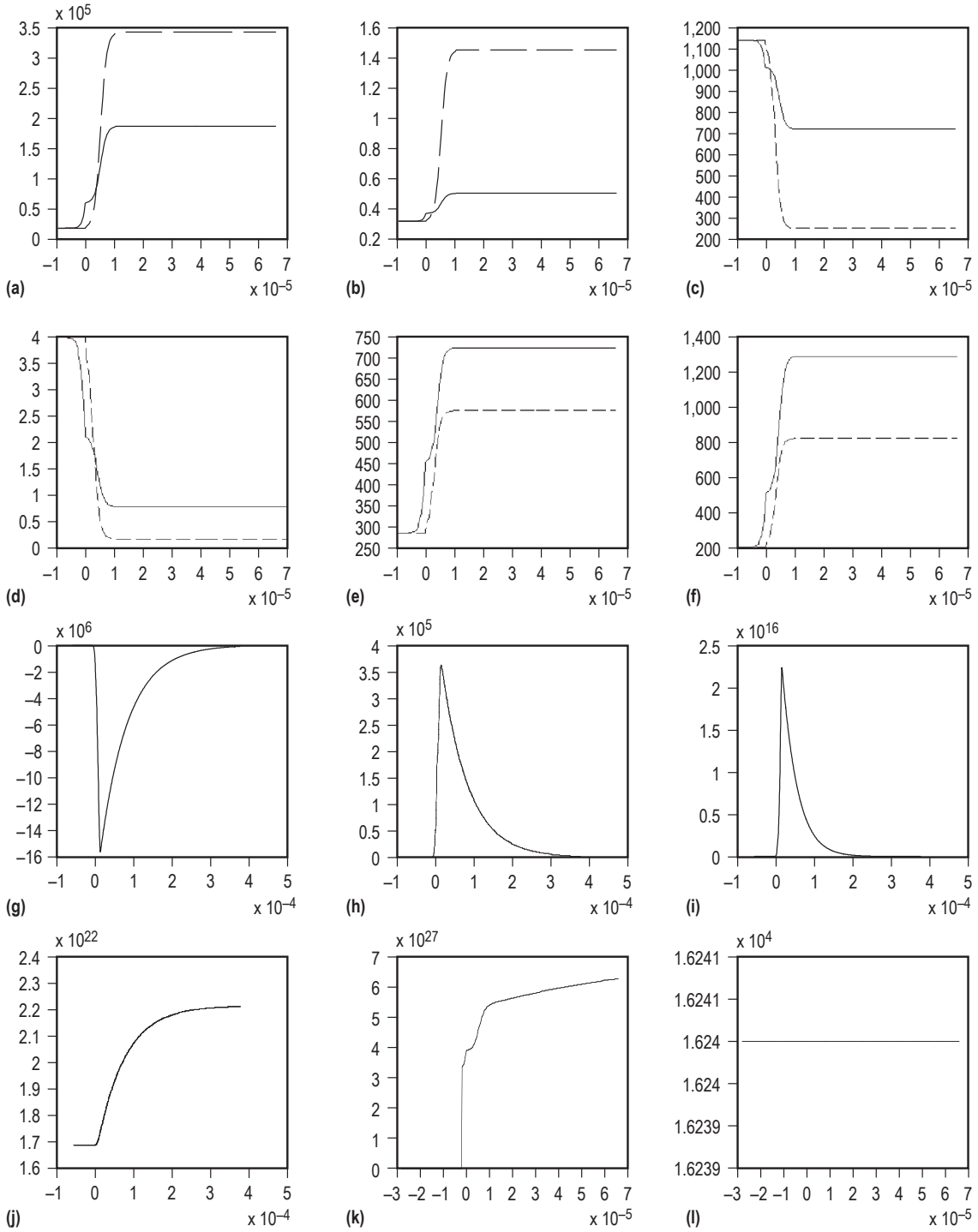

Figure 24. Shock structure for a Mach 4 flow at 40,000 ft with a 1.4-eV source: (a) Pressure, (b) density, (c) velocity, (d) Mach number, (e) speed of sound, (f) temperature, (g) electric field, (h) electron velocity, (i) ohmic heating, (j) ion and electron densities, (k) ionization rate, (l) electron temperature.

A.2 Shock Structure of a Mach 12 Flow at 70,000 ft With a 0.85-eV Source

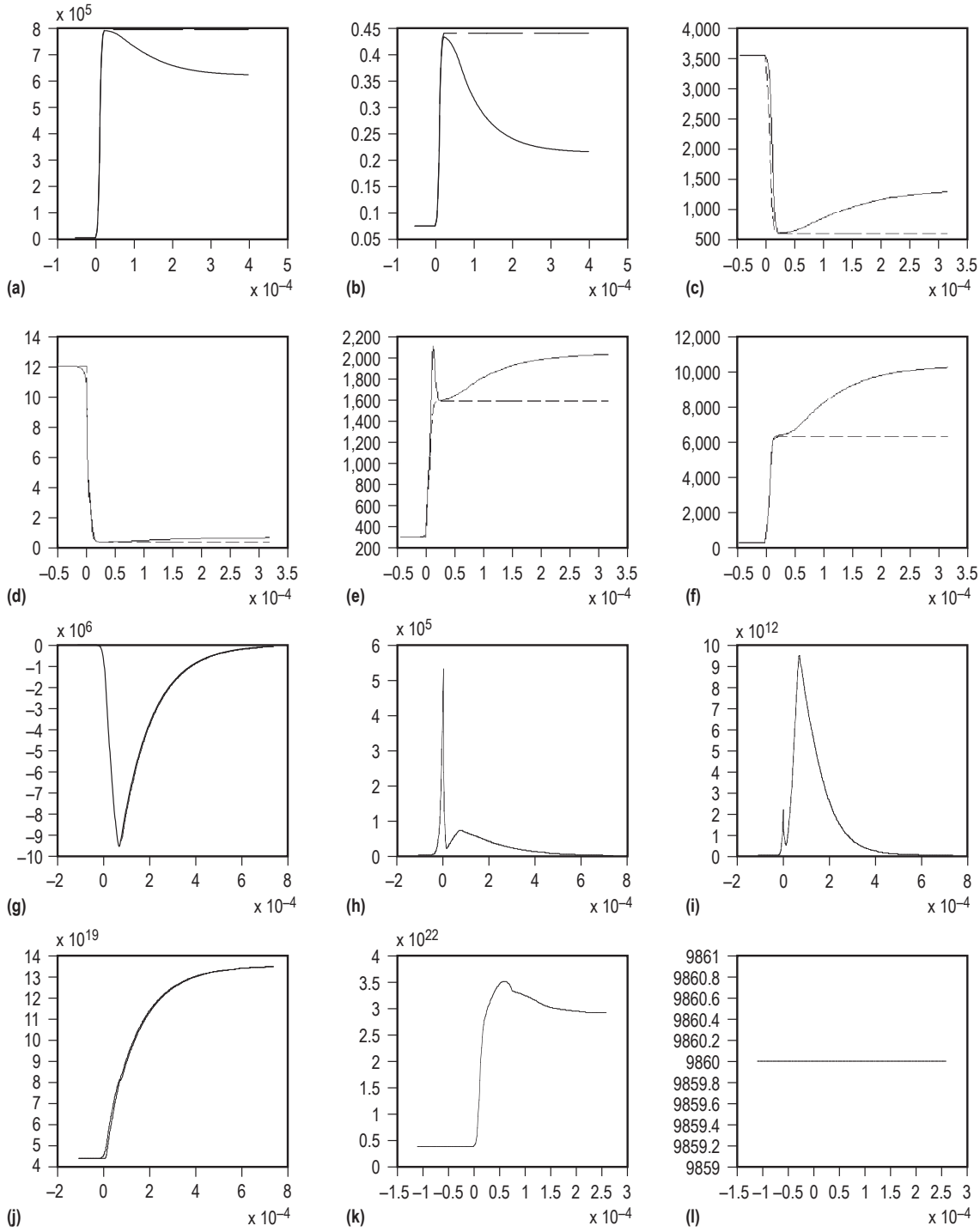

Figure 25. Shock structure for a Mach 12 flow at 70,000 ft with a 0.85-eV source: (a) Pressure, (b) density, (c) velocity, (d) Mach number, (e) speed of sound, (f) temperature, (g) electric field, (h) electron velocity, (i) ohmic heating, (j) ion and electron densities, (k) ionization rate, (l) electron temperature.

A.3 Shock Structure of a Mach 2 Flow at 10,000 ft With a 0.9-eV Source

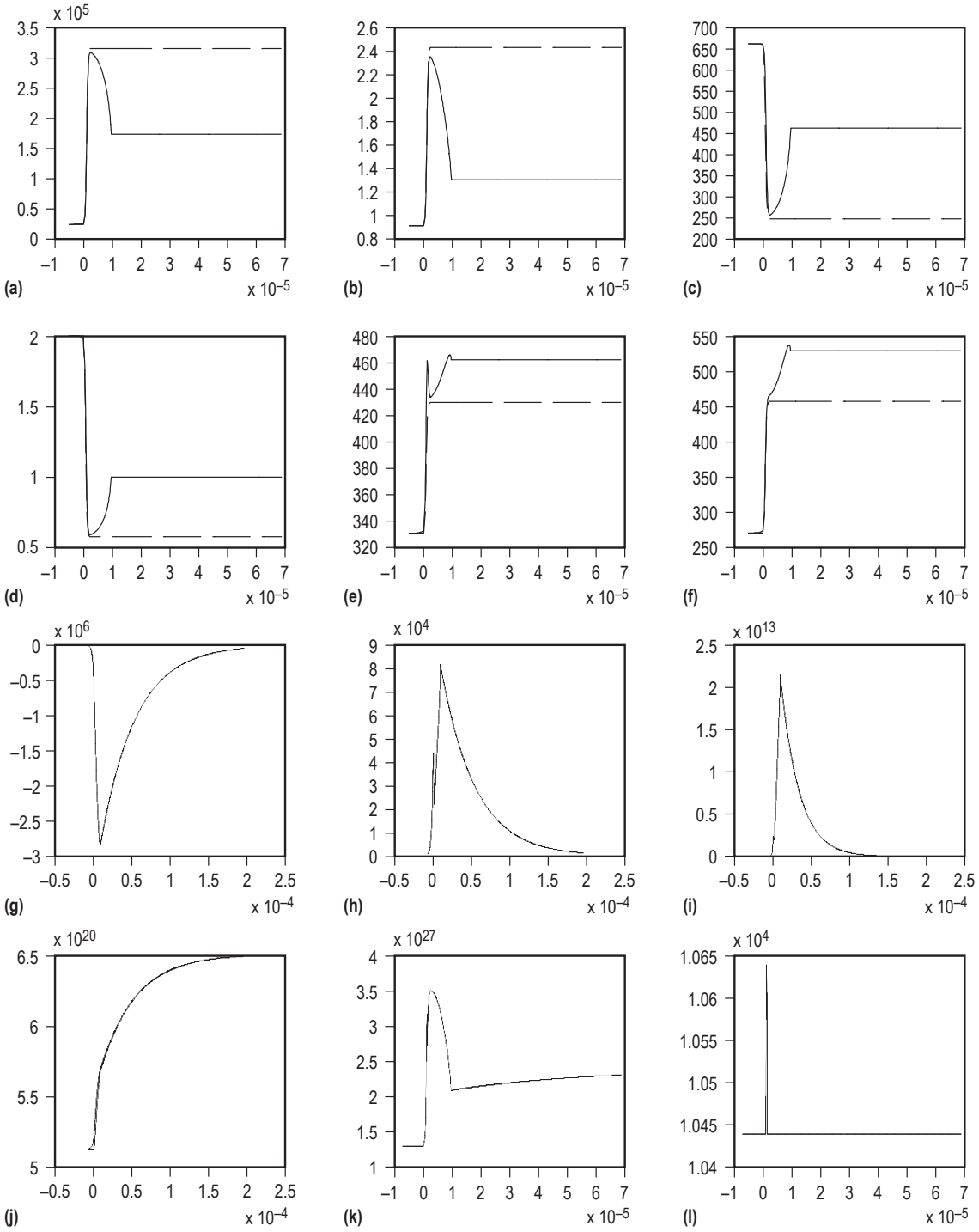

Figure 26. Shock structure for a Mach 2 flow at 10,000 ft with a 0.9-eV source: (a) Pressure, (b) density, (c) velocity, (d) Mach number, (e) speed of sound, (f) temperature, (g) electric field, (h) electron velocity, (i) ohmic heating, (j) ion and electron densities, (k) ionization rate, (l) electron temperature.

APPENDIX B—APPROXIMATE ANALYTIC DERIVATION OF THE MODIFIED PRESSURE AND DENSITY RATIOS

The purpose of this appendix is to provide an alterative approximate analytic derivation of the effective Mach numbers that bypasses the empirical derivation used in section 5.1. To this end, start with the inequalities

$$1 \le \frac{\overline{\rho}_{\mathrm{dn}}}{\rho_{\mathrm{up}}} \le \frac{(\gamma+1)M_{\mathrm{up}}^2}{(\gamma-1)M_{\mathrm{up}}^2+2} \quad \text{and} \quad 1 \le \frac{\overline{p}_{\mathrm{dn}}}{p_{\mathrm{up}}} \le \frac{2\gamma M_{\mathrm{up}}^2-(\gamma-1)}{(\gamma+1)} \ , \tag{75}$$

where $\overline{\rho}_{\mathrm{dn}}/\rho_{\mathrm{up}}$ and $\overline{p}_{\mathrm{dn}}/p_{\mathrm{up}}$ are upper bounded by the "no ionization" case since ionization reduces the density and pressure ratios across the shock, and lower bounded by the "no shock" case where $\overline{\rho}_{\mathrm{dn}} = \rho_{\mathrm{up}}$ and $\overline{p}_{\mathrm{dn}} = p_{\mathrm{up}}$. Substituting the density inequalities into the expression for the downstream shock intensity

$$\sqrt{(\overline{p}_{\mathrm{dn}}\overline{\rho}_{\mathrm{dn}})/(p_{\mathrm{up}}\rho_{\mathrm{up}})} = M_{\mathrm{up}} \tag{76}$$

with ionization, one may derive tighter upper and lower bounds for $\overline{p}_{\mathrm{dn}}/p_{\mathrm{up}}$ via

$$M_{\mathrm{up}}^2 = \frac{\overline{p}_{\mathrm{dn}}}{p_{\mathrm{up}}}\frac{\overline{\rho}_{\mathrm{dn}}}{\rho_{\mathrm{up}}} \le \frac{\overline{p}_{\mathrm{dn}}}{p_{\mathrm{up}}}\frac{(\gamma+1)M_{\mathrm{up}}^2}{(\gamma-1)M_{\mathrm{up}}^2+2} \ , \tag{77}$$

or equivalently

$$\frac{\overline{p}_{\mathrm{dn}}}{p_{\mathrm{up}}} \ge M_{\mathrm{up}}^2\frac{(\gamma-1)M_{\mathrm{up}}^2+2}{(\gamma+1)M_{\mathrm{up}}^2} = \frac{(\gamma-1)M_{\mathrm{up}}^2+2}{(\gamma+1)} \ . \tag{78}$$

Similarly, one may derive an upper bound for $\overline{p}_{\mathrm{dn}}/p_{\mathrm{up}}$ using the opposite inequality in equation (75) yielding

$$M_{\mathrm{up}}^2 = \frac{\overline{p}_{\mathrm{dn}}}{p_{\mathrm{up}}}\frac{\overline{\rho}_{\mathrm{dn}}}{\rho_{\mathrm{up}}} \ge \frac{\overline{p}_{\mathrm{dn}}}{p_{\mathrm{up}}}1 = \frac{\overline{p}_{\mathrm{dn}}}{p_{\mathrm{up}}} \ . \tag{79}$$

Although there remains a considerable gap between the upper and lower bounds of equations (78) and (79), they are tighter than the bounds of equation (75). In particular, both the upper and lower bounds

grow with M_{up}^2 for large upstream Mach numbers. As such, approximate $\bar{p}_{dn}/p_{up}$ by a value that is midway between the upper and lower bounds of equations (78) and (79); i.e.,

$$\frac{\bar{p}_{dn}}{p_{up}} \approx \frac{M_{up}^2 + \frac{(\gamma-1)M_{up}^2+2}{(\gamma+1)}}{2} = \frac{\gamma M_{up}^2 + 1}{(\gamma+1)} \quad . \tag{80}$$

Although equation (80) has a maximum percent error of $100/\gamma$ (74 percent in air and 60 percent in a monotonic gas), it represents the "best" estimate for $\bar{p}_{dn}/p_{up}$ given the available data. Substituting equation (80) into equation (76) yields a corresponding approximation for the density ratio

$$\frac{\bar{\rho}_{dn}}{\rho_{up}} \approx \frac{(\gamma+1)M_{up}^2}{\gamma M_{up}^2 + 1} \quad . \tag{81}$$

Finally, one may obtain expressions for the pressure effective and density effective Mach numbers by equating the expressions for $\bar{p}_{dn}/p_{up}$ and $\bar{\rho}_{dn}/\rho_{up}$ of equations (80) and (81) with the defining equalities for $\hat{M}_{up}$ and $\tilde{M}_{up}$ of equation (53):

$$\frac{2\gamma\hat{M}_{up}^2 - (\gamma-1)}{(\gamma+1)} \equiv \frac{\bar{p}_{dn}}{p_{up}} \approx \frac{\gamma M_{up}^2 + 1}{(\gamma+1)} \quad \text{and} \quad \frac{(\gamma+1)\tilde{M}_{up}^2}{(\gamma-1)\tilde{M}_{up}^2 + 2} \equiv \frac{\bar{\rho}_{dn}}{\rho_{up}} \approx \frac{(\gamma+1)M_{up}^2}{\gamma M_{up}^2 + 1} \quad , \tag{82}$$

yielding

$$\tilde{M}_{up}^2 \approx \frac{2M_{up}^2}{1+M_{up}^2} \quad \text{and} \quad \hat{M}_{up}^2 \approx \frac{1+M_{up}^2}{2} \quad , \tag{83}$$

while

$$\begin{aligned} \bar{M}_{up} &= \sqrt{\hat{M}_{up}\tilde{M}_{up}} = \sqrt{\sqrt{\frac{1+M_{up}^2}{2}}\sqrt{\frac{2M_{up}^2}{1+M_{up}^2}}} \\ &= \sqrt[4]{\left(\frac{1+M_{up}^2}{2}\right)\left(\frac{2M_{up}^2}{1+M_{up}^2}\right)} = \sqrt[4]{M_{up}^2} = \sqrt{M_{up}} \quad . \end{aligned} \tag{84}$$

As such, with the aid of the (admittedly "loose") approximation of equation (80), one can replicate the theory of section 5.1—including the empirical formula for the effective Mach number with ionization.

APPENDIX C—TWO-DIMENSIONAL AERODYNAMIC ANALYSIS WITHOUT IONIZATION

The purpose of this appendix is to provide an overview of the classical two-dimensional aerodynamic analysis techniques used in section 6 including the following:

- The characterization of the shock and the flow behind the shock without ionization,
- The Prandtl-Meyers expansion analysis used to evaluate the flow on the top and lower rear surfaces of the two-dimensional lifting body.
- The wave drag and lift formulae.
- The model used for evaluating the friction drag due to the turbulent flow along the surfaces of the lifting vehicle.
- A method for computing skin temperature of the lifting body.
- The boundary layer thickness.

C.1 Shock Angle and Downstream Flow

For a hypersonic lifting body without ionization, one may assume that the shock is attached—in which case, its properties are similar to the properties of the attached shock with ionization described in section 5.3, using the classical pressure and density ratio formulae and oblique shock curves rather than the modified formula of section 5.3. In particular, the attached shock is wedge shaped, the streamlines downstream of the shock are parallel to the surface of the wedge, and the flow variables are constant in the region between the shock and the wedge. As such, one may

(1) Compute the shock angle using the classical oblique shock curves of figure 15 or by solving

$$M_{\text{up}} = \frac{1}{\sin(\beta)} \sqrt{\frac{2}{(\gamma+1)\cot(\beta)\tan(\beta-\chi)-(\gamma-1)}} \tag{85}$$

for β given the wedge angle, χ, and M_{up}

(2) Use the classical pressure and density ratios of equation (52) to compute the pressure and density downstream of the shock.

(3) Use the inverse of the density ratio to evaluate the normal velocity of the downstream flow via

$$u_{\mathrm{dn}}^{n} = \frac{\rho_{\mathrm{up}}}{\rho_{\mathrm{dn}}} u_{\mathrm{up}}^{n} = \frac{\rho_{\mathrm{up}}}{\rho_{\mathrm{dn}}} \sin(\beta) u_{\mathrm{up}} \tag{86}$$

(4) Let $u_{\mathrm{dn}} = u_{\mathrm{dn}}^{n} / \tan(\beta - \chi)$.

C.2 Prandtl-Meyers Expansion

To evaluate the flow on the upper and lower rear surfaces of the lifting body, use a classical Prandtl-Meyers expansion since there is no ionization involved in either case.[31] To compute the flow variables, M_{tp}, p_{tp}, ρ_{tp}, and u_{tp}, along the upper surface of the lifting body given the upstream flow variables M_{up}, p_{up}, ρ_{up}, and u_{up}, use the following procedure:[31]

(1) Compute the Mach number of the flow along the upper surface of the lifting body via

$$M_{\mathrm{tp}} = v^{-1}\left(\alpha + v\left(M_{\mathrm{up}}\right)\right) \tag{87}$$

where

$$v(M) = \sqrt{\frac{\gamma+1}{\gamma-1}} \operatorname{atan}\left(\sqrt{\frac{\gamma-1}{\gamma+1}}\left(M^2 - 1\right)\right) - \operatorname{atan}\left(\sqrt{M^2 - 1}\right) \tag{88}$$

is the Prandtl-Meyers function plotted in figure 27.

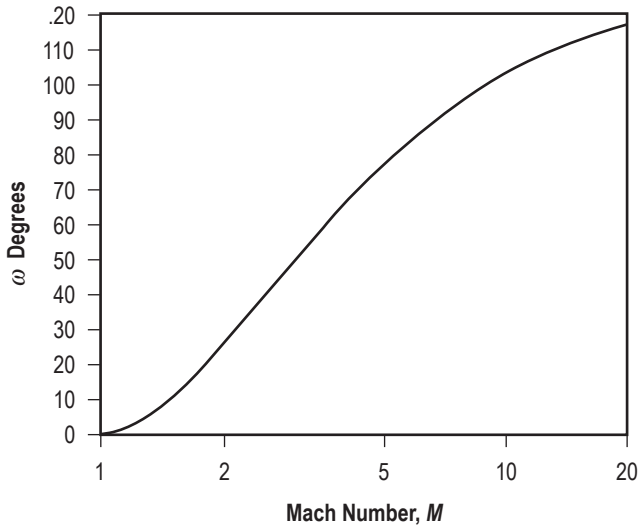

Figure 27. Prandtl-Meyers function.

(2) Given M_{tp}, one may now compute p_{tp}, ρ_{tp}, and u_{tp} via the total pressure and density expressions

$$\frac{p_{tp}}{p_{up}} = \left[\frac{2 + (\gamma - 1)\left(M_{up}\right)^2}{2 + (\gamma - 1)\left(M_{tp}\right)^2} \right]^{\gamma/(\gamma - 1)} , \tag{89}$$

$$\frac{\rho_{tp}}{\rho_{up}} = \left[\frac{2 + (\gamma - 1)\left(M_{up}\right)^2}{2 + (\gamma - 1)\left(M_{tp}\right)^2} \right]^{1/(\gamma - 1)} , \tag{90}$$

while

$$u_{tp} = M_{tp} \sqrt{\gamma p_{tp} / \rho_{tp}} \ , \tag{91}$$

yielding a complete description of the air flow variables along the upper surface of the lifting body.

Similarly, one can compute the flow variables, M_{lr}, p_{lr}, ρ_{lr}, and u_{lr} along the lower rear surface of the lifting body given the flow variables downstream of the shock along the lower forward surface of the lifting body, M_{dn}, p_{dn}, ρ_{dn}, and u_{dn}, via a Prandtl-Meters expansion. Since the ionization at the shock does not effect the expansion process, one can use the same Prandtl-Meyers algorithm with or without ionization. The ionization at the shock, however, indirectly effects the expansion via its effect on the flow variables downstream of the shock along the lower forward surface of the lifting body.

C.3 Wave Drag and Lift

The wave drag and lift forces on the lifting body are the horizontal and vertical components of the forces on the lifting body due to the air pressure on its surfaces, respectively, as shown in figure 28. The wave drag and lift forces are computed by multiplying the pressure on the surface by the area of the surface projected in the horizontal or vertical direction, respectively. For instance, the lift on a unit width of the lower forward surface is $L_{dn} = p_{dn} l_1 \cos(\alpha + \eta)$. Of course, the downward force due to the pressure on the upper surface of the lifting body, L_{tp}, cancels part of the lift from the pressure on the lower surfaces, while the sum of the lift terms must equal the gravitational forces on the lifting body to maintain a constant altitude. Similarly, the pressure on the upper and lower rear surfaces of the lifting body partially compensates for the wave drag on the lower forward surface, while the sum of the wave drag terms must be balanced by thrust from the engine. Finally, to maintain trim, the moments produced by all of the forces on the lifting body must be balanced by the moments produced by the control surfaces or attitude control jets of the lifting body (not shown in fig. 28).

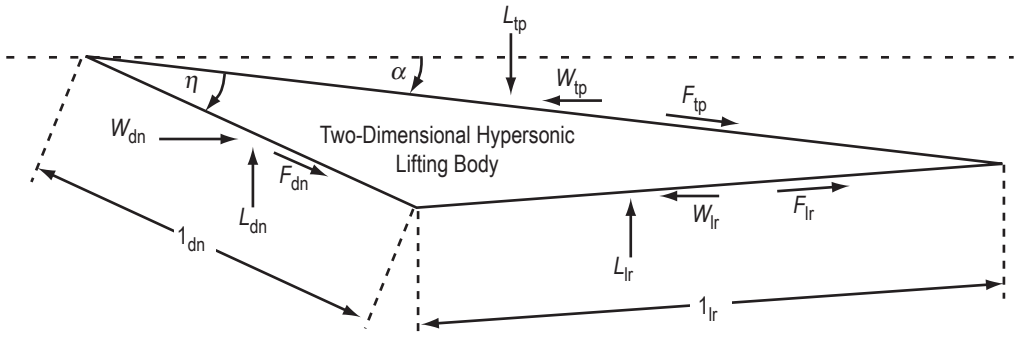

Figure 28. Wave, lift, and friction drag forces on a two-dimensional lifting body.

C.4 Friction Drag

To model the friction drag along the surfaces of the lifting body at hypersonic speeds, one must account for the turbulent flow along the surface and the effects of the boundary layer. Since the analysis requires consideration of the air flow within the boundary layer along the surface of the lifting body, use the superscripts "*w*", "∞", and "*m*" to distinguish between the air flow variables at the wall or skin of the lifting body, the outer edge of the boundary layer, and the mean value between the wall and the outer edge, where the air flow variables at the outer edge of the boundary layer coincide with the free air flow variables generated by the shock and expansion analysis; i.e., $\rho_{dn}^{\infty} = \rho_{dn}$, etc. In the following analysis, the subscript is dropped when dealing with a generic location.

Typically a supersonic flow over a flat surface is laminar at the upstream end of the surface, transitioning to turbulent flow as it passes over the surface, with the friction due to the turbulent flow typically dominate. As such, to simplify the friction drag analysis, assume that the flow over the entire surface of the lifting body is turbulent. Following Schlichting, the force on a surface of length, *l*, and unit width due to friction drag (in the direction of the flow in parallel with the surface) is given by (ref. 42)

$$F = 3.6\times10^{-6}\rho^{m}\left(u^{\infty}\right)^{2}1\left(u^{\infty}1\rho^{m}/\mu^{m}\right)^{-1/5} \quad , \tag{92}$$

where the selection of a mean reference level in the boundary layer is based on experimental evidence.[42] Here, μ is the air viscosity, which may be characterized by Sutherland's equation:[23]

$$\mu = 1.458\times10^{-6}T^{3/2}\left(T+110.4\right)^{-1} \quad . \tag{93}$$

Since the air flow variables at the edge of the boundary layer can be evaluated via the shock and expansion analysis described above, ρ^{m} and μ^{m}, in equation (90), may be expressed in terms of the "∞" variables at the edge of the boundary layer. To this end, let

$$\rho^{m} = \rho^{\infty}\frac{\rho^{m}}{\rho^{\infty}} = \rho^{\infty}\frac{T^{\infty}}{T^{m}} \quad , \tag{94}$$

where the last equality in equation (92) follows from the observation that the air pressure is constant in the boundary layer together with the perfect gas law.[42] Now, following Schlichting,[42]

$$\frac{T^{\infty}}{T_m} = \frac{2}{2 + \frac{\gamma - 1}{2}\left(M^{\infty}\right)^2} \quad , \tag{95}$$

where M^{∞} is the Mach number of the flow at the edge of the boundary layer (equal to the Mach number of the free air flow). As such,

$$\rho^m = \rho^{\infty}\frac{T^{\infty}}{T_m} = \rho^{\infty}\left(\frac{2}{2 + \frac{\gamma - 1}{2}\left(M^{\infty}\right)^2}\right) , \tag{96}$$

as required. Similarly, to express μ^{m} in terms of μ^{∞}, observe from Sutherland's equation (eq. (91)) that, at the relatively high temperatures in the boundary layer, μ can be approximated by $1.458\times10^{-6}T^{1/2}$ (where any approximation error will be further damped out by the fact that viscosity appears to a 1/5 power in the friction drag equation (eq. (90)). As such,

$$\mu^m = \mu^{\infty}\frac{\mu^m}{\mu^{\infty}} \approx \mu^{\infty}\left(\frac{T^m}{T_{\infty}}\right)^{1/2} = \mu^{\infty}\left(\frac{2}{2 + \frac{\gamma - 1}{2}\left(M^{\infty}\right)^2}\right)^{-1/2} \quad . \tag{97}$$

Substituting equations (96) and (97) into the friction drag equation (eq. (92)) now yields the desired expression for force due to skin friction on a surface of length, l, and unit width:

$$F = 3.6\times10^{-6}\rho^{\infty}\left(\frac{2}{2+\frac{\gamma-1}{2}\left(M^{\infty}\right)^2}\right)\left(u^{\infty}\right)^2 1\left(\frac{u^{\infty}1\rho^{\infty}\left(\frac{2}{2+\frac{\gamma-1}{2}\left(M^{\infty}\right)^2}\right)}{\mu^{\infty}\left(\frac{2}{2+\frac{\gamma-1}{2}\left(M^{\infty}\right)^2}\right)^{-1/2}}\right)^{-1/5}$$

$$= 3.6\times10^{-6}\rho^{\infty}\left(u^{\infty}\right)^2 1\left(\frac{u^{\infty}1\rho^{\infty}}{\mu^{\infty}}\right)^{-1/5}\left(\frac{2}{2+\frac{\gamma-1}{2}\left(M^{\infty}\right)^2}\right)^{7/10}$$

$$= 7.2\times10^{-6}Q^{\infty}1\left(R^{\infty}\right)^{-1/5}\left(\frac{2}{2+\frac{\gamma-1}{2}\left(M^{\infty}\right)^2}\right)^{7/10} \quad , \tag{98}$$

where $Q^{\infty} = \rho^{\infty}\left(u^{\infty}\right)^2 \Big/ 2$ is the dynamic pressure of the air flow at the edge of the boundary layer and $R^{\infty} = u^{\infty}1\rho^{\infty} \Big/ \mu^{\infty}$ is the Reynolds number of the air flow at the edge of the boundary layer. Alternatively, upon grouping variables and expressing the viscosity via Sutherland's equation, *F* reduces to

$$F = 3.98\times10^{-3}\left(\rho^{\infty}\right)^{4/5}\left(u^{\infty}\right)^{9/5}1^{4/5}\left(T^{\infty}\right)^{3/10}$$
$$\left(T^{\infty}+110.4\right)^{-1/5}\left(2+\frac{\gamma-1}{2}\left(M^{\infty}\right)^2\right)^{-7/10} \quad , \tag{99}$$

Using this model, with the superscript "∞" variables equated to the appropriate free air flow variables, one can evaluate the friction drag on each of the three surfaces of the two-dimensional hypersonic lifting body of figure 27.

C.5 Skin Temperature

To evaluate the thermal loads on the two-dimensional lifting body, one needs to compute the skin or wall temperatures, T^w. To this end, employ the relationship (ref. 42).

$$\frac{T^w}{T^{\infty}} = 1+\frac{\gamma-1}{2}\left(M^{\infty}\right)^2 \quad . \tag{100}$$

C.6 Boundary Layer Thickness

Following Landau and Lifshitz,[16] the thickness of a boundary layer along a surface at a distance, x, from the upstream edge of the surface is $\delta = \sqrt{\mu x / u^{\infty}}$. Taking μ to be the mean value of the viscosity in the boundary layer, and expressing μ^m via equation (97), this reduces to

$$\delta = \left(\frac{\mu^m x}{u^{\infty}} \right)^{\frac{1}{2}} = \left(\frac{\mu^{\infty} x}{u^{\infty}} \right)^{\frac{1}{2}} \left(\frac{2}{2 + \frac{\gamma - 1}{2} \left(M^{\infty} \right)^2} \right)^{\frac{1}{4}} . \tag{101}$$

Finally, using the "high" temperature approximation of Sutherland's equation, $\mu^{\infty} = 1.458 \times 10^{-6} T^{1/2}$, one may express the boundary layer thickness at x via

$$\delta = 1.435 \times 10^{-3} \times \left(\frac{x}{u^{\infty}} \right)^{\frac{1}{2}} \left(\frac{T^{\infty}}{2 + \frac{\gamma - 1}{2} \left(M^{\infty} \right)^2} \right)^{\frac{1}{4}} . \tag{102}$$

In particular, the maximum thickness of the boundary along a surface of length, l, is

$$\delta^{\max} = 1.435 \times 10^{-3} \times \left(\frac{l}{u^{\infty}} \right)^{\frac{1}{2}} \left(\frac{T^{\infty}}{2 + \frac{\gamma - 1}{2} \left(M^{\infty} \right)^2} \right)^{\frac{1}{4}} . \tag{103}$$

REFERENCES

1. Liberman, M.A.; and Velikovich, A.L.: *Physics of Shock Waves in Gases and Plasmas*, Springer-Verlag, Heidelberg, 1986.

2. Beaulieu, W.; Byturin, V.; Klimov, A.; et al.: "Plasma/Wind Tunnel Experiment With 1/6 Scale Model of Nose Part F–15," Proc. of the *3rd Weakly Ionized Gases Workshop*, Norfolk, November 1999, AIAA Paper 99–4825, 1999.

3. Klimov, A.I.; Koblov, A.N.; and Mishin, G.: "Evolution of Anomalous Dynamic Properties," *Sov. Tech. Phys. Lett.*, Vol. 8, pp. 290–291, 1982.

4. Klimov, A.I.; Koblov, A.N.; Mishin, G.I.; et al.: "Shockwave Propagation in a Glow Discharge," *Sov. Tech. Phys. Lett.*, Vol. 8, p. 192, 1982.

5. Kunhardt, E.; Saeks, R.; Mankowski, J.; and Suchomel, C.: "One Dimensional Shock Characteristics in Weakly Ionized Gases," Proc. of the *3rd Weakly Ionized Gases Workshop*, Norfolk, VA, AIAA Paper 99–4941, 1999.

6. Lowry, H.; Stepanek, C.; Blanks, J.; et al.: "Shock Structure of a Spherical Projectile in Weakly Ionized Air," Presented at the *2nd Weakly Ionized Gases Workshop* (*Supplement*), Norfolk, VA, April 24–25, 1998, pp. 273–300, 1998.

7. Popovic, S.; Kessaratikoon, P.; Markhotek, A.; et al.: "Shock Wave Propagation and Dispersion in a Microwave Cavity Discharge," *33rd AIAA Plasmadynamics and Lasers Conference*, Maui, HI, AIAA Paper 2002–2279, 2002.

8. Vine, F.; Saeks, R.; Mankowski, J.; and Chow, A.: "Plasma Shock Wave Modification Experiments in a Temperature Compensated Plasma," *JANNAF*, Colorado Springs, CO, 2003.

9. Appleton, J.P.; and Bray, K.N.C.: "The Conservation Equations for a Non-Equilibrium Plasma," *J. Fluid Mech.*, Vol. 20, pp. 659–672, 1964.

10. McIntyre, T.J.; Houwing, A.F.P.; Sandeman, R.J.; and Bachor, H.-A.: "Relaxation Behind Shock Waves in Ionizing Neon," *J. Fluid Mech.*, Vol. 227, pp. 617–640, 1991.

11. Magretova, N.N.; Pashchenko, N.T.; and Raizer, Yu.P.: "Structure of a Shock Wave Experiencing Multiple Ionization of Atoms," *Zh. Prikl. Mekh. Tekh. Fiz.*, Vol. 5, No. 11, 1970.

12. Liu, W.S.; and Glass, I.I.: "Ionizing Argon Boundary Layers," *J. Fluid Mech.*, Vol. 91, pp. 679–696, 1979.

13. Popovic, S.; and Vuskovic, L.: "Ionization-Recombination Model for the Supersonic Flow in Weakly Ionized Gas," *9th Inter. Space Planes and Hypersonic Systems and Technologies Conference—3rd Weakly Ionized Gases Workshop*, Norfolk, VA, AIAA Paper 99–4905, 1999.

14. Saeks, R.; Mankowski, J.; Vine, F.; and Cooper, S.: *Plasma Shock Wave Modification*, Report to the U.S. Government on Contracts *NAS8–00137*, *NAS8–09007*, *N00178–01–C–1039*, *N00014–99–C–1085*, and *N00178–99-C–1043*, Accurate Automation Corp. (Revised 2003), 2002.

15. Sutton, G.W.; and Sherman, A.: *Engineering Magnetohydrodynamics*, McGraw-Hill, New York, 1965.

16. Landau, L.D.; and Lifshitz, E.M.: *Course of Theoretical Physics*: *Volume 6—Fluid Mechanics*, 2nd ed., Butterworth Heinemann, Oxford, 1987.

17. Raizer, Yu.P.,: *Gas Discharge Physics*, Springer, Heidelberg, 1991.

18. Lowke, J.J.; and Murphy, A.B.: "Plasma Flows," *The Handbook of Fluid Dynamics*, R.W. Johnson, ed., CRC Press, pp. 15-1–15-32, 1998.

19. Hoffert, M.I.; and Lien, H.: "Quasi-One-Dimensional Nonequilibrium Gas Dynamics of Partially Ionized Two-Temperature Argon," *Physics of Fluids*, Vol. 10, pp. 1769–1777, 1967.

20. Stevefelt, J.; Boulmer, J.; and Delpech, F.-F.: "Collisional-Radiative Recombination in Cold Plasmas," *Phys. Rev. A*, Vol. 12, pp. 1246–1251, 1975.

21. Murray, J.; and Saeks, R.: "Analysis of the Modified Rankine Hugoniot Equations," *34th AIAA Conf. on Plasmadynamics and Lasers*, Orlando, FL, AIAA Paper 2003–4180, 2003.

22. Yamasaki, H.; Abe, M.; and Okuno, Y.: "Characterization of Shock-Wave Under Lorentz Force and Energy Exchange," Proc. of the *IVTNN Workshop on Weakly Ionized Plasmas*, Moscow, Russia, pp. 105–111, 2001.

23. Bertin, J.J.; and Smith, M.L.: *Aerodynamics or Engineers*, 3rd ed., Prentice-Hall, Englewood Cliffs, 1998.

24. Shapiro, A.: *The Dynamics and Thermodynamics of Compressible Flow*, Vols. I & II, The Ronald Press, New York, 1953.

25. Shapiro, A.H.; and Kline, S.J.: "On the Thickness of Normal Shock Waves in Air," *8th International Conference on Theoretical and Applied Mechanics*, Istanbul, Turkey, 1952.

26. Conde, L.; Ibanez, L.F.; and Ferro-Fontan, C.: "Electron Impact Ionization by Drifting Electrons in a Weakly Ionized Plasma," *Physics Review*: *Part E*, Vol. 64, pp. 1–5, 2001.

27. Ishiguro, S.; Kamura, T.; and Sata, T.: "Double Layer Formation Caused by Contact Between Different Temperature Plasmas," *Physics of Fluids*, Vol. 28, pp. 2100–2105, 1985.

28. Raadu, M.A.: "The Physics of Double Layers and Their Role in Astrophysics," *Physics Reports*, Vol. 178, pp. 25–97, 1989.

29. Kuo, S.P.; Kalkhoran, I.M.; Bivolaru, D.; and Orlick, L.: "Observation of Shock Elimination by a Plasma in a Mach 2.5 Flow," *Physics of Plasmas*, Vol. 7, pp. 1345–1348, 2000.

30. Kuo, S.P.; and Bivolaru, D.: "Plasma Effect on Shock Waves in a Supersonic Flow", *Physics of Plasmas*, Vol. 8, pp. 3258–3264, 2001.

31. Anderson, J.D.: *Modern Compressible Flow With Historical Perspective*, 2nd ed., McGraw-Hill, New York, 1990.

32. Bain, L. (ed.): *Proceedings of the Workshop on Weakly Ionized Gasses*, USAF Academy, CO, June 9–13, 1997.

33. Martin, J.J.: *Atmospheric Reentry*, Prentice-Hall, Englewood Cliffs, 1965.

34. Beaulieu, W.; Klimov, A.I.; Leonov, S.B.; et al.: "Development of Cold Plasma Technology Joint BNA and Russian Program," Proceedings Supplement for the *2nd Workshop on Weakly Ionized Gasses*, Norfolk, VA, pp. 207–230, 1998.

35. Bletzinger, P.; Ganguly, B.N.; and Garscadden, A.: "Strong Double Layer Formation by Shock Waves in Nonequilibrium Plasmas," *Physical Review*: *Part E*, Vol. 67, pp. 047401-1–047401-4, 2003.

36. Bain, L. (ed.): Proc. of the *2nd Workshop on Weakly Ionized Gasses*, AIAA, Norfolk, VA, April 24–25, 1998.

37. Klimov, A.; Byturin, V.; Charitonov, A.; et al.: "Shock Wave Propagation Through a Non-Equilibrium Cluster Plasma," *40th AIAA Aerospace Sciences Meeting and Exhibit*, Reno, NV, AIAA Paper 2002–0639, 2002.

38. Mishin, G.I.: "Sound and Shock Waves in a Gas Discharge Plasma," *Proceedings of the Workshop on Weakly Ionized Gasses*, USAF Academy, CO, Paper E, 1997.

39. Settles, G.S.: *Schlieren and Shadowgraph Techniques*, Spring, Berlin, 2001.

40. Liu, W.S.; Whitten, B.T.; and Glass, I.I.: “Ionizing Argon Boundary Layers,” *J. Fluid Mech.*, Vol. 87, p. 609, 1978.

41. Chan, C.; and Hershkowitz, N.: “Electron Temperature Differences and Double Layers,” *Physics of Fluids*, Vol. 26, pp. 1587–1595, 1983.

42. Schlichting, H.: *Boundary-Layer Theory*, 7th ed., McGraw-Hill, New York, 1979.

REPORT DOCUMENTATION PAGE

Form Approved
OMB No. 0704-0188

1. AGENCY USE ONLY *(Leave Blank)*	2. REPORT DATE	3. REPORT TYPE AND DATES COVERED
	August 2006	Technical Publication

4. TITLE AND SUBTITLE
Shock Structure Analysis and Aerodynamics in a Weakly Ionized Gas Flow

5. FUNDING NUMBERS

6. AUTHORS
R. Saeks,* S. Popovic,** and A.S. Chow

7. PERFORMING ORGANIZATION NAME(S) AND ADDRESS(ES)
George C. Marshall Space Flight Center
Marshall Space Flight Center, AL 35812

8. PERFORMING ORGANIZATION REPORT NUMBER
M–1171

9. SPONSORING/MONITORING AGENCY NAME(S) AND ADDRESS(ES)
National Aeronautics and Space Administration
Washington, DC 20546–0001

10. SPONSORING/MONITORING AGENCY REPORT NUMBER
NASA/TP—2006–214602

11. SUPPLEMENTARY NOTES
Prepared by the Academic Affairs Office, Office of Human Capital
*Accurate Automation Corporation, Chattanooga, TN **Old Dominion University, Norfolk, VA

12a. DISTRIBUTION/AVAILABILITY STATEMENT
Unclassified-Unlimited
Subject Category 02
Availability: NASA CASI 301–621–0390

12b. DISTRIBUTION CODE

13. ABSTRACT *(Maximum 200 words)*
The structure of a shock wave propagating through a weakly ionized gas is analyzed using an electrofluid dynamics model composed of classical conservation laws and Gauss' Law. A viscosity model is included to correctly model the spatial scale of the shock structure, and quasi-neutrality is not assumed. A detailed analysis of the structure of a shock wave propagating in a weakly ionized gas is presented, together with a discussion of the physics underlying the key features of the shock structure. A model for the flow behind a shock wave propagating through a weakly ionized gas is developed and used to analyze the effect of the ionization on the aerodynamics and performance of a two-dimensional hypersonic lifting body.

14. SUBJECT TERMS
shockwave, weakly ionized gas, aerodynamics, electrofluid dynamics, shock structure

15. NUMBER OF PAGES
92

16. PRICE CODE

17. SECURITY CLASSIFICATION OF REPORT	18. SECURITY CLASSIFICATION OF THIS PAGE	19. SECURITY CLASSIFICATION OF ABSTRACT	20. LIMITATION OF ABSTRACT
Unclassified	Unclassified	Unclassified	Unlimited

National Aeronautics and
Space Administration
IS20
George C. Marshall Space Flight Center
Marshall Space Flight Center, Alabama
35812